An experimental and simulation study of the influence made by inserts on chromatographic packed bed hydrodynamics

A thesis submitted to the University College London

for the degree of

DOCTOR OF PHILOSOPHY

Tian Lan

2012

The Advanced Centre for Biochemical Engineering

Department of Biochemical Engineering

University College London

London UK

Declaration

I, Tian Lan confirm that the work presented in this thesis is my own. Where information has been derived from other sources, I confirm that this has been indicated in the thesis.

Sign:

Date:

To my loving family

Acknoledgements

I would like to thank my supervisor Prof. Nigel Titchener-Hooker for his support and guidance throughout my PhD studies, and also my advisor Dr. Martina Micheletti. The contribution and expertise provided by the many people at Department of Biochemical Engineering are warmly acknowledged, with specific appreciation given to Spyridon Gerontas for his assistance with model, Yu-Chih Chang for his help with experiment.

To my parents, thank you very much for unwavering support and love. I would like to give a special thanks to my wife Fang Qi for encouraging me to take on this endeavour.

In addition, I want to gratefully acknowledge the support of the Innovative Manufacturing Research Centre (IMRC) in Bioprocessing. The IMRC and the EPSRC Centre are each part of The Advanced Centre for Biochemical Engineering, Department of Biochemical Engineering, University College London, with collaboration from a range of academic partners, biopharmaceutical and biotechnology companies.

Abstract

The biopharmaceutical industry, which relates to human health, witnessed very fast development in the last few years to match the biodrug market demand. Manufacture of high value therapeutics usually requires the use of at least 2 or 3 chromatographic steps, which contributes to the significant cost of downstream processes. Therefore, chromatographic process optimization is an essential part of bioproduct manufacture development. In chromatographic separation, the compressible agarose-base matrices, which are most widely, used as column packing material.

Over the past years there has been a steady move toward the adoption of more rigid, porous particles in order to combine ease of manufacture with increased levels of productivity. The latter is still constrained by the onset of compression where the level of wall support becomes incapable of withstanding flow-induced particle drag. In this study it investigates how, by the installation of cylindrical column inserts, it is possible to enhance the level of wall support to improve the column hydrodynamic performance.

Experiments were conducted to examine the effect of the position of the insert in the column, and also of the insert dimensions on the critical velocity at which the onset of compression occurs. It was found that when installed at the bottom of the

column, single inserts in different dimensions can provide 5% to 15% critical velocity increment, and inserts combination can provide up to a 20% increase in critical velocity without significantly affecting column hydrodynamics (less than 10%), as measured by the level of axial dispersion.

A solid mechanics model was established to simulate the pressure drop, flowrate, and packing material compression properties in a chromatography column. Based on the Biot's theory, which describes consolidation of porous materials, the model can relate the pressure drop to compression in chromatographic process. Darcy's law is also applied, and combines with the Konezy-Carman equation for permeability. Comsol Multiphysics software, which can solve physical phenomenon by the finite element method, was employed for the model established. The inverse method in Matlab is used for parameter determination. With this simulation, the Young's modulus, and bed voidage fraction were specified in one experiment condition. The determined parameters were then input to the model to simulate the flowrate, pressure drop, and bed displacement. The simulation results fit the experimental result quite well. The average error between experimental and simulation data was 3% for linear velocity and 4% for pressure drop. The simulation could also predict the superficial critical velocity for the same column packed but with inserts in different dimensions.

Besides the experimental and simulation study on hydrodynamics in

chromatography column having inserts, the effects of inserts applied on protein separation were also considered. The column inserts allowed higher operational flowrates, and process duration, which is positive to process productivity. However, it had a negative effect on the resolution, and caused larger elution volumes, especially when more than one insert present. In a case study of column inserts affecting on productivity, the productivity could increase 18% by two inserts setup in a 1 L column. These inserts lead 20% critical velocity increment, and 10% plate number decrement.

Table of Contents

Declaration 2

Acknoledgements 4

Abstract 5

Table of Contents 8

List of Figures 13

List of Tables 19

Nomenclature 20

Chapter One: Introduction 24

1.1 Perspective and motivation 24

1.2 Aims of this project 25

1.3 Chromatography in bioprocesses 26

1.3.1 Modes of chromatography operation 28

1.3.2 Packed matrix properties 28

1.3.2.1 Base matrices 29

1.3.2.2 Ligands 30

1.3.3 Basic chromatographic theory 35

1.3.3.1 Resolution 35

1.3.3.2 Column efficiency 36

1.4 History of chromatographic process development 38

1.5 Bed compression in chromatographic process 41

1.5.1 Limitations with compressible materials 41

1.5.2 Theory of wall effects 42

1.5.3 Column inserts 44

1.6 Organisation of thesis 45

Chapter Two: Materials and Methods 47

2.1 Experiments for critical velocity determinations and column efficiency tests 47

2.1.1 Experimental setup 47

2.1.1.1 Pump and detector systems 47

2.1.1.2 Chromatography columns 48

2.1.1.3 Packing materials 49

2.1.1.4 Inserts 51

2.1.2 Column packing procedure 53

2.1.3 Pressure-flowrate curve and critical flow velocity determination 55

2.1.4 Column efficiency determination 57

2.2 Mathematical simulation 58

2.2.1 Model of solid mechanics established with Comsol Multiphysics 58

2.2.2 The finite element method 61

2.2.3 Inverse method 62

2.3 Statistical analysis 64

Chapter Three: System Characterisation 66

3.1 Introduction 66

3.2 Impact of column insert on critical velocity 69

3.2.1 Effect of experimental runs on critical velocity..... 69

3.2.2 Effect of insert position on critical velocity..... 71

3.2.3 Effects of insert length on critical velocity 73

3.2.4 Effect of single insert diameter on critical velocity 75

3.2.5 Effect of insert number on critical velocity 77

3.2.6 Effect of column aspect ratio on the critical velocity 79

3.3 Impact of insert on column efficiency 82

3.3.1 Effect of packing procedure on experimental result 82

3.3.2 Effect of insert type..... 85

3.3.3 Effect of insert material 87

3.5 Conclusions..... 95

Chapter Four: Model Establishment 96

4.1 Introduction..... 96

4.2 Theory 97

4.2.1 Flow condition in chromatographic columns 97

4.2.1.1 Newtonian fluid 98

4.2.1.2 Laminar flow..... 98

4.2.2 Darcy's Law..... 100

4.2.3 Mathematical modeling of compression in a chromatography column

..... 103

4.2.3.1 Liquid phase equations 104

4.2.3.2 Solid phase equations 105

4.2.4 Simulations 108

4.2.4.1 Young's modulus 108

4.2.4.2 Voidage fraction 108

4.2.4.3 Evaluate packing material property 109

4.3 Results and discussion 110

4.3.1 Coefficient determination by experimental data 110

4.3.2 Bed displacement versus pressure 112

4.3.3 Parameters distribution 113

4.4 Conclusions 115

Chapter Five: Application of a two-dimensional structural mechanics model for predicting the pressure-flow profile and compression properties during operation of columns with internal inserts 117

5.1 Introduction 117

5.2 Results and discussion 118

5.2.1 Comparing simulation and experiment results 119

5.2.2 Key parameter profiles in columns with single insert 120

5.2.3 Simulation on the effect of insert length on critical velocity 122

5.2.4 Simulation on the effect of insert diameter on critical velocity 123

5.2.5 Simulation the effect of column insert number on critical velocity 125

5.3 Conclusions 128

Chapter Six: Conclusions and Future Work 130

6.1 Conclusions 130

6.2 Future directions 134

6.2.1 Impact of column inserts on process productivity 134

6.2.2 Insert material 134

6.2.3 Industry scale study 135

References 136

Appendix 149

List of Figures

Figure 1.1 A typical platform of bioprocess for protein production, involving two or three chromatographic processes. 27

Figure 1.2 Typical Chromatogram. The void volume, V_0, is defined as the elution volume of an un-retained solution. 36

Figure 1.3 The height equivalent of a theoretical plate (HETP) at different flowrate. 38

Figure 2.1 Experimental setup 49

Figure 2.2 a Stainless steel insert configurations. The support bars can be removed to enable single or double inserts to be used. Design for both XK 50 and BPG 100 columns. The inserts diameters were 15 mm and 30 mm, and their length was 45 mm. all supporting bars were 50 mm long. b Plastic insert configuration. The support bar is fixed. The insert size is same as stainless steel inserts. 52

Figure 2.3 Insert in a BPG 100 column. The insert is constructed of stainless steel, and it is 75 mm in diameter, and 90 mm in length. This column is a 100 mm diameter column. 55

Figure 2.4 Initial experimental date of automatic pressure step method. The experiment was taken at BPG 100 column with P6XL at 110±5 mm bed height. The solid line is flowrate, and the dash line is pressure. This is for independent critical velocity determination experiment. 56

Figure 2.5 Flowchart for model formulation in Comsol Multiphysics. In the first step the 2D-asymmetry was selected to deal with the cylindrical column. Secondly, the mathematical model describing the flow in chromatography column was chosen. Thirdly, the geometry was drawn. In the fourth step, the parameters were input. Next, the equations need to be specified in the model domain. Then, the mesh was generated, and the model solved. Finally, the results were evaluated and exported. 60

Figure 2.6 Flowchart for evaluating parameters in hydrodynamic equation (Young's modulus as a function of packing material deformation, and permeability as a function of bed voidage) by using inverse method in Comsol Multiphysics and Matlab. 63

Figure 3.1 The experimental critical velocity results for different runs. The experiments used a BPG 100 column packed with P6XL to 110±5 mm in height. The solid points and hollow points represent the critical flowrate result with and without column repacking respectively. For non-repacked column experiments, a one hour period for bed expansion was allowed for between determination of critical velocity. 70

Figure 3.2 Inserts at different column positions. All use an XK 16 column packed with Sepharose 6b-CL material at 100±5 mm bed height. Insert (9 mm in diameter and 45 mm in length) constructed of plastic and placed at three different positions: top (55 mm from column base), middle (27.5 mm from column base), and bottom (resting on column base) of bed prior to determination of the critical velocity. 71

Figure 3.3 Effect of insert position on critical velocity of XK 16 column packed with Sepharose CL-6B to a bed height of 100±5 mm. Critical 72

velocity without insert; 360 cm h^{-1}. Data points are mean±SD from 3 independent experiments.

Figure 3.4 Effect of insert length on critical velocity of BPG 100 column packed with P6XL resin to a bed height of 100±5 mm. Critical velocity without insert; 219cm h^{-1}. Insert constructed of stainless steel. Insert lengths (mm): 30, 45, 60, 75 and 90, and insert diameter: 30 mm. Data points are mean±SD from 3 independent experiments. Line shows best fit to the linear equation: $\frac{\Delta u_{crit}}{u_{crit\,0}} = 0.08 \times L_{insert}$, R^2=0.98 74

Figure 3.5 Effect of insert diameter on critical velocity of BPG 100 column packed with P6XL resin to a bed height of 100±5 mm. Critical velocity without insert; 219 cm h^{-1}. Inserts constructed of stainless steel. Inserts all had a length of 45 mm. Data points are mean±SD from 3 independent experiments. Line shows fit to polynomial equation: $\frac{\Delta u_{crit}}{u_{crit\,0}} = -17.5 \times \left(\frac{D_{insert}}{D_{bed}}\right)^3 + 13.7 \times \left(\frac{D_{insert}}{D_{bed}}\right)^2 + 11.4 \times \left(\frac{D_{insert}}{D_{bed}}\right)$. 76

Figure 3.6 Effect of insert configuration on critical velocity of BPG 100 column packed with P6XL resin to a bed height of 100±5 mm. Critical velocity without insert; 219 cm h^{-1}. Inserts were constructed of stainless steel, length 45 mm. Data points are mean±SD from 3 independent experiments. 78

Figure 3.7 Effect of scale on critical velocity change. Constant ratio of insert to column diameter packed with P6XL resin to a bed height of 100±5 mm. Inserts constructed of stainless steel. All inserts were 45 mm in length. Insert diameter was 35 mm (XK 50 columns) or 70 mm (BPG 100 columns). The

ratio of insert to column diameter was 10:7. Critical velocity without insert; 234 cm h^{-1} (XK 50 column) and 219 cm h^{-1} (BPG 100 column). Data points are mean±SD from 3 independent experiments. 80

Figure 3.8 Effect of resin type on critical velocity in a XK 16 column with a bed height of 100±5 mm. Inserts constructed of stainless steel. Critical velocity without insert; Sepharose CL-6B resin 360 cm/h; P6XL resin 234 cm/h; Sepharose 4B 200 cm h^{-1}. Data points are mean±SD from 3 independent experiments. 81

Figure 3.9 Impact of stainless steel insert on column efficiency of XK 50 column packed with P6XL resin to a bed height of 120±5 mm. All inserts were 45 mm in length. Figure 3.9a: HETP for no insert (——), 16 mm diameter insert (– – –), 35 mm diameter insert (-----), and 16 mm and 35 mm diameter double inserts (–·–··). Figure 3.9b: Variation in plate numbers for column tested in Figure 3.9a, the initial plate number is 3483 plates m^{-1}. Figure 3.9c: Variation in asymmetry factor for column tested in Figure 3.9a, the initial asymmetry is 1.25. Data points are mean±SD from 3 independent experiments. 86

Figure 3.10 Impact of insert materials of construction on column efficiency for an XK 50 column packed with P6XL resin to a bed height of 50±2 mm. All inserts were 45 mm in length. Volume of inserts; plastic insert is 4 mL; stainless steel inserts is 0.14 mL. No insert (——), Plastic insert (–·–··), Stainless steel insert (-----). a: tracer absorbance as a function of retention volume, b: tracer absorbance normalized as a function of column volume. 88

Figure 3.11 Change in productivity with flow velocity with different inserts (35 mm, 70 mm diameter insert, and double inserts) in 100 mm diameter 92

column packed to 127 mm bed height with Mabselect SURE™ .The solid line is the productivity change with operational flow velocity.

Figure 3.12 Productivity with flow velocity at different DBC gradient. It is in 100 mm diameter column packed to 127 mm bed height with Mabselect SURE™.

93

Figure 4.1 Experimental (●) versus simulated (——) pressure-flow data. The experimental data were best fitted to a structural mechanics model in order to calculate the mechanical properties of the resin (Young modulus empirical equation constants) and permeability coefficient, and to generate the simulated pressure-flow profile and bed height.

111

Figure 4.2 Bed displacement profile of a 0.86 L chromatographic column (100 mm in diameter, and 110 mm in original packed height) packed with P6XL. The six figures represent the profile at different pressure drops, which lead to achieving the condition corresponding to the onset of the critical velocity. 113

Figure 4.3 Pressure, stress, and voidage fraction profile of a 0.86L chromatographic column (100 mm in diameter, and 110 mm in height) packed with P6XL, at the point the column achieves critical velocity. 114

Figure 5.1 Experimental (●) versus simulated (——) pressure-flow data for chromatographic column packed with column inserts. In practice, the column was 100 mm in diameter, and packed to 110 mm bed height. The column inserts were 30 mm diameter for single insert, and 30 mm & 75 mm for 120 double inserts. All column inserts were 45 mm in length, and 1.1 mm in

thickness. The packed material was P6XL.

Figure 5.2 Axial-stress, voidage fraction, and bed displacement profile of a 0.86L chromatographic column (100 mm in diameter, and 110 mm in height) packed with single column inserts (75mm in diameter and 45 mm in length), at the point the column achieves critical velocity. The packed material was P6XL. 121

Figure 5.3 Simulation result on the impact of column insert length on superficial critical velocity. The simulation was conducted at a 100 mm diameter column packed to 110 mm bed height. The inserts was 30 mm in diameter, and 1.1 mm in thickness. The insert length of the simulation was from 7.5 to 90 mm. 123

Figure 5.4 Simulation result on the impact of column insert length on superficial critical velocity. The simulation was conducted at a 100 mm diameter column packed to 110 mm bed height. The inserts were 45 mm in length, 1.1 mm in diameter. The insert diameter of the simulation was from 7.5 to 90 mm. 125

Figure 5.5 Bed Voidage fraction, and displacement profile of a 0.86L chromatographic column (100 mm in diameter, and 110 mm in height) packed with double column inserts (32mm & 64 mm in diameter and 45 mm in length), and triple column inserts (25 mm & 50 mm &75 mm diameter and 45 mm in length), at the point the column achieves critical velocity. The packed material was P6XL. 127

List of Tables

Table 1.1 Types of ligand chemistries used in preparative protein chromatography. 30

Table 2.1 Summary of basic materials and experimental conditions 51

Table 2.2a Plastic and stainless steel insert dimensions (mm) 53

Table 2.2b Stainless steel insert dimensions (mm) 53

Table 3.1 Theoretical plate number and asymmetry with different packing procedure. 84

Table 3.2 The time for each step was determined depending on the screening conditions 91

Table 4.1 Reynolds number of flow for different column geometries tested 99

Table 4.2 Physical constants used in modeling simulations 112

Table 4.3 Best-fit values for the empirical modulus of equation (4.19 and 4.20) 112

Table 5.1 Critical velocity increment with insert number 128

Nomenclature

A	the cross-sectional area (m^2)
a	1. the distance from the leading edge of the peak to the midpoint of the peak (mm)
	2. coefficient in equation 4.20 (-)
A_s	asymmetry factor (-)
b	1. the distance from the midpoint of the peak to the trailing edge (mm)
	2. coefficient in equation 4.20 (-)
C	permeability constant (-)
D	column diameter (mm)
e	void ratio (-)
d	the pipe diameter (mm)
D_{bed}	column diameter (mm)
D_{insert}	insert diameter (mm)
d_p	the particle diameter (m)
E	elasticity modulus (Pa)
E_0	6% agarose Young's modulus (Pa)
G	shear modulus (Pa)
g	gravitational acceleration ($m\ s^{-1}$)
H	column bed height (mm)
H_0	the initial height of the uncompressed column (mm)

k	the permeability (-)
k_p	the permeability coefficient for water (-)
L_{insert}	insert length (mm)
N	plate number (m^{-1})
n	safety margin (-)
P	pressure (Pa)
	process productivity ($g\ h^{-1}\ L^{-1}$)
ΔP	the hydrodynamic pressure drop across the column (Pa)
R_e	Reynolds number (-)
t_C	cycle time (h)
t_R	retention time (s)
U_0	superficial flow velocity ($cm\ h^{-1}$)
U_{crit}	critical flow rate ($mL\ min^{-1}$)
u	operational flow velocity ($cm\ h^{-1}$)
u_{crit0}	initial critical velocity ($cm\ h^{-1}$)
V	volumetric flow rate ($mL\ min^{-1}$)
V_L	column volume (L)
V_{sp}	packing material volume (L)
v	superficial flow velocity ($cm\ h^{-1}$)
$W_{1/2}$	the width of the peak at one half the maximum height (mm)
Y	yield of mAb purification with MabSelect SuRe^{TM} resin (%)

Greek symbols

α	1.the constant of coefficient (-)
	2. the angle of inclination of the flow path with respect to the horizontal (°)
β	the constant of coefficient (-)
δ	the constant of coefficient (-)
ε	1. bed voidage fraction (-)
	2. strain (mm)
σ	stress (Pa)
λ	Lame's coefficient (-)
μ	fluid viscosity (Pa s^{-1})
μ_f	the wall friction coefficient (-)
ν	Poisson's ratio (-)
ρ	density (kg m^{-3})

Abbreviation

AEX	Anion exchange chromatography
AFC	Affinity chromatography
CEX	Cation exchange chromatography
CFD	Computational fluid dynamics
CV	Column volume

DBC	Dynamic binding capacity
FDA	Food and drug administration
HETP	Height equivalent to a theoretical plate
HIC	Hydrophobic interaction chromatography
IEX	Ion exchange chromatography
PI	Proportional-integral
SD	Standard deviation
SEC	Size-exclusion chromatography

Chapter One: Introduction

1.1 Perspective and motivation

Nowadays, the benefit from biopharmaceutical industry is increasing dramatically (Aggarwal, 2011). Each company is trying to deliver safer and cheaper medicines and manufacturing development crucial to this. Biotech drugs or biologics include therapeutic proteins, recombinant vaccines, peptide conjugates, gene therapy, RNA interference, and regenerative medicine. These biologics have a bigger share of the pharmaceutical market. In the drug industry as a whole 101 drugs each brought in more than $1 billion in worldwide sales in 2006 (Lawrence, 2007), of these, 18 were biotech drugs. It has grown from only 3 biologics in 2000 (Lawrence, 2007). In the US biotech market, the total sales grew from $40 billion in 2006 to $51.3 billion in 2010 (Aggarwal, 2009; Aggarwal, 2011). That means the biopharmaceutical industry is attracting more and more attention, and this situation is leading to greater level of competition in this industry. Each company faces enormous pressure to increase productivity while reducing costs. This is driving new technology developments. For the biopharmaceutical industry, antibody therapeutics is one of the most important products (Reichert, 2008). Seven new mAbs reached the market during 2010-2011, and there are now 34 US-Food and Drug Administration (FDA)-approved mAbs in the market (Aggarwal, 2011). There are several critical challenges: improving process efficiency, achieving regulatory requirements, and reducing costs(Roque and Lowe, 2004). With these

improvements, the bioproduct will be made more affordable to the purchaser.

In the total manufacturing cost of a therapeutic antibody, the downstream processing occupies more than 50%, and the main cost in the downstream is the need for several chromatographic processes (Aldridge, 2006; Roque and Lowe, 2004). Therefore, developing the chromatographic process is very important to antibody manufacturing development; and, it is important to improve the economy and efficiency of chromatographic systems. To achieve this goal, how to increase the throughput whilst meeting quality requirements is a prime motivation.

1.2 Aims of this project

This thesis seeks to demonstrate the effect of column inserts on chromatographic column hydrodynamics. It will target chromatographic columns packed with compressible materials. Column inserts are designed to provide extra wall support, and hence lead to a larger superficial critical velocity. The superficial critical velocity is the maximum flow velocity the column can achieve when packed with compressible materials. By enabling the operating flowrate to increase, and the period of process operation could be reduced. Higher levels of process productivity could be expected. In this thesis, the effects were studied both experimentally and via mathematical simulation. The objective of the experimental work was to provide experimental results on the critical velocity and column efficiency change

with various column inserts. The purpose of establishing the mathematical model was to provide theoretical supporting evidence to explain the column inserts impact on column hydrodynamics and bed consolidation. Moreover, with the model, it was expected to predict pressure-flow profile, and bed compression in a chromatographic column packed with a range of column inserts (different diameters, lengths, or number).

1.3 Chromatography in bioprocesses

In this thesis, the focus is on chromatographic processes in the downstream processing of biotech drugs. The general requirement of the downstream process in biopharmaceutical industry is different from other drugs, such as chemical drug, because the unit operations for the separation of biological molecules differ from their counterparts in the chemical industry. Most biological molecules, and particularly proteins, are destroyed by heat, cannot be evaporated or distilled, are generated at low concentrations, and have a three-dimensional structure that can change during purification, resulting in loss of the molecule's function. Therefore, bioproducts are recovered, purified, and concentrated by membranes, adsorption, chromatography, crystallization, and other techniques that do not require heat or extreme pH to achieve fractionation. Therefore, some processes, such as filtration, adsorption, chromatography, and crystallization, which do not require extreme heat or pH to achieve fractionation have been chosen for downstream purification steps in the biopharmaceutical industry (Sofer and Hagel, 1997).

Among these purification steps, chromatographic processes play an important role of bioproduct purification, especially for protein separation due to its high efficiency and selectivity. The downstream processes, almost always contains two or three chromatography steps, which is shown in Figure 1.1. The first step is normally for product capture. The second step of chromatography is for additional purification of the product from residual host-cell contaminants. Sometimes, a third chromatography step is required as a polishing step to clear residual impurities, which are hard to remove.

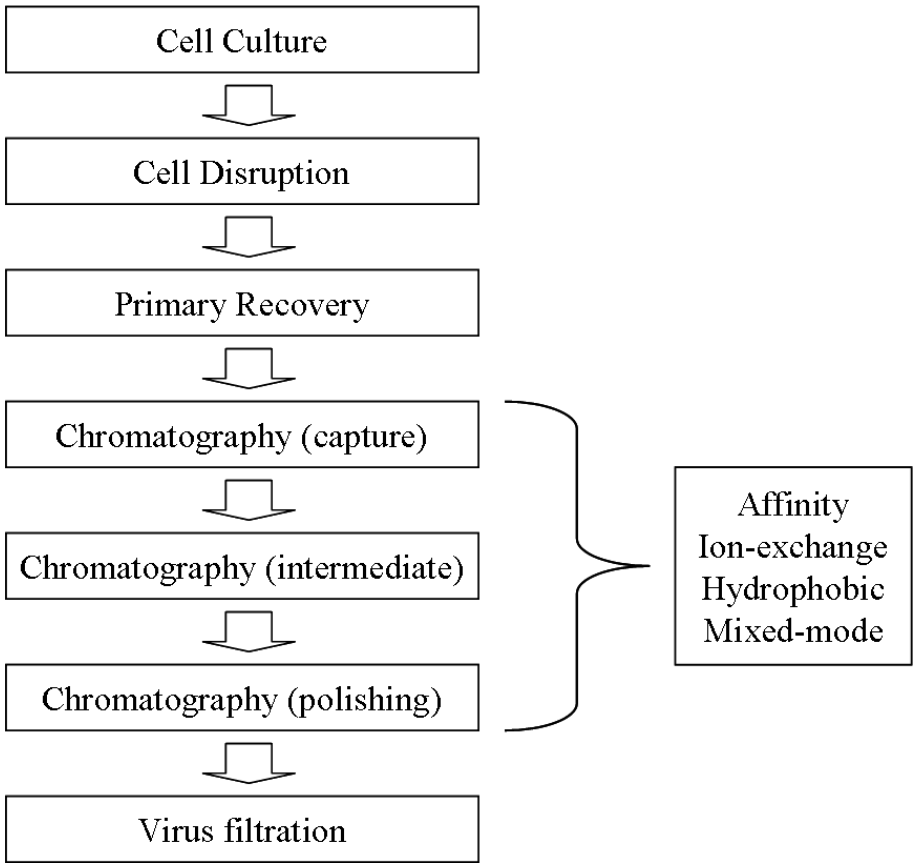

Figure 1.1 *A typical platform of bioprocess for protein production, involving two or three chromatographic processes.*

1.3.1 Modes of chromatography operation

Process chromatography is usually operated in one of two modes, involving 'bind-and-elute' or 'flow-through'. In bind-and-elute mode, the protein product is bound to the column and then separated across the length of the column under isocratic, or linear gradient elution conditions (Harrison et al., 2003; Guiochon et al., 2006). The steps of the typical bind-and-elute chromatography are a column equilibration stage, sample loading, one or more wash steps, and product elution. By contrast, in flow-through mode, the feedstock or sample is loaded continuously to the column with the goal being to bind contaminants to the column while the product ‘flows-through’ for recovery after passing the bed. The typical steps in this mode include column equilibration stage, sample loading, one or more wash as stripping steps after the load, and column regeneration.

1.3.2 Packed matrix properties

Chromatography packed materials are characterised by their base support material and surface chemistry ligand. The matrices are usually produced by attaching a binding ligand to the base matrix. While the surface chemistry determines the primary separation mechanism, the base matrix can strongly influence the mass transport properties of the separation and contribute to secondary binding effects.

Secondary binding effects include the impact of the matrix structure such as pore size in determining the level of product separation achieved (Boschetti, 1994; Muller, 2005).

1.3.2.1 Base matrices

The base matrix may either be porous or non-porous, with the majority of base matrices used in preparative protein chromatography being porous. Both inorganic and organic materials are used in the preparation of base matrices (Muller, 2005). Inorganic base matrices include hydroxyapatite, alumina, silica, and controlled pore glass. The main feature of this kind of sorbent is its incompressibility. Organic polymers include cellulose, agarose-based matrices, cross-linked dextran, polyacrylates, and polyvinyl polymers (Beyzavi, 1999). They are compressible materials. Among them, agarose gels are typical natural and neutral macroporous polysaccharidics used as base matrix. After cross-linking, it can improve them mechanical properties. Because they are inert and hydrophilic, they are widely used in bioseparations (Boschetti, 1994). In this study, agarose gels were the main group considered. Composite materials, such as silica-polymer, have also been developed in order to combine the rigidity of one material with the biocompatibility and stability of another (Muller, 2005).

1.3.2.2 Ligands

The attached ligand property determines the chromatography separation mechanism.

The different types of chromatography are summarised in Table 1.1.

Table 1.1 Types of ligand chemistries used in preparative protein chromatography.

Type	Examples of Ligand Type	Separation Principle
Cation-exchange	*Sulfopropyl (SP)* *Methylsulfonate (S)* *Carboxymethyl (CM)*	Electrostatic interaction
Anion-exchange	*Diethylaminoethylene (DEAE)* *Quaternary aminoethyl (QAE)* *Quaternary ammonium (Q)*	Electrostatic interaction
Hydophobic Interaction	*Phenyl-* *Butyl-* *Octyl-*	Hydrophobic complex formation
Reversed phase	*4-carbon alkyl (C4)* *18-carbon alkyl (C18)*	Hydrophobic complex formation
Size-exclusion chromatography	*N/A (porous inert base matrix)*	Steric exclusion
Affinity, Pseudo-affinity	*Protein A/G* *Glutathione* *Heparin* *Dye* *Antibody* *Recombinant protein* *Biomimetic* *Lectin* *Immobilised metal affinity*	Biospecific interaction, coordination complex formation

Ion-Exchange Chromatography

Ion-exchange chromatography separates molecules based on their surface charge. As all proteins carry a net negative or positive charge, (depending on the pH and the relative numbers of basic and acidic amino acids), they can be bound by ionic forces to immobilized groups of opposite charge. Ion-exchange matrices consist of hydrophilic particles to which charged groups have been covalently bonded. Once bound, proteins can be eluted by either changing the pH of the mobile phase or by increasing the salt concentration. The steric mass-action (SMA) ion-exchange equilibrium formalism, accounts explicitly for the steric hindrance of salt counterions upon protein binding in multicomponent equilibria. The SMA model describes protein adsorption in an ion change system as a stoichiometric exchange. At higher protein concentrations, the finite capacity of the stationary phase sites for the adsorbed molecules play important roles in equilibrium adsorption. Velayudhan (Velayudhan, 1990) observed that the number of blocked sites is proportional to the adsorbed protein concentration. Brook and Cramer (Brook and Cramer, 1969) have utilized this insight to form the basis of the SMA formalism. The SMA model has been shown capable of describing the linear and nonlinear adsorption of proteins in ion-exchange chromatographic system over a range of salt concentrations. Since biopharma is dominated by mAbs most commonly used are quaternary ammonium (Q) as an anion exchanger and Methylfonate (S) as a cation exchanger.

Hydrophobic Interaction Chromatography

This type of chromatography makes separation of the fact that many proteins have hydrophobic sites exposed on their surfaces. The separation is achieved by the changing strengths of the resultant interactions with an uncharged matrix containing hydrophobic groups, i.e., alkyl chains or phenyl rings (Burton, 1998; Chen, 2008).

Raising the ionic strength of the solution by adding a neutral salt increases the strength of hydrophobic interactions. Thus it is usual when performing hydrophobic interaction chromatography to adsorb the sample to the matrix at high ionic strength. Adsorbed substances are then separated by selective desorption in which the elution conditions are altered so as to progressively reduce the strength of the hydrophobic interactions with the matrix. This can be achieved by one or more of the following methods:

• Reducing the ionic strength

• Changing the ion to a more chaotropic one

• Raising the pH of eluant

• Reducing the polarity of the eluant by including, for example, ethylene glycol

• Including a detergent

Operation is very similar to ion exchange chromatography in that elution may be by either step or continuous gradient. HIC interactions are also affected by temperature. Adsorption will be stronger at increasing temperatures (Sofer and Hagel, 1997).

Reversed Phase Chromatography

Reversed phase chromatography operates by a similar mechanism but is distinguished from hydrophobic interaction chromatography by an increased degree of substitution (hydrophobic content) on the matrix and subsequently stronger sample/matrix interaction. In the case of proteins, the interaction is so strong that the internal hydrophobic sites of the proteins are exposed, resulting in denaturation. Elution is usually effected by organic solvents. Reversed phase chromatography is highly useful for small molecules and peptides where denaturation is not a problem. Hydrophobic interaction chromatography is used for larger proteins, where the gentle binding and elution conditions prevent denaturation and lead to higher recovery (Sofer and Hagel, 1997; Boschetti, 1994).

Size Exclusion Chromatography

Size exclusion chromatography separates compounds base on different molecular sizes. The stationary phase consists of insoluble, hydrophilic, porous particles (usually called the gel) packed into the column. Small molecules are able to penetrate the pores fully, while large molecules are excluded from entering the gel particles. Medium sized particles can partially penetrate the pores. Thus, different proportions of the column volume are accessible to molecules of different sizes. The large molecules travel fastest and are eluted first since they are unable to penetrate the pores and have only the interstitial or void volume to traverse. Small molecules that can fully penetrate the particle pores have the largest volume to

traverse and are eluted last. Molecules that can penetrate the particles to varying degrees have varying volumes to traverse and are eluted in order of decreasing size (DePhillips and Lenhoff, 2000).

Affinity Chromatography

Proteins have highly specific binding sites for other molecules, which allow them to carry out their biological functions. The size and the shape of the bound species as well as the hydrophobic and the hydrophilic interactions determine the nature of the binding. The affinity of a protein for a specific molecule (a ligand) can be employed in order to separate the target protein from a complex mixture (Clonis, 2006; Roque et al., 2005). This is the basis of affinity chromatography, which utilizes a sample-specific ligand covalently coupled to a support matrix. This binding ligand is then able to adsorb the sample from the mobile phase. Desorption is achieved by changing the elution conditions so as to reduce the ligand-protein interaction. Affinity matrices used for practical large-scale purification fall into two categories:

• Those which are specific to the desired protein. In the case of an enzyme for instance, the ligand might be a substrate, substrate analogue, inhibitor, or a specific antibody.

• Those which will interact with a group of species because they carry a group-specific or general ligand. Such group-specific ligands include immobilized cofactors (for example, 5-AmP or NAD) which are specific for classes of enzymes, or dyes which can interact with a large number of different proteins. In the case of

group-specific ligands, purification depends on the variable affinity of different enzymes for the ligand and in the susceptibility to differing elution conditions. Desorption may be achieved by eluting with either a specific co-factor or substrate which will compete with the immobilized ligand for the protein. It may also be attained by altering the pH or ionic strength, which will perturb the protein/matrix interaction. In theory, a specific affinity matrix offers ideal purification, with the potential for a one-step process from a crude protein mixture to the single desired product. In practice, however, ligands specific for a given enzyme are either substrates or inhibitors of that enzyme. For that reason, they are often difficult and expensive to prepare in quantity. In addition, after the enzyme substrate is coupled to the matrix, it may no longer be capable of binding the enzyme. The use of group-specific matrices has been more common to-date. In particular, the immobilized dyes have found many uses. A variety of commercially produced dye-ligand matrices are available.

1.3.3 Basic chromatographic theory

1.3.3.1 Resolution

The separation efficiency or resolution of a system depends on two different properties: selectivity, measured by the volume separating the peaks of two adjacent sample components; and the band broadening properties of the system. Both of these properties are taken into account when defining resolution. The calculation of

two peaks' resolution in Figure 1.2 can follow the equation below:

$$R_s = \frac{V_{r2} - V_{r1}}{\frac{1}{2}(W_{b1} + W_{b2})} \tag{1.1}$$

Where R_s is resolution. V_{r2} and V_{r1} are the retention volume/time of the two peak. W_{b1} and W_{b2} are the width of the two peaks.

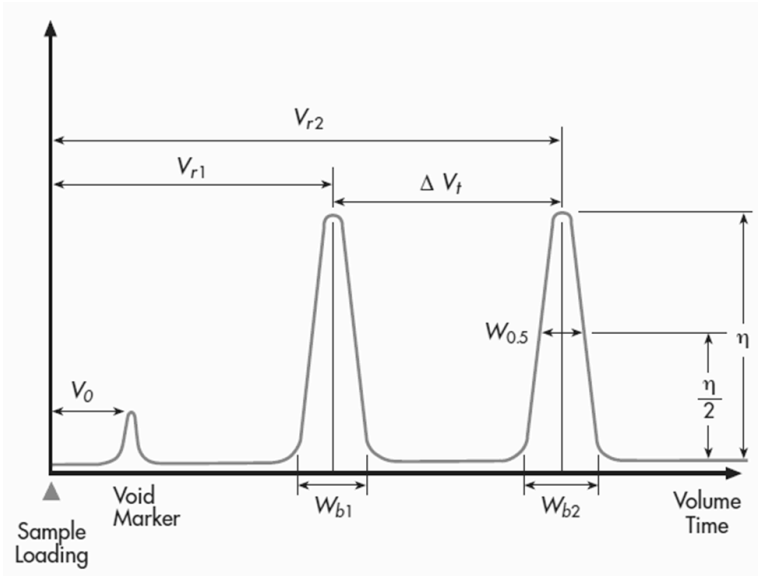

Figure 1.2 *Typical Chromatogram. The void volume, V_0, is defined as the elution volume of an un-retained solution.*

1.3.3.2 Column efficiency

The method of determining a normalized peak width has been developed to compare fairly the effects of such factors as particle size, column packing technique or ancillary equipment on efficiency. A defined band of a single test injection, usually such as a salt (NaCl), or a dilute solution of acetone, is applied to the column. Retention volume and peak width are measured. These are used to

calculate the theoretical plate number for the peak in Figure 1.2, (N): (Martin and Synge, 1941; Craig, 1944)

$$N = 5.54\left(\frac{V_{r2}}{W_{0.5}}\right)^2 \tag{1.2}$$

The plate number (N) is proportional to the column bed length (L). To make the comparison of the efficiency of different columns, the height equivalent of a theoretical plate of HETP is used:

$$HETP = \frac{L}{N} \tag{1.3}$$

The HETP gives a measurement of the separation efficiency per unit length of column, when operated under a given set of conditions. It will vary with the concentration, nature and volume of the test solute and should thus only be used for comparative purposes. More efficient columns have lower HETP values. The calculation of HETP allows ready comparison of the loss of efficiency in a column after a number of applications, or the difference between different columns. The dependence of HETP on flow rates given by the Van Deemter equation: (Van Deemter et al., 1956)

$$HETP = A + \frac{B}{u} + Cu \tag{1.4}$$

where u is the flow rate. A is a constant associated with eddy diffusion, B is coefficient associated with axial diffusion, and C reflects the mass transfer kinetics. Figure1.3 shows how the HETP related to flowrate.

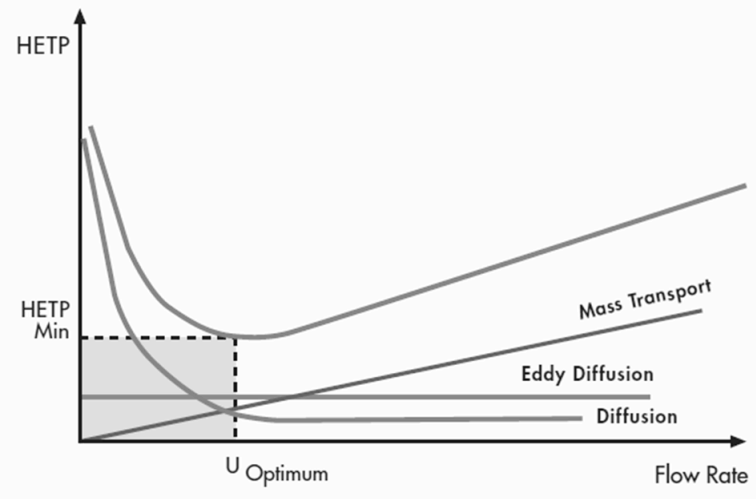

Figure 1.3 *The height equivalent of a theoretical plate (HETP) at different flowrate.*

1.4 History of chromatographic process development

There is a long history of process chromatography use in protein purification, and this work will focus on the re-design the chromatography column with soft matrix packing. Therefore, it is necessary to introduce the five decades history of process chromatography briefly.

The first development of chromatography was by Russian botanist Tswett at the beginning of the 20th century in the separation of plant pigments (Tswett, 1906). Process chromatography was first applied to the removal of low molecular weight solutes from whey by gel filtration about 50 years ago. Milestones of process chromatography: it can be summarized as from size exclusion chromatography, to Ion-exchange chromatography, then to affinity chromatography.

a) The Nobel Prize in Chemistry 1948 was awarded to Arne Tiselius for his research on electrophoresis and adsorption analysis, especially for his discoveries concerning the complex nature of the serum proteins (Tiselius, 1948). Martin and Synge invented the partition chromatography for the Nobel Prize in Chemistry (1952), "This tool has enabled research workers in chemistry, biology, and medicine to tackle and solve problems which earlier were considered almost hopelessly complicated." (Tiselius, 1952)

b) In 1970s size exclusion chromatography was scaled up for insulin production, which was only used as an analytical method. At the same time, ion exchange also became a viable technology for the same application. Ion exchange was adopted as the industry workhorse as robust resins became available and formed the backbone of chromatographic processing of blood plasma fractionation in alternatives to and extensions of ethanol precipitation (Curting, 2007).

c) The high cost of affinity chromatography restricted it only in the laboratory until the production of mAbs made efficient immunoaffinity indispensable in high purity coagulation factor production in the 1980s. Since then, an powerful toolbox of chromatographic methods has been developed, and a process chromatographic capture–purify–polish regime is now almost popularized. Affinity capture of antibodies on Protein A adsorbents is used throughout the industry with widespread

discussion of affinity versus ion exchange.

Compressible matrix

In 1960s, the low porosity, hydrophobic styrene-divinyl benzene resins were replaced by porous and hydrophilic supports for protein chromatography. Cellulose ion exchangers was developed by Peterson and Sobers in 1956, (Peterson and Sober, 1954) cross-linked dextrans (Sephadex) by Porath and Flodin in 1959,(Porath and Flodin, 1959) and polyacrylamide and agarose by Hjertén (Hjertén, 1961, Hjertén, 1964) in 1961 and 1964 respectively. This was a revolution in protein chromatography.

Scale-up

Before 1970s the chromatographic process scale-up was restricted to the use of rigid gels, such as Sephadex G-25 in stainless steel columns or "Gel Filters," which were developed and introduced in 1968 by Pharmacia Fine Chemicals. The "Stack" or sectional column was developed by Janson (Janson, 1971) to overcome the pressure-flow restrictions of soft gels. At that time, the maximum column dimensions could be achieved was 16 cm bed height by 37 cm diameter, only because this was the largest polypropylene mold size which could be made. These early columns had fixed bed heights and the gel filters could be pump packed, is still predating today's packing methods in these several decades.

Since the 1960's, manufactures of chromatographic resins have developed increasingly robust media for process scale chromatography. They continue to search for improvements in stationary phases to keep pace with the increasing demands of the biotechnology industry for improved product throughput. The development challenge was and still is overcoming mass transfer limitations due to diffusion, in turn limited by residence time, bead porosity, bead size, and matrix morphology in the case of continuous stationary phases.

1.5 Bed compression in chromatographic process

1.5.1 Limitations with compressible materials

Soft material, such as agarose based matrices are widely used in the chromatography column packing (Sofer and Hagel, 1997). With compressible material packing chromatography column, the low throughput is a problem, especially at a large-scale. The reason is that chromatographic process usually operates at a high pressure, the high pressure leads the bed more compress in soft matrix packed column, and then the resistance from the bed cause a the limitation on the flow rate. With such a low flow rate, the productivity is limited. Therefore, new technology should be developed to reduce the bed compression, increase the flow rate, and then improve the productivity. After achieving this, it can be outstanding in biopharmaceutical industry competition. Therefore, chromatography columns need re-designing to overcome this problem. However, due to the high

selectivity property of chromatographic systems, any column re-design may change the bed efficiency. Therefore, the aim of the re-design column should increase the throughput, and keep the column efficiency constant.

1.5.2 Theory of wall effects

With soft matrix packing, larger pressure drops in the column are not sustainable. The ritical flow velocity is the maximum flow velocity in the chromatography column, which is packed with compressible matrix. At the beginning of any increase in pressure, the flow rate increases, and the matrix undergoes compression. When the matrix reaches the highest compression level, the resistance from the matrix will be constant. With now a tight matrix formation, even more pressure is supplied, but the flow remains constant. This flow rate is termed the critical flow rate (U_{crit}). The critical velocity is the critical flow rate divided by the base area. The critical velocity is very important to the chromatographic process with soft matrix packing; the operating flow velocity < 70% of the critical velocity (Sofer and Hagel, 1997). This critical velocity reflects the level of wall support of the column. It can be imaged that keeping bed height constant, with larger column diameter, the support from the column work will be reduced and the matrix will be more compressed. The resistance from the matrix will be raise, and therefore, the critical velocity will be low. On scale-up of a chromatographic system with soft matrix packing, the wall support should be considered.

Chromatographic processes are usually developed at bench scale with columns of diameter (D) less than 0.03m. Current chromatographic scale-up techniques typically involve increasing column diameter to accommodate the increase in process volume, whilst maintaining the bed height and superficial fluid velocity (Stickel and Fotopoulos, 2001). A key-issue in the scale-up for columns packed with compressible materials is that the maximum flow rate through the column is limited by the collapse of the resin due to compressive stresses imposed by the fluid flowing through it. This does not occur with beds packed with incompressible, rigid resins for which the bed volume and permeability remain constant giving rise to linear pressure-flow profiles in which the increasing pressure drop is a result of increasing fluid velocity only. However, many of the chromatography resins available today exhibit compression to varying degrees, particularly the ubiquitous agarose-based resins. Bed packed with such materials exhibit exponential pressure-flow curves start to rise without limit is defined as the critical velocity (u_{crit}) (Stickel and Fotopoulos, 2001) and this places a practical boundary upon the operating flow rates which can be used for any chromatographic system utilizing compressible media (Tran et al., 2007).

While frictional forces at the walls of the column provide a degree of bed support and can allow higher flow rates, the impact of shear wall stresses decreases with increasing column diameter (Keener et al., 2002). A direct consequence of this

'wall support' effect is that the superficial mobile phase velocities developed and used during bench-scale optimization may not necessarily be suitable for large scale operation. Further to this, temperature, viscosity, pH and ionic strength of the mobile phase can also have a dramatic effect on the structural support of compressible resins (Stickel and Fotopoulos, 2001), as well as the packing techniques used (e.g. sedimentation time etc.).

It is shown that the wall support has reflected on the critical velocity, and more wall support can reduce bed compression, and then the critical velocity can increase. With a higher critical velocity, the operating velocity can also increase. If the operating velocity can increase, and provided no deleterious influence on column efficiency, the productivity can increase, and that means more benefit can be gained. Therefore, to increase the operating velocity, more wall support is required. The idea of insert setup in the column is to increase the wall support.

1.5.3 Column inserts

With scale-up, the bed height is always maintained, to accommodate more material, the diameter of the column increase. However, due to the large change in aspect ratio the medium compression level and hydrodynamic pressure drops will increase, because of the loss of wall support (Mohammed et al., 1992; Colby et al., 1996). To increase the level of wall support, an innovative insert system was put in the

chromatography column to increase the wall support, and then the compression level decreases in the packing bed, the resistance from the packing media will reduce, so a higher critical velocity can be expected. With such an insert setup, there will be potentially some other problems. For example, the hydrodynamic flow and the flow distribution will change in the column, and the theoretical plate height of the column will change. (That means the column efficiency will vary) Therefore, there is a need to perform experimental and theoretical work on the re-design columns with insert setup. It is necessary to research the column hydrodynamic performance in Chapter Three. Only base soft matrix packed in the column will be studied. HETP and critical velocity test in the condition with or without insert will be used to show how both of these changes when an insert is used. Then, a mathematical model will be established to describe the pressure-flowrate relationship for a compressible matrix column with or without insert system in Chapter Four.

1.6 Organisation of thesis

The thesis seeks to characterise the effect of column inserts on chromatographic column hydrodynamics. Both experimental and simulation studies are involved to achieve this objective. In Chapter Two, the materials and methods for experiment and mathematics are provided. Chapter Three lists the main experimental data about critical velocity and column efficiency test results on chromatographic columns

packed with various inserts. The mathematical model, which describes chromatography column hydrodynamics is established in Chapter Four, based on Darcy's Law about flow though porous media, and Biot's Theory about compressible material consolidation. It is an empirical model. The best fit coefficient in the equations which describe the packed material properties (Young's modulus, and bed voidage fraction) is found out by an inverse method. The model application is in Chapter Five. This model will be used to predict the pressure-flow, and bed consolidation in chromatographic columns with different column insert. The optimal column insert design, which can lead to the greatest critical velocity increment, will be estimated. Finally, in Chapter Six, the conclusions and recommendations for future work are presented.

Chapter Two: Materials and Methods

The following sections detail the experimental methods and mathematical modeling approaches developed and used in this work.

2.1 Experiments for critical velocity determinations and column efficiency tests

2.1.1 Experimental setup

To study the effect of column inserts on the chromatographic hydrodynamics of packed bed chromatography a range of different compressible matrices were chosen as packing material. Experiments were conducted at lab-scale and pilot-scale where all columns were packed manually. To deal with different column scales, a range of chromatography operating systems were employed. In this section, the chromatography operating system, columns, packing material, and column inserts are introduced.

2.1.1.1 Pump and detector systems

Three different chromatography systems, all supplied by GE Healthcare, (Uppsala, Sweden,) were used to cover the range of column operating specifications. The ÄKTAexplorer™ system was applied for the critical velocity determination in XK 16 columns packed with P6XL, Sepharose™ CL-6B or Sepharose 4B (maximum flowrate 100 mL min^{-1}), and column efficiency tests for XK16 and XK50 columns. The ÄKTAcrossflow™ system was applied for critical velocity determinations in

XK 50 and BPG 100 columns packed with P6XL (maximum flowrate 600 mL min^{-1}). The ÄKTApilot™ system was applied for critical velocity determinations in XK 50 and BPG 100 columns packed with P6XL (maximum flowrate 800 mL min^{-1}), and column efficiency tests for the BPG100 column. These AKTA series systems were controlled by Unicorn Software. The pressure drop, flowrate, UV, and conductivity were record automatically during operation. Additionally, with this software, a method can be written for automatic column operation, including conducting critical velocity and column efficiency tests. The minimum measurement of the pump systems on all the AKTA system is 0.1 bar. To get more accurate pressure measurements, a Digitron 2082P pressure transducer, supplied by Digitron Instrumentation Ltd.(Cambridge, UK), (Range: 0 – 2 bar) was used. It was positioned at the inlet point of the column to measure the pressure drop. It had a sensitivity of 0.001 bar. The pressure was recorded manually for each experimental step. The difference between the repeat experimental results is no more than 2% when using these pumps.

2.1.1.2 Chromatography columns

XK™ 16 (i.d.: 16 mm diameter) and XK™ 50 (i.d.: 50 mm diameter) columns were used for laboratory-scale experiments, whereas a BPG™ 100 (i.d.: 100 mm diameter) was used for pilot-scale experiments. All columns were purchased from GE Healthcare (GE Healthcare, Uppsala, Sweden). Each column allowed for packing to different bed heights with adjustable top adaptors. The limitation of their

operational pressure is 3 bar, and the operational pressure never exceeded 70% of this limitation for safety reasons. The experimental setup is shown in Figure 2.1.

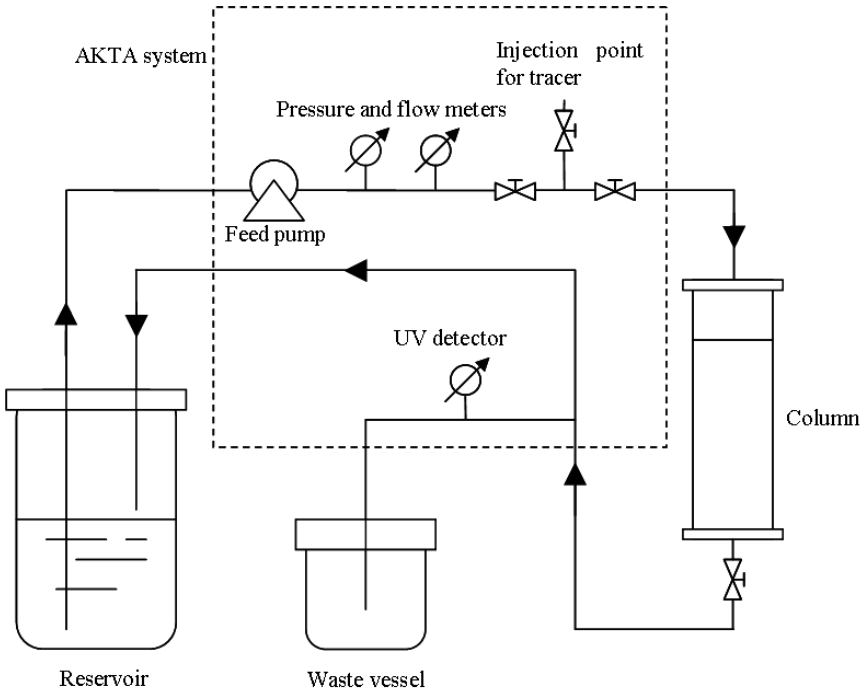

Figure 2.1 *Experimental setup*

2.1.1.3 Packing materials

Sepharose 4B, Sepharose CL-6B (GE Healthcare, Uppsala, Sweden) and Purabead® 6XL (ProMetic Biosciences Ltd, Cambridge, UK) resins were used in these studies. All are agarose-based resins with no ligands attached. The average particle size was in the range of 75-125 μm in all cases. Each resin had a different level of agarose cross-linked structure and hence rigidity. Experiments performed with non cross-linked and cross-linked resins evaluated the effect of resin rigidity on bed compression. Specifically, Sepharose CL-6B and P6XL resin each contain 6% v/v cross-linked agarose to achieve a high level of rigidity. Sepharose 4B

contains 4% v/v agarose, which is not cross-linked, thus it is of lower rigidity than the other two resins. In all experiments, columns were repacked with the same resin before each critical velocity determination. Experiments conducted on column without re-packing showed that the critical velocity reduced after each experiment. The details of the results and discussion will be provided in Chapter three.

The physical properties of the resins, including the Youngs modulus, Poisson ratio, and wall friction coefficient between column and packing material, were calibrated by mathematical modeling, established by employing non-linear curve fitting in Matlab (see section 2.2).

2.1.1.4 Inserts

Table 2.1 Summary of basic materials and experimental conditions

	Diameter (mm)	Pump system		Resin	Insert material
		U_{crit}	A_s & HETP		
XK 16	16	ÄKTAexplorer	ÄKTAexplorer	Sepharose 4B Sepharose CL-6B P6XL	Plastic
XK 50	50	ÄKTAcrossflow ÄKTApilot	ÄKTAexplorer	P6XL	Plastic & Stainless Steel
BPG 100	100	ÄKTAcrossflow ÄKTApilot		P6XL	Stainless Steel

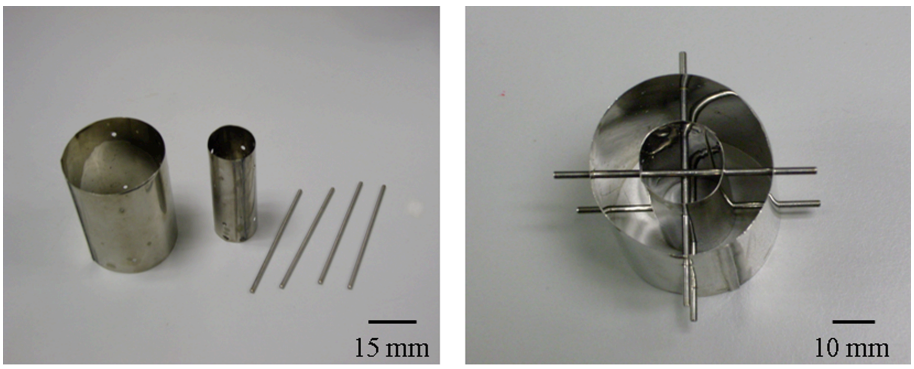

a

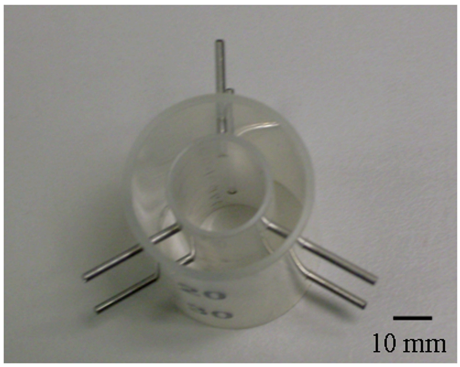

b

Figure 2.2 a *Stainless steel insert configurations. The support bars can be removed to enable single or double inserts to be used. Design for both XK 50 and BPG 100 columns. The inserts diameters were 15 mm and 30 mm, and their length was 45 mm. all supporting bars were 50 mm long. b Plastic insert configuration. The support bar is fixed. The insert size is same as stainless steel inserts.*

All inserts were purpose made and of hollow cylindrical shape constructed of either plastic or stainless steel (Figure 2.2). Inserts were placed concentrically within the columns and their orientation was secured by stainless steel bars (diameter: 1.5 mm) bearing on the column walls to allow precise location of the insert. It was assumed that these bars did not disturb the flow field significantly as their cross sectional area is ~3% of the cross-sectional area of the column. The wall thickness of the

plastic inserts was 1 mm. The wall thickness of the stainless steel inserts was 0.1 mm. Table 2.1 summarises the columns and chromatography systems used and Tables 2.2a+b gives the dimensions of all inserts used. To make it clear in this thesis, 'height' always refers to bed height, and insert height has been present as 'insert length'.

Table 2.2a Plastic and stainless steel insert dimensions (mm)

Column	Diameter	Length
XK 16	8	45
XK 50	16 & 35	45

Table 2.2b Stainless steel insert dimensions (mm)

		Insert diameter					
		15	30	45	60	75	90
	30		√			√	
Insert	45	√	√	√	√	√	√
length	60		√			√	
	75		√			√	
	90	√	√	√	√	√	√

Ticked blocks indicate those inserts fabricated for use either singly or combined.

2.1.2 Column packing procedure

Homogenous slurries of resin (in 20% v/v ethanol) were made to a concentration of 70% v/v gravity settled bed slurry volume and used for column packing. RO water and 100mM sodium chloride was used as the mobile phase and recycled during the

pressure-flow curve and critical velocity determinations. Before column packing, it was necessary to get rid of the air between the filter and mesh on adaptors; otherwise, the air bubbles will affect the flow distribution, and they will affect the column efficiency test results. For bottom mounted inserts the insert was initially placed in the column before packing buffer and the bead slurry was poured into the column. Additionally, there were three packing procedures used, including inserts placed before pouring slurry, inserts placed after that, and inserts placed after pouring slurry with a low upward flow during bed settle. In the Chapter Three, it will show the column efficiency test results on these three packing methods, and discuss the data to determine which packing procedure is better. A measured volume of slurry was poured into the column down the column wall to avoid entrainment of air bubbles. The resin was then gravity settled overnight and the top adaptor was lowered into the supernatant to a point 1 cm above the settled bed. Following this a 10 cm h^{-1} flowrate was applied for 40 minutes in order for the bed height to equilibrate.

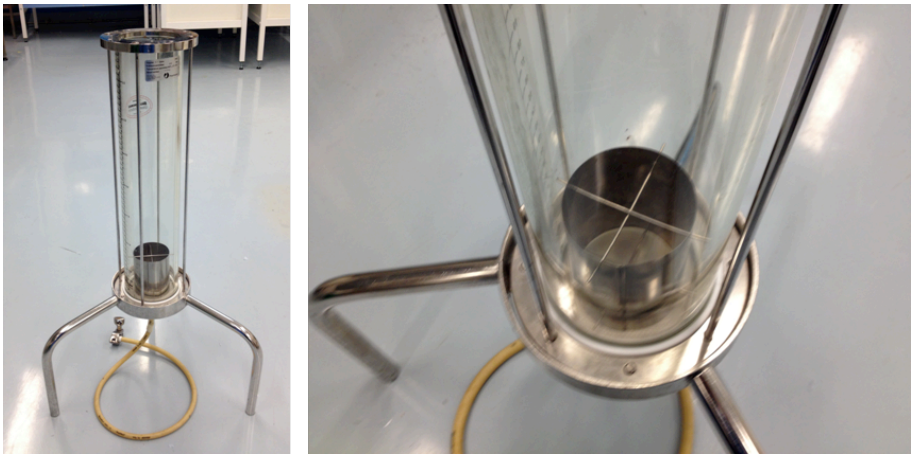

Figure 2.3 *Insert in a BPG 100 column. The insert is constructed of stainless steel, and it is 75 mm in diameter, and 90 mm in length. This column is a 100 mm diameter column.*

2.1.3 Pressure-flowrate curve and critical flow velocity determination

The automatic pressure step method developed by Chang et al. (2012) was applied for critical velocity determination.(Chang et al., 2012) Briefly, a standard proportional-integral (PI) control algorithm was linked to the pressure and flow controller of the pump system. The pressure was increased incrementally from 0.05 MPa in fixed pressure steps (0.02 MPa for the ÄKTAexplorer system and 0.01 MPa for the rest of the systems used). Each step lasted 5 min during which period the system sought to adjust the flow velocity in order to achieve the desired pressure set point. The critical velocity was deemed to have been reached when a change of less than 15 cm h^{-1} in the flow velocity occurred after three consecutive pressure steps. The maximum allowable operational pressure was set at 70% of the column pressure safety limit. To reduce the experimental error, each experiment was repeated in triplicate with the mean results presented with together a standard

deviation.

In the traditional method (Stickel, 2001), the flowrate is the input and is increased in steps. When the pressure drop increases without limited at a certain flowrate step, this flowrate is termed the critical flowrate, Ucrit. If the input flow velocity is close to, or in excess of the real critical velocity, the pressure drop will be equivalent to that at the real critical flowrate. Therefore, it is very difficult to achieve an accurate critical flowrate without prior experience. Moreover, if the input flow velocity is more than the critical velocity, there is a risk of column damage by high pressure. Compared to the traditional flow step method for critical velocity determination, this automatic pressure step can yield more accurate results.

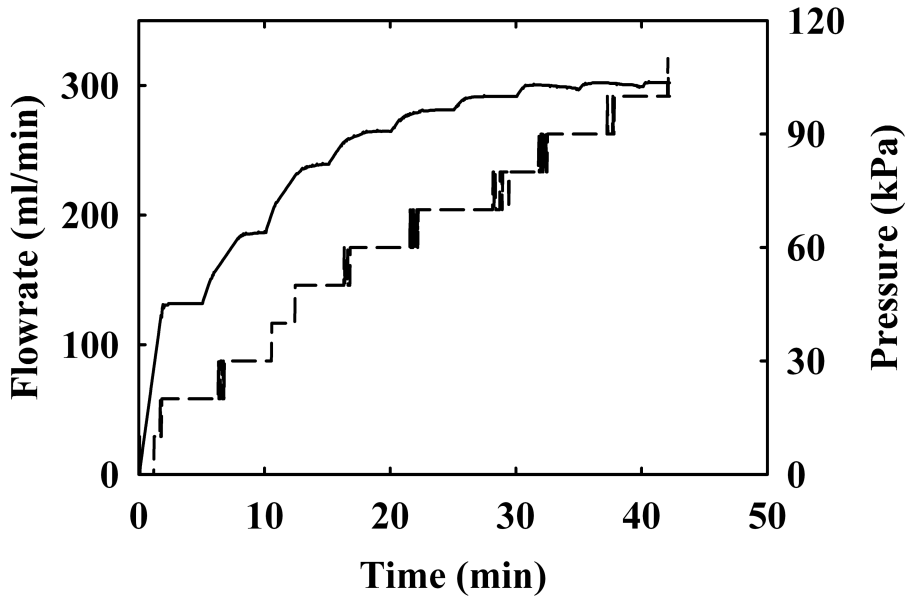

Figure 2.4 *Initial experimental data of automatic pressure step method. The experiment was taken using a BPG 100 column with P6XL at 110±5 mm bed height. The solid line is flowrate, and the dash line is pressure. This is for independent*

critical velocity determination experiment.

In this project, the difference of critical flowrates in a column packed with two types of inserts was sometimes only 2-3%. Such a small difference is hard to locate with the traditional method of U_{crit} determination. Moreover, with the control of flowrate, the pressure increases very fast when the flowrate is close to the critical value. There is hence a potential risk of exceeding the safe pressure of the column which is always relatively low (The safety pressure of XK 16, XK50, and BPG100 column is 3 bar). In the automatic pressure step method, the pressure was controlled and hence the risk of generating a high pressure was avoided by ensuring the pressure steps were always well below the safety pressure limit.

2.1.4 Column efficiency determination

The number of theoretical plates and asymmetry factor for all columns were calculated by running a 1% CV pulse of 1% v/v acetone. The flowrate used for the XK 16, XK 50 and BPG100 columns were 2 mL min^{-1}, 20 mL min^{-1} and 80 mL min^{-1} respectively. In each case, this is about 20-30% of the critical flowrate. The absorbance of the tracer pulse leaving the column was detected at 280 nm. The equations to calculate plate number and asymmetry factor are given below(Martin and Synge, 1941; Foley and Dorsey, 1983):

$$N = 5.54 \frac{t_R^{\ 2}}{W_{1/2}^{\ 2}} \tag{2.1}$$

where N is the number of theoretical plates, t_R is the retention time of the probe

molecule and $W_{1/2}$ is the width of the peak at one half the maximum height.

$$A_s = \frac{b}{a} \tag{2.2}$$

where A_s is the asymmetry factor, a is the distance from the leading edge of the peak to the midpoint of the peak and b is the distance from the midpoint of the peak to the trailing edge. A_s was determined at 10 % of the maximum peak height. These calculations were completed using the Unicorn 5.0 software, supplied by GE Healthcare, Uppsala, Sweden. To reduce the experimental error, each experiment was repeated in triplicate, and the mean result presented with standard deviation data.

2.2 Mathematical simulation

The creation of a mathematical model was essential for this work. Whilst the experiments conducted can lead us to understand the phenomenon and which column inserts affect chromatographic process operation, a mathematics model allows us to research the theory of chromatography bed consolidation by inserts. In this section, the method of model establishment for chromatography bed compression is set out. It involves use of the finite element and the inverse methods.

2.2.1 Model of solid mechanics established with Comsol Multiphysics

Comsol Multiphysics (Comsol Ltd., Hatfield, UK) was applied to simulate the prevailing hydrodynamics in the chromatography columns. Comsol Multiphysics is a finite element analysis, solver and simulation software for various physics and

engineering applications, especially coupled phenomena, or multiphysics. It is based on the finite element method which it uses to solve the differential equation, such as the pressure drop, superficial flow velocity, and porosity distribution in the chromatography column in this case. (The finite element method will be described later.) The column is rotationally symmetric due to its cylindrical shape; therefore the dimensional type of this model can be 2D-symmetry. To simulate the hydrodynamic flow in a chromatography column, flow through the porous media was based on Darcy's law. A solid mechanics model was employed and coupled to the hydrodynamic component. The initial estimates for these parameters were from some published papers. For Young modulus of 6% agarose gels, it is 120 kPa (Chen et al., 2003). The Poisson ratio is 0.26, and the wall friction coefficient between packing material and column wall is 0.16.(Keener et al., 2004; McCue et al., 2007) The equations which describe the pressure drop, flow velocity, porosity, and Young modulus were also input. The detail of the equations will be discussed later. Figure 2.5 shows the steps of model formulation.

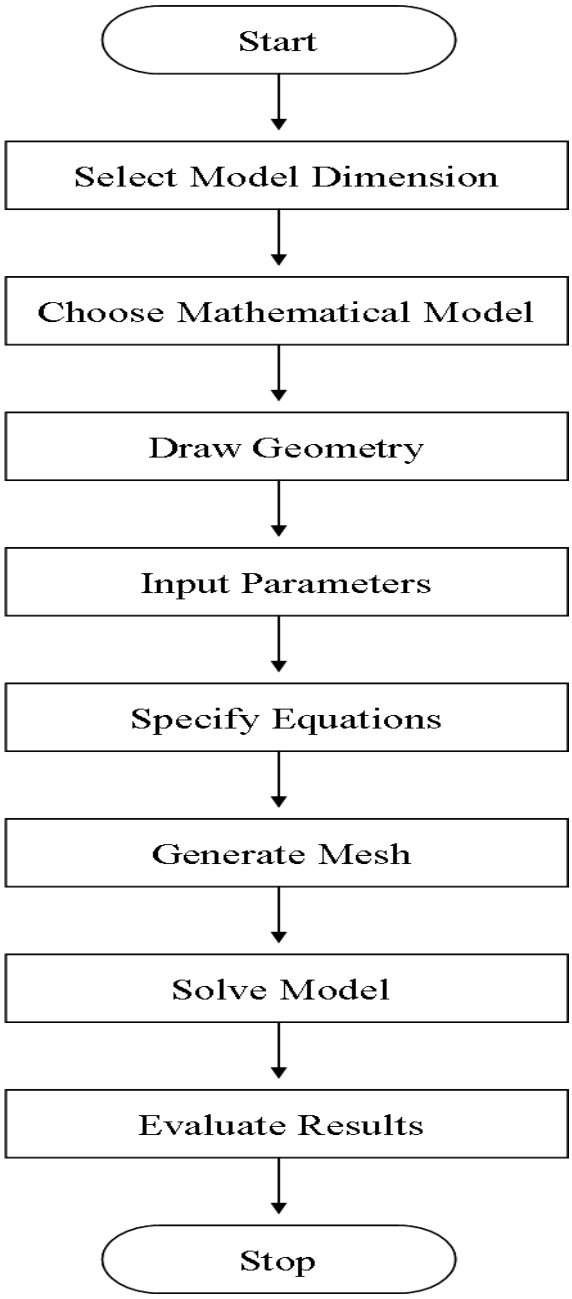

Figure 2.5 *Flowchart for model formulation in Comsol Multiphysics. In the first step the 2D-asymmetry was selected to deal with the cylindrical column. Secondly, the mathematical model describing the flow in chromatography column was chosen. Thirdly, the geometry was drawn. In the fourth step, the parameters were input. Next, the equations need to be specified in the model domain. Then, the mesh was generated, and the model solved. Finally, the results were evaluated and exported.*

2.2.2 The finite element method

Most phenomenon in nature such as sound, heat, electrostatics, electrodynamics, fluid flow, or elasticity can be described with the aid of the Laws of Physics, in term of partial differential equations relating various quantities of interest.(Reddy, 1993) Their solution by exact methods is often impossible because of the complicated geometry or complex function involved. Therefore, approximate methods of analysis are employed.

The finite element method is a numerical technique for finding approximate solutions to partial differential equations and their systems. The finite element method originated from the need for solving complex elasticity and structural analysis problems in civil and aeronautical engineering. Its development can be traced back to the work by Alexander Hrennikoff (1941) and Richard Courant (1942) (Pelosi, 2007).

The finite method is a technique where a given domain is divided into subdomains. Each subdomain is called an element and their union is called a finite element mesh. It is a uniform mesh, where all elements (length/area/volume) are same; otherwise it is a non-uniform mesh. The points where the elements are connected to each other are called nodes. The dimension of the elements depends on the dimension of the problem to be solved. In one-dimensional problems, the element is a line segment. In two-dimensional problems, the element is a triangle. In three-dimensional

problems, the element is a tetrahedron (Gerontas et al., 2010; Reddy, 1993).

After the whole has been divided into parts, the functions which approximate the solution are developed over each of the elements. The algebraic relations among the nodal values of the solution over each part are derived, and then an assembly of the element equations and a solution for the whole domain results (Reddy, 1993).

2.2.3 Inverse method

The inverse method was used to evaluate the parameters, including the Young's modulus of the resin, the wall friction coefficient and the permeability constant. This inverse problem was implemented in 5 steps using Comsol Multiphysics wrapped around Matlab^{TM} (The MathWorks Inc., Natick, USA). The flowchart for this is given in Figure 2.6. Firstly, the Comsol model was developed in Comsol's graphical user interface using arbitrary values for the parameters of interest. It was then saved as a Matlab file. In this form the file can run in Matlab's graphical user interface without the option to alter the values of the parameters of interest and to calibrate the model with experimental data. This was achieved by editing the file as a Matlab function, so as to treat the system of differential equations of the model as a functional representation between the parameters of interest which are the input and the sum of squared residuals (a residual is defined as the difference between the experimental and the fitted value) which is the output. This Matlab function was

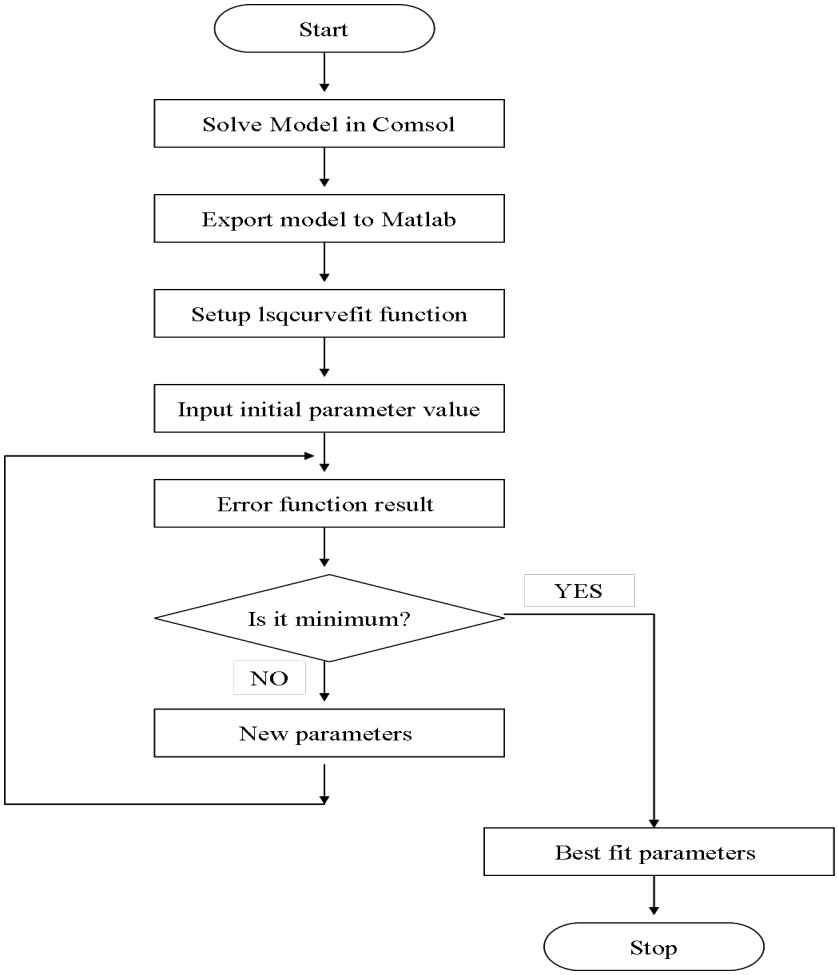

Figure 2.6 *Flowchart for evaluating parameters in hydrodynamic equation (Young's modulus as a function of packing material deformation, and permeability as a function of bed voidage) by using inverse method in Comsol Multiphysics and Matlab. There are 5 steps involved. In the first step, the model was solved in Comsol Multiphysics. In the second step, the model was saved as a Mablab file. In the third step, the model function was created, which is the sum of square of different between simulation and experiment result. In the fourth step, the reasonable initial guess and range of parameters were input. At last, Matlab calculated the error results for each parameter and found to best-fit parameter values which are minimizing the error function.*

referred to as the forward model function. Its role used to help Matlab recognise, which parameters of the Comsol model need to be estimated. Then, the nonlinear least-squares Matlab function “lsqcurvefit” (default settings) was used to minimise the forward model function. This was achieved by solving the nonlinear data-fitting problems using the Levenberg-Marquardt algorithm, and searching for optimal parameter values within the range imposed by the upper and lower bounds of these parameters. Using it without setting bounds could lead to results with no physical meaning. The parameter values were estimated in 4 h CPU times on an Intel Hexa-Core Pentium Xeon 5680/3.33 GHz processor with 96 Gb memory. Both cores were under load during simulation and 48 Gb out of 96 Gb memory were allocated for Comsol Multiphysics.

2.3 Statistical analysis

Experimental works were conducted to seek the effect of column inserts on critical velocity and column efficiency change. The experimental data included critical velocity and plate number of chromatographic column with different dimensional column inserts. To validate the experimental data, triplicate experiments were taken for each independent experiment. To claim the significant difference between these groups, a two sample t-test in Minitab 15 (Lead Technologies Inc.) software was applied. For example, to compare the theoretical plate number when two different kinds of column insert were present, the experimental data were input to Minitab,

and a two sample t-test then run. If the P value is < 0.005, it can be claimed that there is significant change of theoretical plate number with columns having these two kinds of inserts (Schiff and Agostina, 1996).

Chapter Three: System Characterisation

3.1 Introduction

In this chapter, the critical velocity determination and column efficiency experimental results carried out on columns having different types of inserts, from lab-scale to pilot scale are reported. Some empirical equations are specified to describe the critical velocity change versus insert dimension. The majority work in this chapter is devoted to showing the phenomenon by which the inserts affect the column hydrodynamics, and presents some discussions of this. The development and application of a theoretical simulation will be given in the next two chapters.

Chromatography is widely used in the purification of proteins, contributing significantly to the cost of the overall downstream process. Normally, the development of chromatographic processes is from laboratory columns with diameters less than 30 mm, and then goes to pilot scale and large scale. Scale-up is conventionally conducted by increasing the column diameter to accommodate more packing material, keeping the bed height and superficial velocity constant. However, on scale-up, this can result in an increased hydrodynamic pressure drop due to loss of wall support. The majority of commercially available chromatography media are compressible, such as agarose base matrices (Stickel and Fotopoulos, 2001; Sofer and Hage, 1997; Tran et al., 2007; McCue et al., 2007), and the pressure drop can become very large. Over time, the chromatography bed will be over-compressed

and the performance of the column will deteriorate. As a result, in large scale manufacturing, chromatography columns have to be repacked periodically. Therefore, for chromatographic process scale-up, it is necessary to study the effect of wall support on bed compressibility. In a chromatographic process, the mobile phase viscosity is always higher than the viscosity of water, which is used for model development. However, there is a linear relationship between viscosity and other parameters, such as pressure, permeability, and flowrate, therefore, when viscosity changes, the model is still applicable.

The superficial critical velocity is an indirect measure of column compressibility. The superficial critical velocity defined as the maximum flow velocity the column can achieve before the pressure starts to rise without limit.(Keener et al., 2002; Keener et al., 2004; Östergren et al., 1998) For a given column geometry a high critical velocity means that the resin is less compressible and the bed height is not reduced significantly over a wide range of operating flowrates. Therefore, the column can operate at high flow rates, potentially resulting in high levels of productivity. However, for commercially available agarose based chromatography column packing material, due to its soft property, the critical velocity is relatively low and the creates a limit on the process throughput that can be achieved.

Wall support is one of key parameters which affect the critical velocity. It derives from the frictional forces acting at the column walls and is affected by the aspect

ratio (diameter/length) of the packed bed.(Colby et al., 1996; Soriano et al., 1997; Parker et al., 1987) The frictional force acts the opposite direction of pressure drop, and slow down the displacement of the chromatography bed, and then lead to higher bed porosity even at high flowrate. This will enable the mobile phase to flow more easily though the column, and a corresponding large critical velocity. The impact of this force is negligible when the aspect ratio of the packed bed is above 2 which means that for most production columns wall support is minimal.(Stickel and Fotopoulos, 2001) In this study, column inserts were design and placed in chromatography column packed with compressible material to gain extra wall support, and then lead to a higher critical velocity.

In this chapter the ability of cylindrical inserts, of negligible wall thickness, to increase the critical velocity without significantly affecting column efficiency was studied. The idea of using inserts is primarily focused on providing a greater operating range for more traditional, compressible beads and hence to extend the hydraulic capability of existing equipment. The inserts were made from cylinders constructed of plastic or stainless steel, rest on the bottom of the column and mounted concentrically. The column inserts were constructed of stainless steel (grade is 316), and plastic (polyethylene) each of which are stable to CIP chemical such as 1 M NaOH. Recognizing, however, that the introduction of any elements within the packed structure may disturb the even flow distribution through the column, we also assessed the impact of the inclusion of inserts on column

efficiency as measured by the theoretical plate number and the degree of peak asymmetry for a non-retained tracer molecule.

3.2 Impact of column insert on critical velocity

In this chapter, an experimental approach was investigated to characterise the effect of column insert design and position on column compression and the impact on column efficiency. The position of the insert(s) in the column, their diameter, their material of construction, the aspect ratio of the column supported by inserts and the resin rigidity were examined independently and in concert.

3.2.1 Effect of experimental runs on critical velocity

To determine experimentally the accurate critical velocity of a chromatography column, repeat tests are necessary. In Chapter Two, it has mentioned that the column needs to be repacked according to the column packing procedure before each test. At the beginning of this project, a series of repeat experiments were taken hourly without column repacking. The results for each run are given in Figure 3.1. The critical velocity keeps decreasing after each run. The reason is that the deformation of the packing material is irreversible after the high pressure operating. The change in apparent critical velocity after each run means that such data can not be used as accurate values of the actual critical velocity. Based on these data it was decided that column repacking was necessary after each run. The solid line in

Figure 3.1 shows the critical velocity test results obtained for columns which had been repacked each time. The difference between runs at a given condition is in 1%, and the average of results can be claimed to be an accurate values of the actual critical velocity. All the critical velocity test results presented in this work were hence columns repacked before each determination. No statistical analysis of the data in Fig 3.1 was presented, because each point represents just one critical velocity test result.

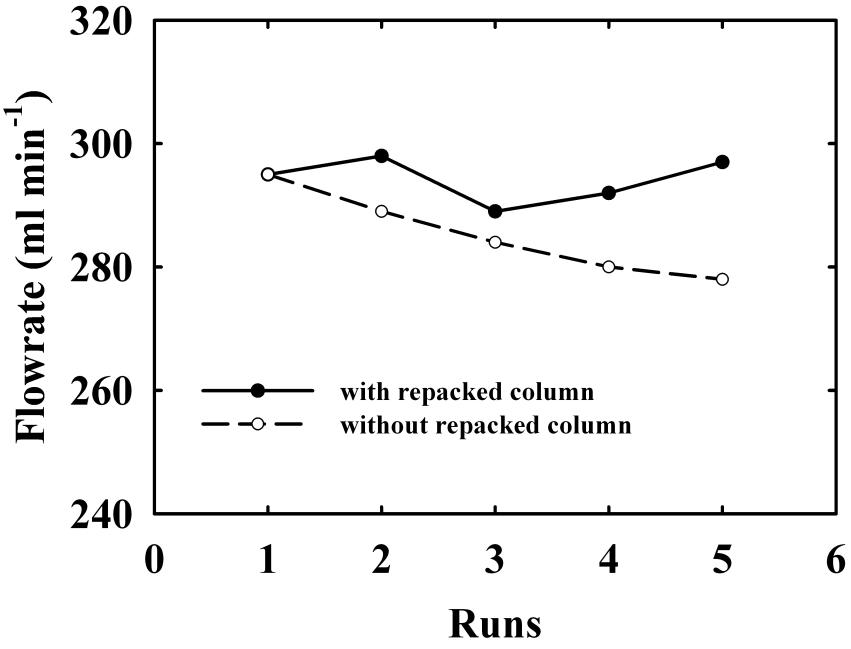

Figure 3.1 *The experimental critical velocity results for different runs. The experiments used a BPG 100 column packed with P6XL to 110±5 mm in height. The solid points and hollow points represent the critical flowrate result with and without column repacking respectively. For non-repacked column experiments, a one hour period for bed expansion was allowed for between determination of critical velocity.*

3.2.2 Effect of insert position on critical velocity

The impact of insert position on the critical velocity was tested in a lab-scale column. The three positions examined were top, middle and bottom in an XK 16 column packed with Sepharose CL-6B (see Figure 3.2). The standard operating procedure for column packing was followed using a single insert 9 mm in diameter and 45 mm in length (The bottom of insert was positioned as follows: TOP, 55 mm from column base; MIDDLE, 27.5 mm from column base; and, BOTTOM, resting on column base as shown in Figure 3.2). Figure 3.3 shows that there was a considerable change in critical velocity when the insert was placed at the bottom of the column. This was expected as the axial stress in the bottom region of the column is greatest and consequently this leads to more bed compression.(Yuan et al., 1999) Hence an insert placed at the base of the column exerts the greatest impact.

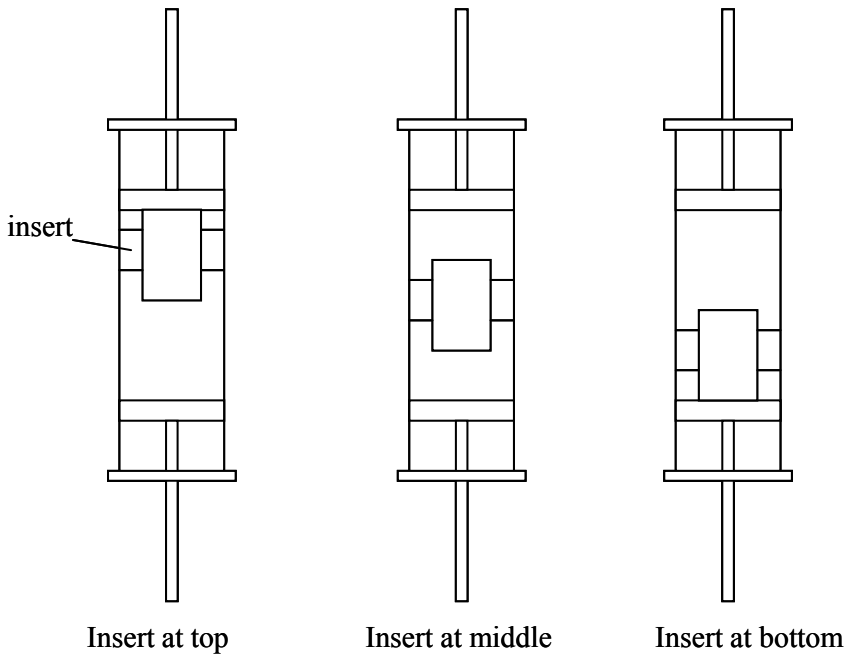

Figure 3.2 *Inserts at different column positions. All use an XK 16 column packed with Sepharose 6b-CL material at 100±5 mm bed height. Insert (9 mm in diameter and 45 mm in length) constructed of plastic and placed at three different positions: top (55 mm from column base), middle (27.5 mm from column base), and bottom (resting on column base) of bed prior to determination of the critical velocity.*

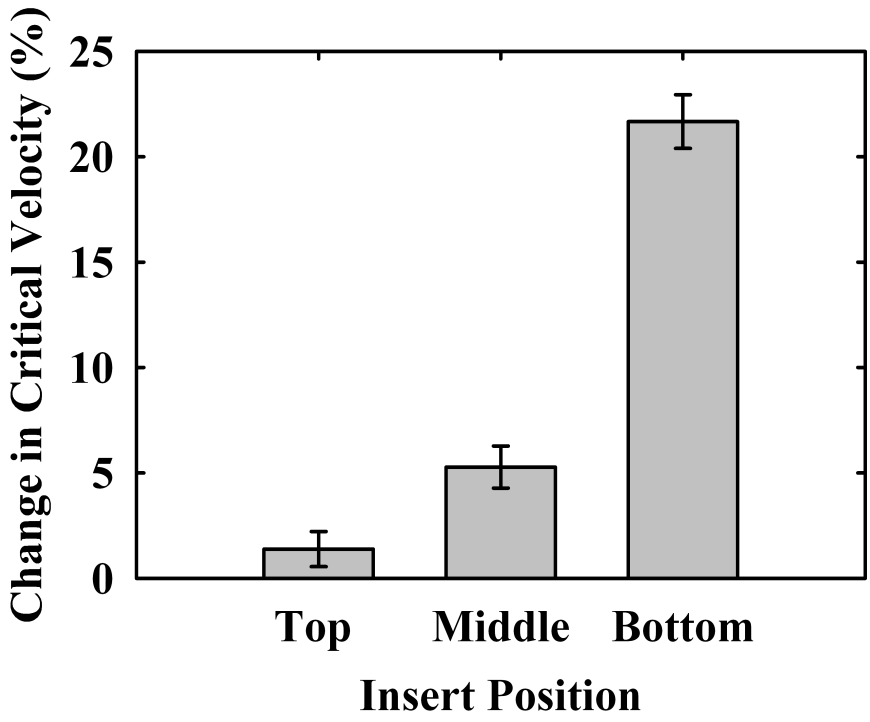

Figure 3.3 *Effect of insert position on critical velocity of XK 16 column packed with Sepharose CL-6B to a bed height of 100±5 mm. Critical velocity without insert; 360 cm* h^{-1}*. Data points are mean±SD from 3 independent experiments.*

Logically when placing an insert in either the middle or top part of the column this results in the less compressed regions of the bed not being supported, thus failing to reduce the compression effect so significantly. The results in Figure 2 support this.

A 20% increase in critical velocity was seen for the best case and provided the impetus for further studies, all of which were based upon placing inserts at the base of the column. In this thesis, SD refers to one standard deviation.

3.2.3 Effects of insert length on critical velocity

Having determined the best location for the positioning of an insert, Figure 3.4 shows the effect of insert length on the critical velocity for a fixed column insert and resin combination. For the combinations studied a linear relationship between the increase in critical velocity and insert length presumably as a result of providing more wall support to the bed structure was developed:

$$\frac{\Delta u_{crit}}{u_{crit0}} = \alpha L_{insert} \tag{3.1}$$

where Δu_{crit} is the change in critical velocity, u_{crit0} is the critical velocity in a column without insert(s), cm h^{-1}, L_{insert} is the insert length, mm, and α is the constant of coefficient. In this case for BPG 100 column packed with P6XL having single insert system, α =0.08.

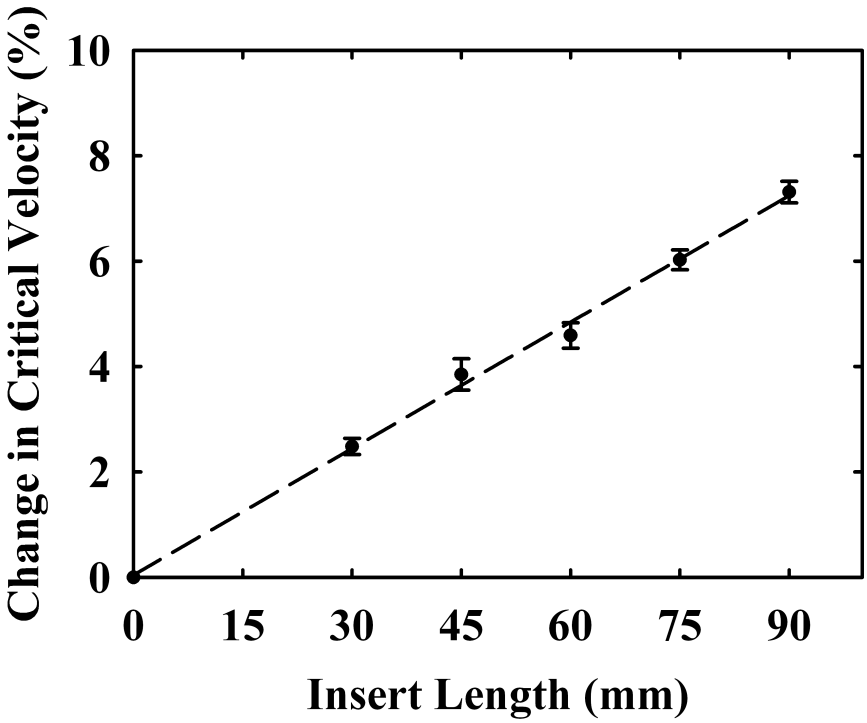

Figure 3.4 *Effect of insert length on critical velocity of BPG 100 column packed with P6XL resin to a bed height of 100±5 mm. Critical velocity without insert; 219cm* h^{-1}*. Insert constructed of stainless steel. Insert lengths (mm): 30, 45, 60, 75 and 90, and insert diameter: 30 mm. Data points are mean±SD from 3 independent experiments. Line shows best fit to the linear equation:* $\frac{\Delta u_{crit}}{u_{crit0}} = 0.08 \times L_{insert}$*,* R^2*=0.98*

Further analysis of the results in Figure 3.4 shows that the axial stress at bottom is greatest in a chromatography column packed with compressible material. It can be noticed that the increment of critical velocity with 30mm, 45 mm length insert is about 2.5%, 4% and it with 60 mm, 90 mm length insert is 4.5%, 7.5%. When the length of the insert doubled, the increment of critical velocity was less than double. It can be consider as evidence to claim that the bottom of insert makes more impact

on critical velocity increment due to the more stress distribution at bottom of the packed bed. There will be a simulation study to model the axial-stress profile in a chromatography column in Chapter Five.

However, there is a practical limit to the length of the insert used. If the insert length becomes comparable to the length of the packed length of the column, there will be only a small space within which the top adaptor may move and consequently for the column to be compressed. This may limit process productivity as the column may have to operate at relatively low linear velocities so as to avoid extensive resin compression. In this study, the maximum insert length was restricted to be no more than 90% of the flow packed bed height.

3.2.4 Effect of single insert diameter on critical velocity

Figure 3.5 shows the effect of insert diameter on the critical velocity for a fixed column/resin combination. The following empirical equation was used to express the increase of critical velocity as a function of the ratio of insert to column diameter:

$$\frac{\Delta u_{crit}}{u_{crit0}} = \alpha\left(\frac{D_{insert}}{D_{bed}}\right)^3 + \beta\left(\frac{D_{insert}}{D_{bed}}\right)^2 + \delta\left(\frac{D_{insert}}{D_{bed}}\right) \quad (3.2)$$

where Δu_{crit} is change in critical velocity, u_{crit0} is the critical velocity in column without insert(s), D_{insert} is the insert diameter and D_{bed} is the column diameter. α,

β, and δ are empirical constants. In this case for BPG 100 column packed with P6XL having single insert system, their values are -17.5, 13.7, and 11.4 respectively. The equation 3.2 was developed as a secondary polynomial equation because of its ability to fit the experimental data. The error between the result from equation and experiment was approximately 5%.

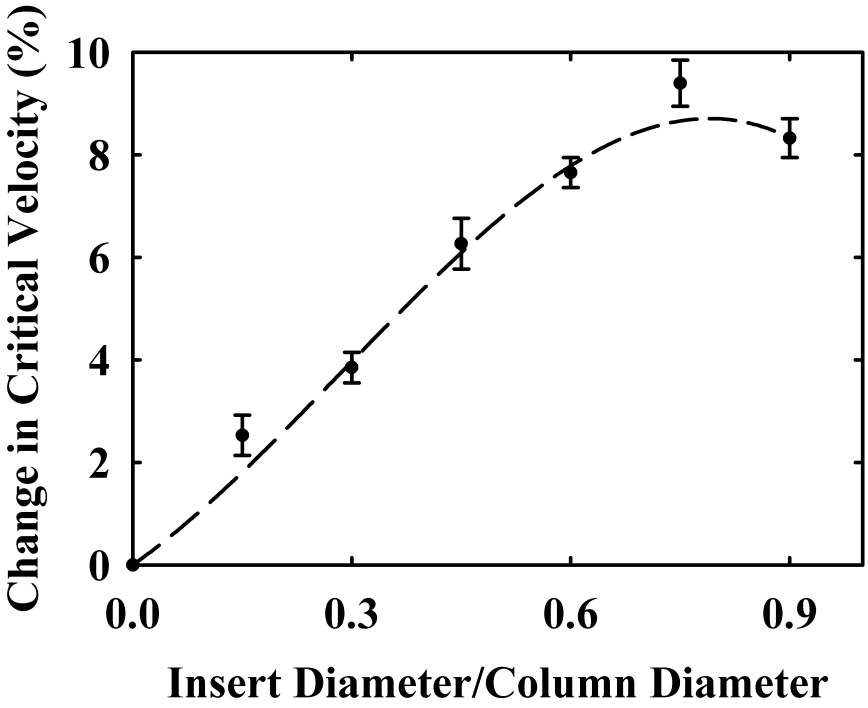

Figure 3.5 *Effect of insert diameter on critical velocity of BPG 100 column packed with P6XL resin to a bed height of 100±5 mm. Critical velocity without insert; 219 cm* h^{-1}*. Inserts constructed of stainless steel. Inserts all had a length of 45 mm. Data points are mean±SD from 3 independent experiments. Line shows fit to polynomial equation:* $\frac{\Delta u_{crit}}{u_{crit0}} = -17.5 \times \left(\frac{D_{insert}}{D_{bed}}\right)^3 + 13.7 \times \left(\frac{D_{insert}}{D_{bed}}\right)^2 + 11.4 \times \left(\frac{D_{insert}}{D_{bed}}\right)$.

Inspection of Figure 3.5 indicates that the increment of critical velocity keeps

increasing with larger diameter inserts from 15 mm to 75 mm. At an insert diameter of 75% of column diameter, the critical velocity change is maximised. After this dimension, the increment reduces. It can be explained that a larger column insert provides increasing levels of wall support up to the threshold diameter and lead to higher critical velocity increment. Beyond this only the small amount of resin contained in the annulus between the column wall and the insert gains effective support. By contrast, the inner part of the resin cannot be supported well. The aggregate effect is to cause the overall critical velocity to decrease for inserts >75% column diameter.

Some prediction can be made from the experimental result. The cross-sectional area of the inner column and annulus (when using one insert) are equal when $D_{insert}/D_{column} = 1/\sqrt{2} = 0.71$. This is quite close to the experimentally observed maximum at about $D_{insert}/D_{column} = 0.75$. Subsequent work will use these data to verify a structural mechanics model developed to optimize the insert dimensions so as to obtain the highest critical velocity (see Chapter Five).

3.2.5 Effect of insert number on critical velocity

The change in critical velocity when the column was supported by multiple inserts is explored in Figure 3.6. It can be seen that additional inserts serve to increase the critical velocity as more wall support is provided. However, there is a limit to this benefit with the incremental improvement in critical velocity reducing as the

number of concentric inserts used increases. From the experimental results, the critical velocity did not increase significantly from column packed with double inserts to triple inserts. This may be explained by the reducing annular volumes of resin affected as the number of inserts rises and hence an asymptotic relationship between the level of improvement seen and the number of inserts used. This trend needs to be explored further for manufacturing scales of operation but was beyond the experimental capabilities to hand. Clearly there will also be a practicable limit to the complexity of the concentric insert arrangements deployed. Additionally, the more column inserts are used, the greater the likely dispersion. This will be explained later in the column efficiency test result of this chapter.

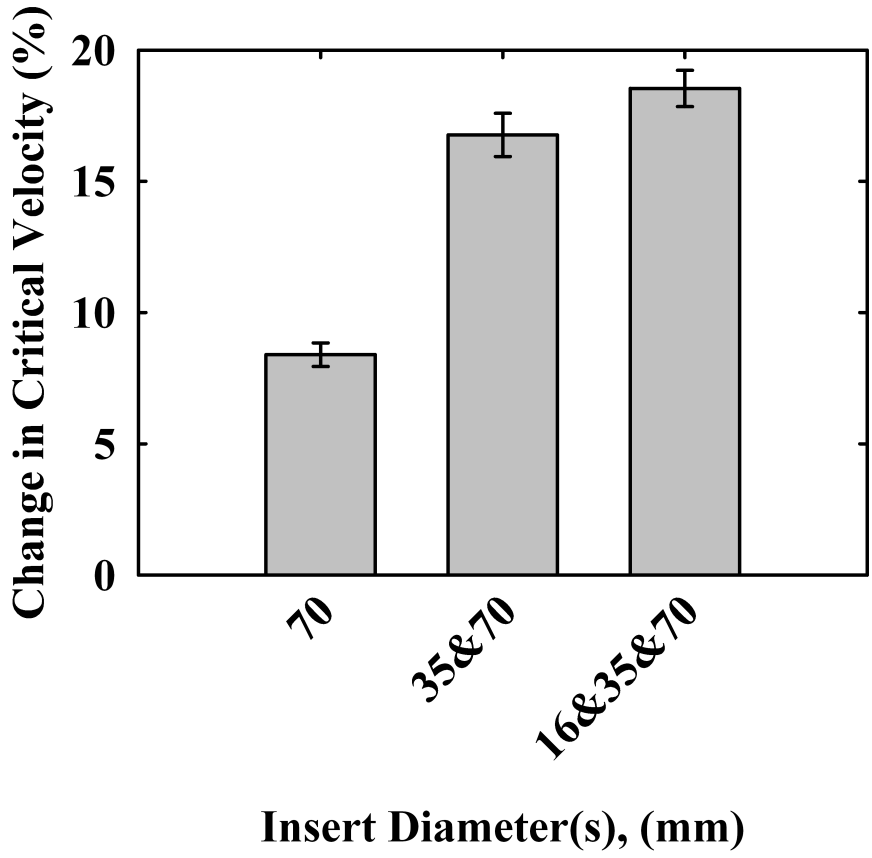

Figure 3.6 *Effect of insert configuration on critical velocity of BPG 100 column*

packed with P6XL resin to a bed height of 100±5 mm. Critical velocity without insert; 219 cm h^{-1}. Inserts were constructed of stainless steel, length 45 mm. Data points are mean±SD from 3 independent experiments.

3.2.6 Effect of column aspect ratio on the critical velocity

From section 3.2.2 to 3.2.5, the role of insert position, length, diameter, and number affecting on the critical velocity in fixed chromatography columns with the same packing material have been assessed. In this section, the critical velocity change with column insert in different scale columns is studied. To make the results in different columns comparable, the column insert diameter/column diameter is constant.

Figure 3.6 shows how the critical velocity changes with an increase in the diameter of the column, while keeping the column / insert aspect ratio constant. The changes in critical velocity for the XK 50 and BPG 100 with an insert 70% of the column diameter were 6% and 8.5% respectively. The greater level of improvement achieved for the larger diameter column is consistent with the relatively low level of wall support offered in the original column before addition of an insert.

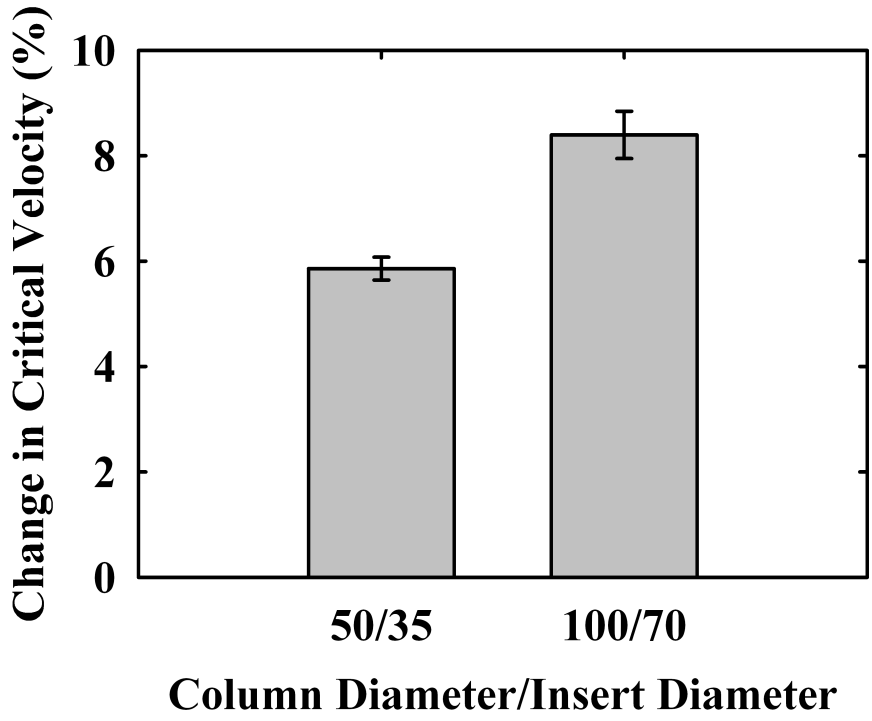

Figure 3.7 *Effect of scale on critical velocity change. Constant ratio of insert to column diameter packed with P6XL resin to a bed height of 100±5 mm. Inserts constructed of stainless steel. All inserts were 45 mm in length. Insert diameter was 35 mm (XK 50 columns) or 70 mm (BPG 100 columns). The ratio of insert to column diameter was 10:7. Critical velocity without insert; 234 cm* h^{-1} *(XK 50 column) and 219 cm* h^{-1} *(BPG 100 column). Data points are mean±SD from 3 independent experiments.*

3.2.7 Effect of resin type on critical velocity.

Figure 3.8 shows the effect of the rigidity of the resin on the critical velocity in columns containing inserts. As expected, columns packed with soft resins e.g. Sepharose 4B showed the greatest level of improvement. All resin types, irrespective of rigidity, were capable of withstanding greater process velocities

before the onset of compression when inserts were included. Experimental data show for example that when a column was packed with the soft Sepharose 4B resin with inserts, this combination could operate at a higher critical velocity than a normal column packed with a more rigid resin such as P6XL. Inserts can hence allow columns to operate with more compressible material but at flow rates normally associated with operation of columns packed with rigid material.

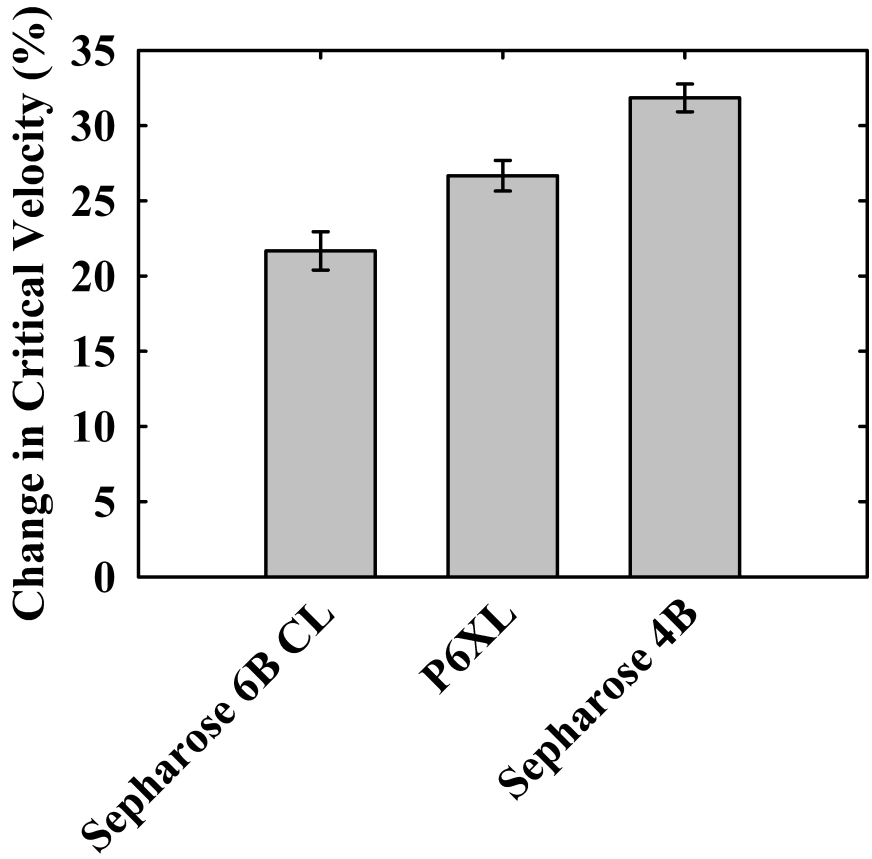

Figure 3.8 *Effect of resin type on critical velocity in a XK 16 column with a bed height of 100±5 mm. Inserts constructed of stainless steel. Critical velocity without insert; Sepharose CL-6B resin 360 cm/h; P6XL resin 234 cm/h; Sepharose 4B 200 cm* h^{-1}*. Data points are mean±SD from 3 independent experiments.*

3.3 Impact of insert on column efficiency

In section 3.2, the impact of column inserts was seem as positive, because it can increase the critical velocity, and hence increases the operating flowrate range. However, column inserts will potentially also affect the dispersion and resolution of packed bed by creating additional obstructions in the flow path. In this section, the experimental results demonstrating how column inserts affect column efficiency as measured by the column theoretical plate number and the asymmetry of an inert tracer with be presented.

3.3.1 Effect of packing procedure on experimental result

The column inserts were designed for specifically chromatographic processes. The column packing procedure is an important element in determining overall column efficiency and hence the influence of packing method with and without inserts was studied first.

In this section, HETP and asymmetry test results were collected and are presented in Table 3.1. Three different packing procedures were applied for comparison. The first one (1) is where column inserts were placed within the column before pouring of the slurry. In the procedure second (2) column inserts were placed in the columns after pouring of the slurry. The third variant (3) compression placing column insert after pouring of the slurry and under a low flow upwards from the bottom adapter

before allowing the bed to settle. The purpose of choosing these three different packing procedures was to find out which one can lead to the most homogenous and consistent packed bed as assessed by a higher theoretical plate number and an asymmetry value approaching 1.

Comparing the outcomes of the different packing procedures 1 and 2 in Table 3.1, it is clear that a higher theoretical plate number was achieved when column inserts were placed in the column before packing first. That means a more homogenous bed can be gained in this way. Comparing the results of packing procedures 1 and 3 in Table 3.1, there was no significant change on the theoretical plate number and asymmetry. It was thought that the composition of a period of upward flow input achieve a more homogenous bed, but the benefit, if any is not very obvious. Therefore, the packing procedure for all the other column efficiency experiments reported in the later section of this thesis employed the first packing method in which inserts were placed with the empty column before pouring of the slurry to form a packed bed.

Table 3.1 Theoretical plate number and asymmetry with different packing procedure

Insert diameters	Method	Mean N (m^{-1})	σ of N	Mean A_s(-)	σ of A_s
16mm	1	3381	60.91	1.25	0.025
	2	3021	112.32	1.23	0.024
	3	3385	30.45	1.24	0.022
35mm	1	3336	15.30	1.10	0.020
	2	3123	153.3	1.15	0.025
	3	3330	58.40	1.13	0.018
16mm & 35mm	1	2916	87.89	1.05	0.021
	2	2543	146.71	1.11	0.022
	3	2908	55.75	1.02	0.025

1: column inserts placed before pouring slurry.

2: column inserts placed after pouring slurry.

3: column insert placed after pouring slurry, a low flow upwards from bottom adapter before bed settle.

The column efficiency test experiments reported in Table 3.1 were all for an XK 50 column packed with P6XL resin to a bed height of 120±5 mm. All inserts were 45 mm in length. The mean theoretical plate number and asymmetry and the standard deviation was for three independent experiments.

3.3.2 Effect of insert type

In section 3.2, the experimental data was presented about critical velocity change with column inserts. In this section, it would introduce the experimental results about how column inserts affect on column efficiency. Figure 3.9 shows the column exit absorbance-time distribution curves for non-retained tracer for a single column geometry containing different types of inserts. The consequence of adding an insert is in all cases to broaden the residence time distribution of the tracer, most especially by the creation of a trailing peak. This increase in peak area will result in slightly larger elution volumes, thus increasing the loading volume of the next process step by dilution of the product stream. These data were analyzed further in Figures 3.9b and 3.9c showing a reduction in the theoretical plate number and in the level of asymmetry as inserts were introduced. The behavior can be explained by the fact that the bed void fraction will be high close to the walls of the column and of the inserts where the tracer will flow faster. This additional level of dispersion of the tracer will tend to reduce the theoretical plate number of the column. Because the column inserts could reduce the extent of bed compression, and lead to a higher voidage fraction.

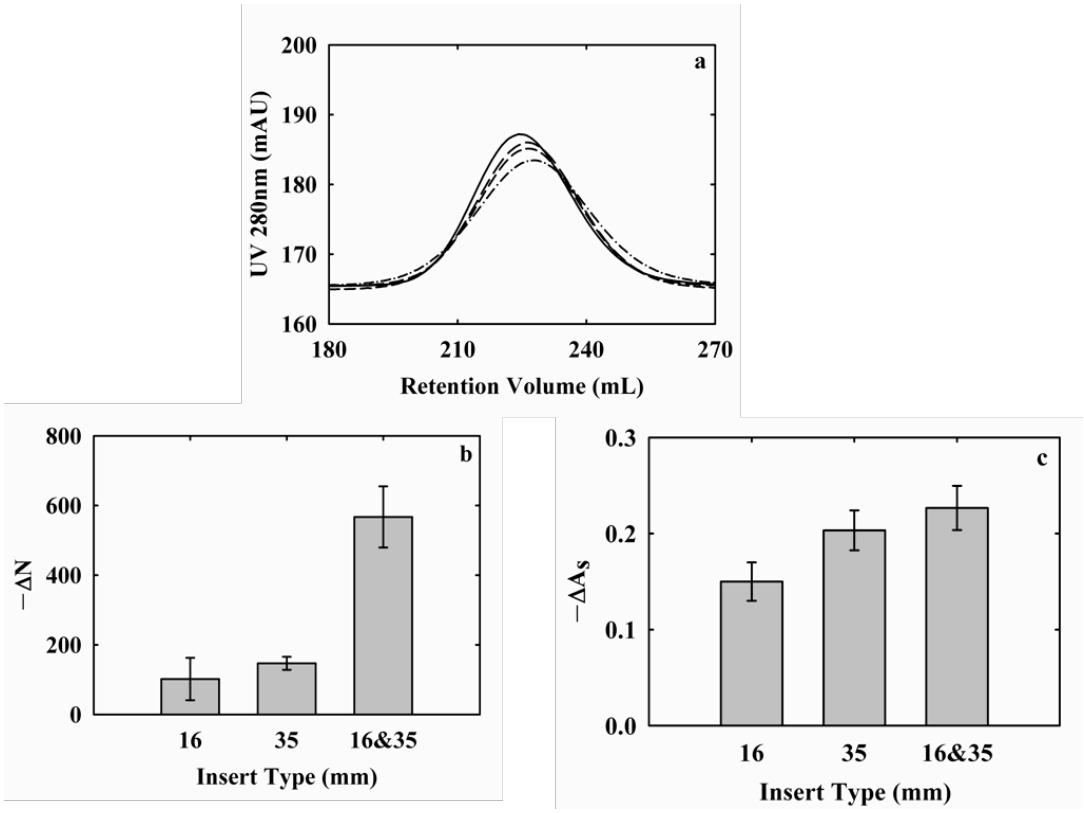

Figure 3.9 *Impact of stainless steel insert on column efficiency of XK 50 column packed with P6XL resin to a bed height of 120±5 mm. All inserts were 45 mm in length. Figure 3.9a: HETP for no insert (——), 16 mm diameter insert (−−−), 35 mm diameter insert (-----), and 16 mm and 35 mm diameter double inserts (−·−··). Figure 3.9b: Variation in plate numbers for column tested in Figure 3.9a, the initial plate number is 3483 plates* m^{-1}*. Figure 3.9c: Variation in asymmetry factor for column tested in Figure 3.9a, the initial asymmetry is 1.25. Data points are mean±SD from 3 independent experiments.*

3.3.3 Effect of insert material

Figure 3.10a shows the absorbance-time distribution curves of a tracer for a given column packed with P6XL to ~120 mm bed height equipped with either plastic or stainless steel inserts. In Figure 3.10b the data were normalized to account for the insert volume, since this is significantly different between the two materials (4 mL for plastic inserts & 0.14 mL for stainless steel). This normalization reduces the difference between the two sets of tracer studies as expected. The small difference remaining between the plastic insert data and that for the stainless steel probably reflects the impact of the insert thickness in causing local axial dispersion as the flow impinges the top of the insert.

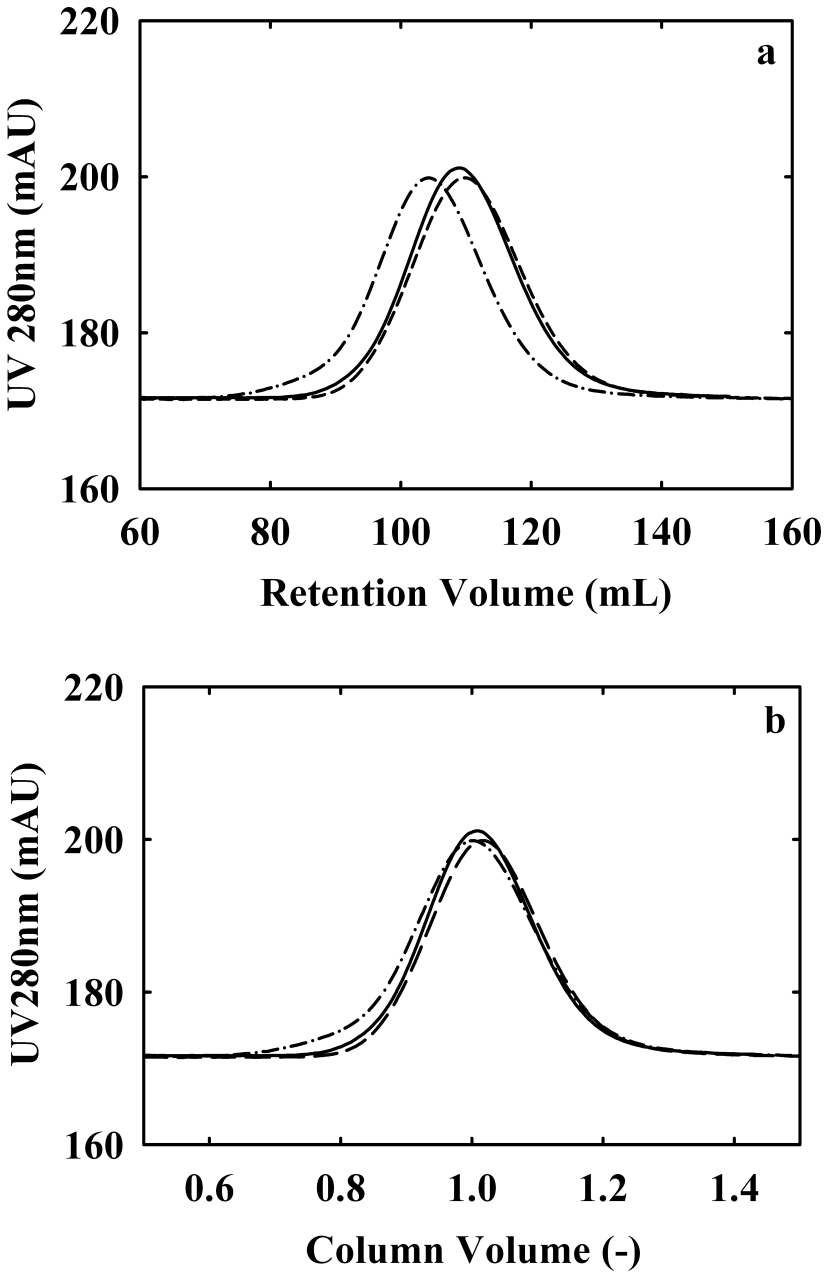

Figure 3.10 *Impact of insert materials of construction on column efficiency for an XK 50 column packed with P6XL resin to a bed height of 50±2 mm. All inserts were 45 mm in length. Volume of inserts; plastic insert is 4 mL; stainless steel inserts is 0.14 mL. No insert (——), Plastic insert (–·–··), Stainless steel insert (-----). a: tracer absorbance as a function of retention volume, b: tracer absorbance normalized as a function of column volume.*

3.4 Impact of insert on productivity

The section sets out to establish the overall impact of the two phenomenon at play when which column inserts are used increasing the critical velocity and decreasing column efficiency. The impact is measured in term of change in the level of productivity reached in columns operating with inserts.

From Sections 3.2 and 3.3, it can be stated that column inserts have a positive effect on the critical velocity, and a negative effect on column efficiency. Both of the factors independently affect the level of process productivity achieved. In order to establish a base case, it was assumed that the maximum operational flow velocity was always 70% of the critical velocity (Sofer, 1997). The broadened elution peak obtained with lower plate numbers will always lead to a larger elution volume. Therefore, it is necessary to study the overall effects of inserts on these two elements together impacting column productivity. A case study on mAb purification by MabSelect SuRe^{TM} was used to research how the productivity changes with the use of inserts. The study was based on a 1 L volume column (100 mm in diameter, and 127 mm in bed height). The column inserts applied were 35 mm and 70 mm in diameter, either singly or in combination. Inserts were all 90 mm long. Earlier results showed the critical velocity increments to be 4%, 10%, and 20% respectively, and the decrement of theoretical plate number to be 5%, 5% and 10%

respectively for these insert combinations.

The process productivity was calculated from:

$$P = \frac{DBC \times V_L \times (1-n)}{t_c \times V_{sp}} \times Y \tag{3.3}$$

where, P is process productivity (g h^{-1} L^{-1}), DBC is the dynamic binding capacity (mg mL^{-1}), V_L is the column volume (L), n is safety margin (-), t_C is cycle time (h), V_{sp} is packing material volume (L), Y is yield of mAb purification with MabSelect SuRe^{TM} resin (%).

Dynamic binding capacity is known to be a function of flow velocity. For MabSelect SuRe^{TM} resin an empirical relationship from GE Healthcare Application notes was used;

$$DBC = \alpha u + \beta \tag{3.4}$$

where $\alpha = -0.042$

$\beta = 47.2$

u is operational flow velocity (cm h^{-1}).

The total cycle time was defined as:

$$t_C = t_e + t_L + t_w + t_E + t_r + t_{w2} + t_{CIP} \tag{3.5}$$

The time for each depends on the buffer volumes used shown in Table 3.2.

Table 3.2 The time for each step was determined depending on the screening conditions (GE Healthcare Application notes)

Element	Steps	Volume (CV)
t_e	Equilibrate with buffer A	5
t_L	Sample loading	*
t_w	Wash with buffer A	5
t_E	Elute the column with a linear gradient to 100% buffer B	10
t_r	Regenerate the column with buffer B	5-10
t_{w2}	Wash the column with buffer A	3
t_{CIP}	Perform CIP	5

* depends on feedstock concentration and DBC

Examples of suitable buffers:

• Buffer A: 20 mM sodium phosphate, 150 mM NaCl, pH 7.2

• Buffer B: 0.1 M sodium citrate, pH 3.0–3.6.

The loading time was calculated as follow:

$$t_{L,i} = \frac{DBC_i \times V_L \times (1-n)}{u_i \times A} \tag{3.6}$$

The elution time was calculated as:

$$t_E = \frac{V_{E,i}}{u_i \times A} \tag{3.7}$$

where, u_i is the operational flow velocity (cm h^{-1}) and $V_{E,i}$ is the elution volume (L).

A is the column cross-section area (cm^2).

The equations 3.3-3.7 were used in a simple Excel spreadsheet to predict the change in process productivity as function of flow velocity. The results are given in Figure 3.11.

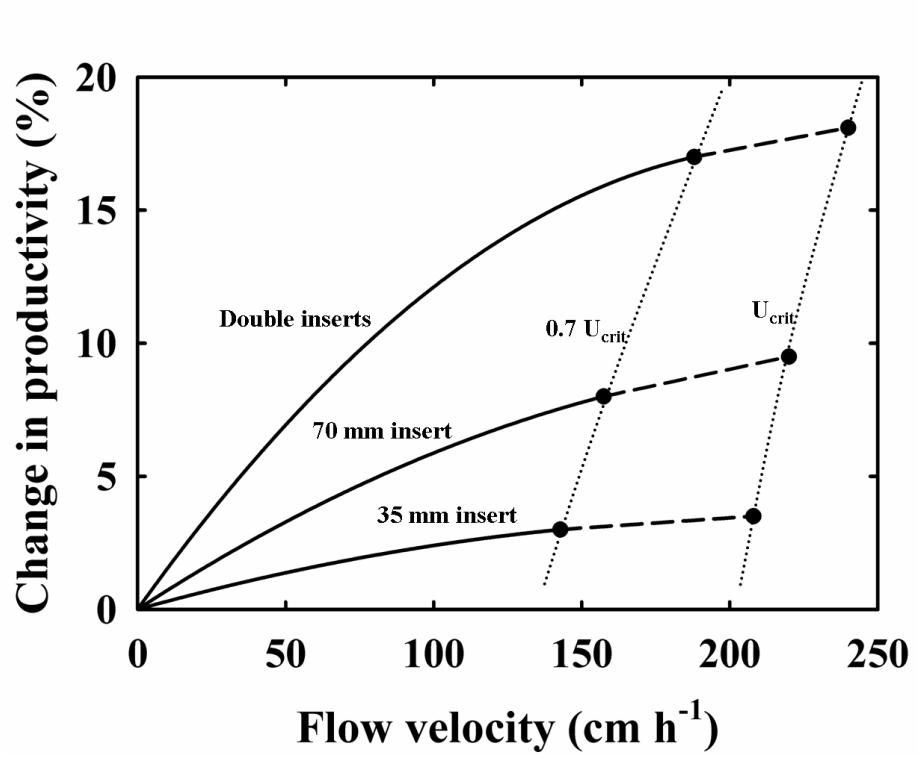

Figure 3.11 Change in productivity with flow velocity with different inserts (35 mm, 70 mm diameter insert, and double inserts) in 100 mm diameter column packed to 127 mm bed height with Mabselect SURE^{TM} .The solid line is the productivity change with operational flow velocity.

As expected from Figure 3.11, the productivity increases with flow velocity. The double inserts lead to a predicted 15-20% operational flow velocity increment, even though such an insert configuration decreases the plate number by 20%. The

negative effect of inserts on column efficiency is clearly small when compared to the benefits in term of critical velocity increment. The overall effect of column inserts is to raise the level of process productivity significantly.

Productivity with different DBC gradient.

It is well known that DBC decreases with flow velocity. In practice, for some resins, the DBC is very sensitive to flow velocity. In figure 3.12, the productivity changes with different levels of DBC sensitivity to flow velocity were studied. From this figure, it was that assumed that the relationship between the DBC and flow velocity is 5 times that in the initial study. Under search a set of assumption the productivity starts to decrease with higher flow velocities. For DBC 5 times that of the base case and at about 120 cm h^{-1} the productivity reaches a maximum. Therefore, the insert system cannot be applied beneficially in this case.

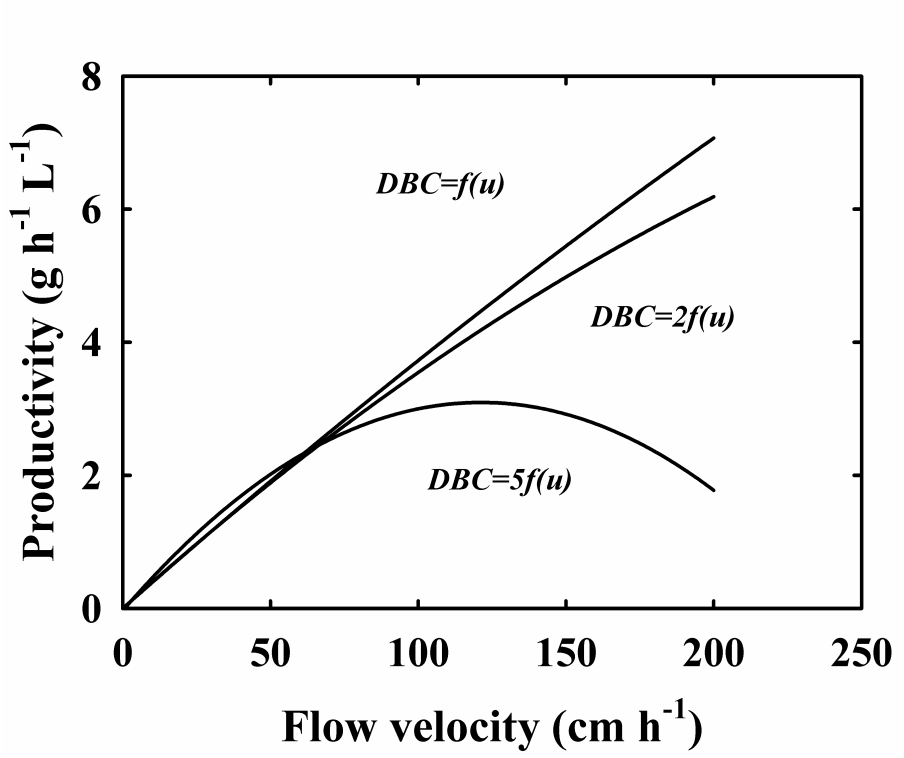

Figure 3.12 Productivity with flow velocity at different DBC gradient. It is in 100 mm diameter column packed to 127 mm bed height with Mabselect SURE^{TM}.

From the simulation results of productivity shown in Figure 3.11, there is approximately an 18% increment of productivity when the operational flowrate is raised by 10% with double column inserts, whilst the column plate number is reduced by about 10%. However, this benefit is depended on the level of DBC, itself a function of flow velocity. In this case study on Mabselect SURE^{TM} resin, there is relatively low DBC change with flow velocity for this kind of material, therefore, nearly a 20% increment of process productivity could be achieved. Apparently, when the level of DCB change is very sensitive to flow velocity, which means that target protein is very hard to bind to the resin even with a little increasing flow velocity, the process productivity could not increase with higher flow velocity. In Figure 3.12, it is clear that when the level of DBC change is 5 times of initial DBC change with flow velocity, the productivity could reduce with higher flow velocity. That means there is no benefit on process productivity improvement with column insert, which could lead to a higher flow velocity. Therefore, when seeking to determine if inclusion of inserts is of benefit it will be important to know the level of DBC change with flow velocity.

3.5 Conclusions

This chapter presents experimental data of critical velocity and column efficiency for a range of chromatography columns (XK 16, XK 50, and BPG 100) packed with compressible material as a function of the design of concentric cylindrical inserts placed within the packed bed has been presented. The results show that inserts installed at the bottom of a column could generate up to a 20% increase in critical velocity and performed better than when inserts were placed at any other axial location. The penalty was a small increase in dispersion. For a single insert the plate number fell by 10%, which was deemed to be insignificant compared to the improvement in throughput. A set of empirical equations were specified to relate the change in critical velocity to insert length and diameter. In the next chapter, a theoretical study linking the pressure-flow profile and bed compression in chromatographic process packed with compressible material will be generated. Hydrodynamic and structural mechanics model will be established to describe the column pressure-flowrate relationships. The model will be used to optimize the dimensions and position of the inserts required to maximise the critical velocity increment without significantly affecting the hydrodynamic efficiency of a column.

Chapter Four: Model Establishment

4.1 Introduction

In Chapter Three, experimental results demonstrating the change of critical velocity and column efficiency due to the influence of chromatography column inserts were presented. These showed that column inserts can provide extra wall support and lead to an increase in critical velocity without significant affecting on column efficiency. However, the experimental work could only exam the phenomenon which column inserts affect chromatographic processes. A theoretical approach is necessary to describe it. A mathematic model is established in this chapter to simulate the flow though a range of chromatographic columns packed with compressible material. This model describes the pressure-flow profile, and the consequences bed compression.

The calculation of the critical velocity of a column is generally conducted through empirical correlations of gravity-settled bed height, column diameter, feed viscosity and compressibility of the chromatographic media used (Tran et al., 2007; Stickel and Fotopoulos, 2001). Additionally, structural mechanics models have been applied to calculate the critical velocity by investigating the stress state in rigid and compressible chromatography resins (McCue, 2007; Chen, 2005; Cherrak, 2001; Keener, 2004; Östergren, 1999). The majority of these models are developed in a two-dimensional coordinate reference system. They describe the pressure-flow

behavior using Darcy's Law and treat the resin as a porous material. They can take into account material nonlinearity in the case of compressible resins by expressing the Young's modulus (modulus of elasticity) as an empirical function of the particle porosity (Wang, 1984). The empirical parameters of the Young's modulus equation are best-fitted to measured independent compression experimental data (McCue et al., 2007). It is expected that the solid mechanics could describe the pressure-flow profile, and the level of bed compression. This model will be further studied to predict the pressure-flow behavior, key parameter profile of a chromatographic column with inserts.

4.2 Theory

In this section, we introduce the physical theory of flow in chromatographic processes, and packed bed consolidation. It will include Darcy's Law for flow through porous media, and Biot's Theory for chromatography bed compression (Biot, 1941; Biot, 1962)

4.2.1 Flow condition in chromatographic columns

It is necessary to study the flow condition in chromatographic column to find out the proper equations, which describe the pressure-flow relationship, before model establishment.

4.2.1.1 Newtonian fluid

Often, the feed stock for chromatographic process is delivered from centrifugation and filtration steps, therefore, cell debris and some contaminations has already been removed, and it has relatively low bio-organism concentration. Most feeds have low viscosity and are Newtonian fluids (Al-Nimr and Aldoss, 2004; Guiochon and Tarafder, 2011), where the viscosity is independent of rate of shear and constant at a given temperature. To determine the pressure-flowrate relationships, the RO water or 100mM NaCl was used as the mobile phase in this project as for previous studies(Keener et al., 2002; McCue et al., 2007), since these are Newtonian fluids. All discussion will be restricted to Newtonian fluids flowing through porous media.

4.2.1.2 Laminar flow

Chromatographic flow is nearly always laminar in nature, seldom molecular or turbulent(Cramers et al., 1981). For the modeling of the pressure-flow relationships, it is necessary to start with the Darcy's Law, which is restricted to laminar flow. Therefore, it is necessary to find out the Reynolds number of flow through chromatographic column. Whether the flow through chromatographic columns is laminar or turbulent depends on the magnitude of the Reynolds number Re, a dimensionless parameter. The calculation of Re for flow through a pipe is

$$\mathrm{Re} = \frac{dv\rho}{\mu} \tag{4.1}$$

Where Re is the Reynolds number (dimensionless); d, the pipe diameter (m); *v*, the superficial flow velocity (m s^{-1}); ρ, the density (kg m^{-3}); and μ, the viscosity (Pa s).

The modified Reynolds number for flow though porous media can be calculated as:(Hellström and Lundström, 2006)

$$\mathrm{Re}' = \frac{d_p v \rho}{\mu} \frac{1}{1-\varepsilon} \tag{4.2}$$

Where ε is the bed voidage fraction; and d_p is the size of particle (m).

From this equation, and experimental data in Chapter Two, the Reynolds number can be calculated as below.

Table 4.1 Reynolds number of flow for different column geometries tested

Column	Insert	Diameter(m)	Critical velocity (cm h^{-1})	Reynolds number
XK16	No	0.016	361	0.15
	Yes	0.016	438	0.19
XK50	No	0.05	243	0.10
	Yes	0.05	283	0.12
XK100	No	0.1	195	0.08
	Yes	0.1	243	0.10

Here, the critical velocity is the maximum flow the column can achieve.

The assumed fluid density is about 1000 kg m^{-3}, the viscosity is about 10^{-3} Pa s, the particle size is 90×10^{-6} m.

In Table 4.1 the flow velocity, which used to calculate Reynolds number, is the critical velocity, as the maximum flow velocity the column can achieve before the onset of bed compression. From the results, the Reynolds number is relatively low (<1). With this condition, Darcy's Law is applicable for the study of flow through a chromatography column. Additionally, if the value of the Reynolds number is greater than 1.0, Darcy's Law has been found to fail adequately to describe flow through a porous medium. A correction factor usually applied in this case (Boomsma and Poulikakos, 2002).

4.2.2 Darcy's Law

To establish a mathematical model of pressure-flowrate relationship in chromatographic columns operating with soft matrix packing, it is usual to start with Darcy's law, which can describe flow through porous media. Fluid through porous media may or may not be one dimension. Furthermore, flow through porous media can be analyzed by the means previously given (Boomsma and Poulikakos, 2002). Thus we will discuss this aspect of flowing fluids is discussed here next.

There are many fluid/media examples to be found: water through soil, solvents through packed beds, air through charcoal, natural gas and oxygen through porous ceramics, and water through biological filters. In each case, the medium through

which the fluid is flowing will be considered at a large dimensional scale so that it will be assumed to be composed not of finite particles with channels, but as a uniform medium that impedes fluid flow.

Darcy's Law is the equation usually used to describe one-dimensional flow through porous media:

$$V = \frac{-kA}{\mu}\left(\frac{\partial p}{\partial L} + \rho g \sin\alpha\right) \tag{4.3}$$

Where V is the volumetric flow rate (m s^{-1}); k, the permeability (m^2); μ, the fluid viscosity (Pa s); A, the cross-sectional area (m^2); $\partial P / \partial L$, the pressure gradient along the flow path (Pa); ρ, the fluid density (kg m^{-3}); g, the acceleration due to gravity (m s^{-2}); and α, the angle of inclination of the flow path with respect to the horizontal (rad).

The second term of Darcy's law takes into account the difference in potential energy of the fluid as it either rises or falls within a gravitational field. When flow is strictly horizontal, or when the fluid density is very small, or when the pressure gradient is much greater than the gravitational potential gradient, then the second term may be neglected, and Darcy's law becomes:

$$V = \frac{-kA}{\mu}\frac{\partial p}{\partial L} \tag{4.4}$$

Notice that the negative sign signifies that flow is positive when the pressure gradient is negative.

The permeability, *k*, is usually an average value of the ease with which a fluid will flow through the medium. The permeability takes into account all the various flow channels that differ in size, shape, direction, and interconnections. The fluid will often flow preferentially through certain flow channels in the medium. The average permeability ignores this fact.

Hydrologists, dealing only with the flow of water, will frequently combine the viscosity and permeability to form a permeability coefficient:

$$k_p = k / \mu \tag{4.5}$$

Where k_p is the permeability coefficient for water as fluid $(N\ S)^{-1}$

In particular, fluid flowing one dimensionally through porous media bounded by surface of a flat plane is given by

$$V = \frac{-kA}{\mu L}\left(p_2 - p_1\right) \tag{4.6}$$

This pressure-flowrate modeling will be established from equation 4.6. In a specific chromatographic process, A is the cross-sectional area of the column, μ is the viscosity of the mobile phase, and L is the bed height.

Here, *k*, the permeability is depended on the media property. When Darcy's Law is applied in Civil Engineering, such as water flow through ground, the k value is always constant, and it is independent of pressure or flowrate. The equation 4.4 can

change to:

$$Q = -KA(\frac{dh}{dL}) \tag{4.7}$$

For example, K for gravels is 0.1-1 cm s^{-1}, and K for sands is 10^{-2}-10^{-3} cm s^{-1}. From equation 4.7, it is quite clear how to calculate the rate of water flow through ground of different property. However, in this project, which analysis flow through compressible chromatography media, the permeability k, is not constant, and it will change with pressure. Therefore, it is necessary to establish the permeability k as a function of the applied pressure.

4.2.3 Mathematical modeling of compression in a chromatography column

The mathematical model which simulates the pressure-flow behavior in chromatography columns packed with compressible resins is based on Biot's theory (Biot, 1962). The model has the following assumptions: (i) the resin is isotropic, (ii) the stress-strain relations are linear, (iii) the strains are small, (iv) the liquid contained in the pores is incompressible, (v) the pores of the resin are saturated with liquid, (vi) the mobile phase flows though the resin according to Darcy's Law, (vii) the relative liquid matrix velocity is equal to the liquid velocity.

4.2.3.1 Liquid phase equations

The pressure drop is related to the superficial velocity according to Darcy's Law for homogenous porous material:

$$U_0 = -\frac{1}{\mu} k \nabla P \qquad (4.8)$$
$$\nabla P = \nabla p - \rho g$$

where U_0 is the superficial velocity (m s^{-1}), μ is the dynamic viscosity of the mobile phase (Pa s), ρ is the density of the mobile phase (kg m^{-3}), P is pressure (Pa), g is the gravitational acceleration (m s^{-2}), and k (m^2) is the permeability.

In this study the permeability is calculated according to the Kozeny-Carman equation (Bear, 1972):

$$k = \frac{{d_P}^2}{C} \frac{\varepsilon^3}{(1-\varepsilon)^2} \qquad (4.9)$$

where ε is the bed void volume fraction and d_p is the particle diameter (m).

The continuity equation for steady state, single phase incompressible flow is:

$$\nabla \cdot (\rho U_0) = 0 \qquad (4.10)$$

(Ostergren et al., 1997)

By combining Eq. (4.8) and Eq. (4.9) the pressure distribution in the liquid phase of the column is described mathematically by:

$$\frac{1}{r}\left(\frac{\partial}{\partial r} \frac{rk\rho}{\mu} \frac{\partial P}{\partial r} + r \frac{\partial}{\partial z} \frac{k\rho}{\mu} \frac{\partial P}{\partial z}\right) = 0 \qquad (4.11)$$

The boundary conditions for equation (4.11) are specified as follows:

At the inlet of the column:

$P(r, H)=\Delta P$, $z=H$ (4.12)

where ΔP is the hydrodynamic pressure drop across the column and H is the compressed bed height, r is the radial coordinate and z is the axial coordinate.

At the outlet of the column:

$P(r, 0)=0, \quad z=0$ (4.13)

At r=0, there is radial symmetry because of the cylindrical shape of the column:

$$\frac{\partial P(0,z)}{\partial r}=0 \tag{4.14}$$

No slip conditions are applied at the insert and column walls:

$$\frac{\partial P(R,z)}{\partial r}=0,\ r=R \tag{4.15}$$

4.2.3.2 Solid phase equations

The relationship between the pressure drop through the column and the solid phase deformation is described mathematically by:

$$-\nabla\cdot[\sigma]=\nabla P \tag{4.16}$$

The above equation expressed in cylindrical coordinates gives:

$$\begin{aligned}
&\frac{\partial \sigma_{rr}}{\partial r}+\frac{1}{r}\frac{\partial \sigma_{r\theta}}{\partial \theta}+\frac{\partial \sigma_{rz}}{\partial z}+\frac{\sigma_{rr}-\sigma_{\theta\theta}}{r}=\frac{\partial P}{\partial r}\\
&\frac{\partial \sigma_{\theta r}}{\partial r}+\frac{1}{r}\frac{\partial \sigma_{r\theta}}{\partial \theta}+\frac{\partial \sigma_{\theta z}}{\partial z}+2\frac{\sigma_{r\theta}}{r}=\frac{1}{r}\frac{\partial P}{\partial \theta}\\
&\frac{\partial \sigma_{zr}}{\partial r}+\frac{1}{r}\frac{\partial \sigma_{z\theta}}{\partial \theta}+\frac{\partial \sigma_{zz}}{\partial z}+\frac{\sigma_{zr}}{r}=\frac{\partial P}{\partial z}
\end{aligned} \tag{4.17}$$

Stress σ and strain ε are related according to Hooke's law:

$$\begin{aligned}
\sigma_{rr} &= 2G\varepsilon_{rr} + \lambda\varepsilon_V \\
\sigma_{\theta\theta} &= 2G\varepsilon_{\theta\theta} + \lambda\varepsilon_V \\
\sigma_{zz} &= 2G\varepsilon_{zz} + \lambda\varepsilon_V \\
\sigma_{\theta z} &= 2G\varepsilon_{\theta z} \\
\sigma_{zr} &= 2G\varepsilon_{zr} \\
\sigma_{r\theta} &= 2G\varepsilon_{r\theta} \\
\varepsilon_V &= \varepsilon_{rr} + \varepsilon_{\theta\theta} + \varepsilon_{zz}
\end{aligned} \tag{4.18}$$

where, σ is stress, ε is strain, and the coefficient G is the shear modulus. λ is Lame's constant, named after the French mathematician G. Lamé. The Lame's constant depends on the material and its temperature. They are related to the modulus of elasticity (Young's modulus) and Poisson's ratio v by

$$\lambda = \frac{Ev}{(1+v)(1-2v)} \tag{4.19}$$

where v is the Poisson ratio, which is the ratio of transverse strain and axial strain.

The displacements are given by:

$$\begin{aligned}
\varepsilon_{rr} &= \frac{\partial u_r}{\partial r} \\
\varepsilon_{\theta\theta} &= \frac{1}{r}\frac{\partial u_\theta}{\partial \theta} + \frac{u_r}{r} \\
\varepsilon_{zz} &= \frac{\partial u_z}{\partial z} \\
\varepsilon_{\theta z} &= \frac{1}{2}\left(\frac{\partial u_\theta}{\partial z} + \frac{1}{r}\frac{\partial u_r}{\partial \theta}\right) \\
\varepsilon_{zr} &= \frac{1}{2}\left(\frac{\partial u_z}{\partial r} + \frac{\partial u_r}{\partial z}\right) \\
\varepsilon_{r\theta} &= \frac{1}{2}\left(\frac{1}{r}\frac{\partial u_r}{\partial \theta} + \frac{\partial u_\theta}{\partial r} - \frac{u_\theta}{r}\right)
\end{aligned} \tag{4.20}$$

The final balance equations expressed in terms of displacement (u_x, u_r) were obtained by combining Eqs. (4.18), (4.19), and (4.20):

$$\frac{1}{r}\frac{\partial}{\partial r}\left(rG\frac{\partial u_z}{\partial r}\right)+\frac{\partial}{\partial z}\left(\left(2G+\lambda\right)\frac{\partial u_z}{\partial z}\right)+S_{u_z}=\frac{\partial P}{\partial z}$$
$$S_{u_z}=\frac{1}{r}\frac{\partial}{\partial r}\left(rG\frac{\partial u_r}{\partial z}\right)+\frac{\partial}{\partial z}\lambda\left(\frac{\partial u_r}{\partial r}+\frac{u_r}{r}\right) \quad (4.21)$$

and

$$\frac{1}{r}\frac{\partial}{\partial r}r\left(\left(2G+\lambda\right)\frac{\partial u_r}{\partial r}\right)+\frac{\partial}{\partial z}\left(G\frac{\partial u_r}{\partial z}\right)-u_r\left(\frac{2G+\lambda}{r^2}-\frac{1}{r}\frac{\partial\lambda}{\partial r}\right)+S_{u_r}=\frac{\partial P}{\partial z}$$
$$S_{u_r}=\frac{\partial}{\partial r}\left(\lambda\frac{\partial u_z}{\partial z}\right)+\frac{\partial}{\partial z}\left(G\frac{\partial u_z}{\partial r}\right) \quad (4.22)$$

S_{ur} is r-direction displacement, and S_{uz} is z-direction displacement.

The boundary conditions for equations (4.21) and (4.22) are the following:

At the inlet of the column:

$$u_r(r,H)=0 \quad \frac{\partial u_z(r,H)}{\partial z}=0 \quad (4.23)$$

At the outlet of the column:

$$u_z(r,0)=0 \quad \frac{\partial u_r(r,0)}{\partial z}=0 \quad (4.24)$$

At r=0 there is radial symmetry because of the cylindrical shape of the column:

$$u_r(0,z)=0,\ \frac{\partial u_r(0,z)}{\partial r}=0,\ \frac{\partial u_z(0,z)}{\partial z}=0 \quad (4.25)$$

At column walls there is no radial displacement of the resin and the wall friction is described through a friction coefficient. Specifically,

$$\delta_{rz}(R,z) = \mu_f \delta_r(R,z), \quad u_r(R,z) = 0 \tag{4.26}$$

where H is the column height, H_0 is the initial height of the uncompressed column, and μ_f is the wall friction coefficient.

4.2.4 Simulations

4.2.4.1 Young's modulus

The modulus of elasticity of the resin (E) is expressed as an empirical function of the voidage fraction, ε (Wang, 1984):

$$E = E_0 \exp(-E_1 \varepsilon) \tag{4.27}$$

where E_0 and E_1 are parameters. Although this is an empirical expression, the parameters do have a physical representation. A high E_0 reflects a high particle rigidity at zero-porosity. The term $\exp(-E_1\varepsilon)$ represents rigidity when the resin is under compression. When pressure is applied to the particle, the porosity, ε reduces, and the value of $\exp(-E_1\varepsilon)$ will increase. That means the material will be more rigid, and harder to compress.

4.2.4.2 Voidage fraction

The Young's modulus changes the voidage fraction from equation (4.27). The voidage fraction also changes with pressure drop. The voidage fraction and pressure relationship has been studied by civil engineers before. Skempton (1944) stated this relationship as a function below (Tripathy and Mishra, 2011),

$$e = a - b \log_{10} P \tag{4.28}$$

The void ratio, e is a linear relationship with logarithm pressure. The void ratio is expressed by voidage fraction as shown below:

$$e = \frac{\varepsilon}{1-\varepsilon} \tag{4.21}$$

4.2.4.3 Evaluate packing material property

The values of $E_{0,} E_1$, a and b were estimated from the pressure-flow experimental data using least squares regression analysis. This inverse problem was applied in two steps using Comsol Multiphysics wrapped around Matlab^{TM} (The MathWorks Inc., Natick, USA). In the first step the Comsol model was developed in Comsol's graphical user interface using arbitrary values for the parameters of interest. It was then saved as a Matlab file. In this form the file can run in the Matlab graphical user interface without the option to alter the values of the parameters of interest in to calibrate the model to experimental data. This was achieved by editing the file as a Matlab function, so as to treat the system of differential equations of the model as a functional representation between the parameters of interest which are the input and the sum of squared residuals (a residual is defined as the difference between the experimental and the fitted value) which is the output. This Matlab function was referred to as the forward model function. Its role is to help Matlab recognise which parameters of the Comsol model need to be estimated. In the second step the nonlinear least-squares Matlab function "lsqcurvefit" (default settings) was used to minimise the forward model function. It solves nonlinear data-fitting problems using the Levenberg-Marquardt algorithm. It searches for optimal parameter values

within the range imposed by the upper and lower bounds of these parameters.

4.3 Results and discussion

In the section, the best fitted empirical coefficients in equation 4.27 and 4.28 will be estimated to make the simulated pressure-flow profile to match the experimental data. The profiles of key parameters including, displacement, pressure, axial stress, voidage fraction will also be presented.

4.3.1 Coefficient determination by experimental data

The physical constants used as input for the simulation are shown in Table 4.2. These constants are from previous works (Keen et al. 1999). The best-fit values for the empirical modulus parameters from least-squares regression analysis are shown in Table 4.3. These values represent the properties of packing material, and they will also be used in further studies of the pressure-flow and bed compression simulation with column inserts.

Figure 4.1 shows the model predictions for the pressure-flow behavior agreed well with experimental data. It can also be noticed that the bed height-flow profile is in agreement with the experimental data, and provided further evidence the model was able to describe the chromatography bed compression.

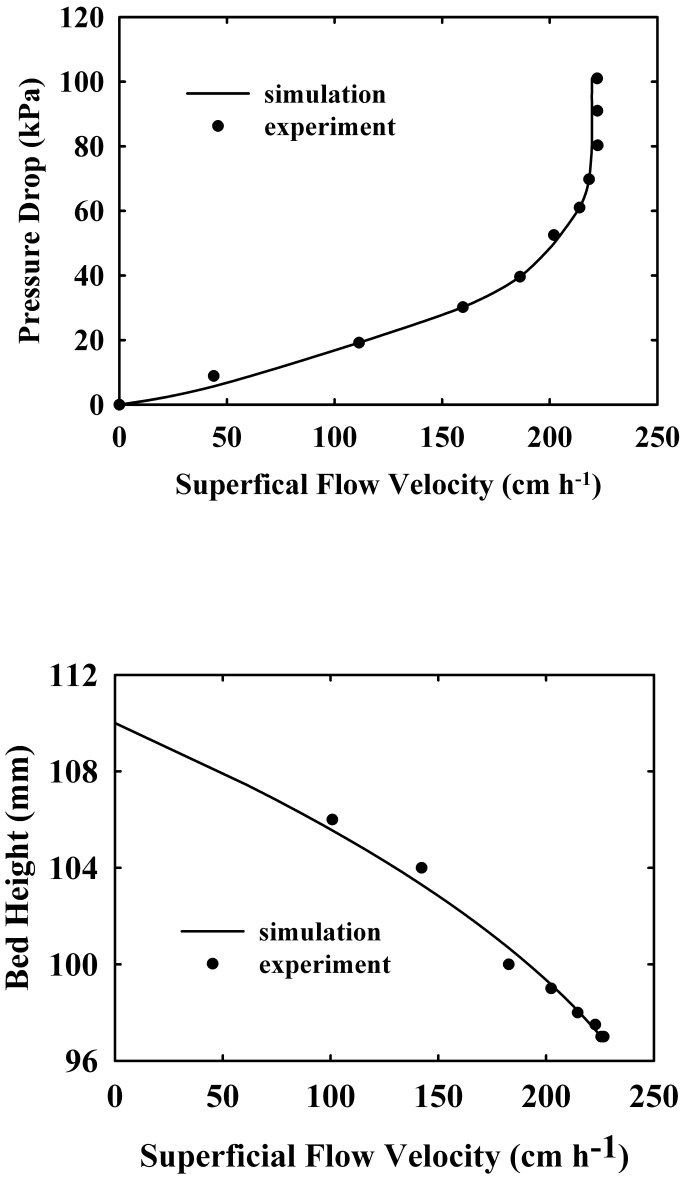

Figure 4.1 *Experimental (●) versus simulated (——) pressure-flow data. The experimental data were best fitted to a structural mechanics model in order to calculate the mechanical properties of the resin (Young modulus empirical equation constants) and permeability coefficient, and to generate the simulated pressure-flow profile and bed height.*

Table 4.2 Physical constants used in modeling simulations

Material	Mean particle size (m) $\times 10^{-6}$	Initial bed porosity (-)	Wall friction coefficient (-)	Poisson ratio (-)
P6XL	90	0.41	0.16	0.26

Table 4.3 Best-fit values for the empirical modulus of equation (4.27 and 4.28)

Young's modulus (P)		Voidage Fraction (-)	
E_0	E_1	a	b
11449	-1.622	1.29	0.23

4.3.2 Bed displacement versus pressure

The bed displacement distribution in the two-dimensional cylindrical coordinate system from simulation results is shown in Figure 4.2. The six graphs show the displacement at different pressures. From simulation result, the critical velocity was achieved with 90kPa pressure. The bed displacement is greater at the top of the bed than at the bottom. At the same bed height, the displacement is different, which is the column centre displacement is higher than it near column wall. This is because of the wall effect. The drag force from the friction of column walls can delay the onset of bed compression. This is evidence of extra wall support from column inserts can lower the bed compression. From Konezy-Carman equation, the higher

voidage fraction (lower compression) leads higher permeability, and the column can achieve larger critical velocity with column inserts.

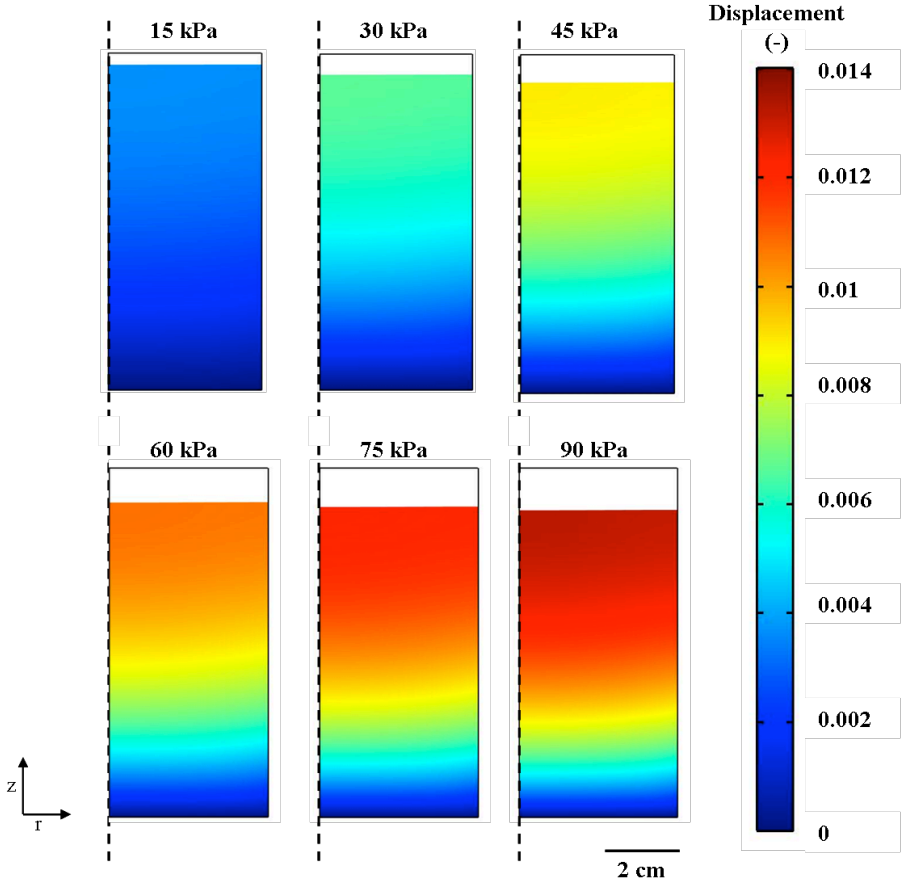

Figure 4.2 *Bed displacement profile of a 0.86 L chromatographic column (100 mm in diameter, and 110 mm in original packed height) packed with P6XL. The six figures represent the profile at different pressure drops, which lead to achieving the condition corresponding to the onset of the critical velocity.*

4.3.3 Parameters distribution

From this model, it is possible to analyse the change in key parameters, including pressure, stress, and bed voidage fraction distribution in the chromatographic

column. The results are shown in Figure 4.3. These graphs are for a column

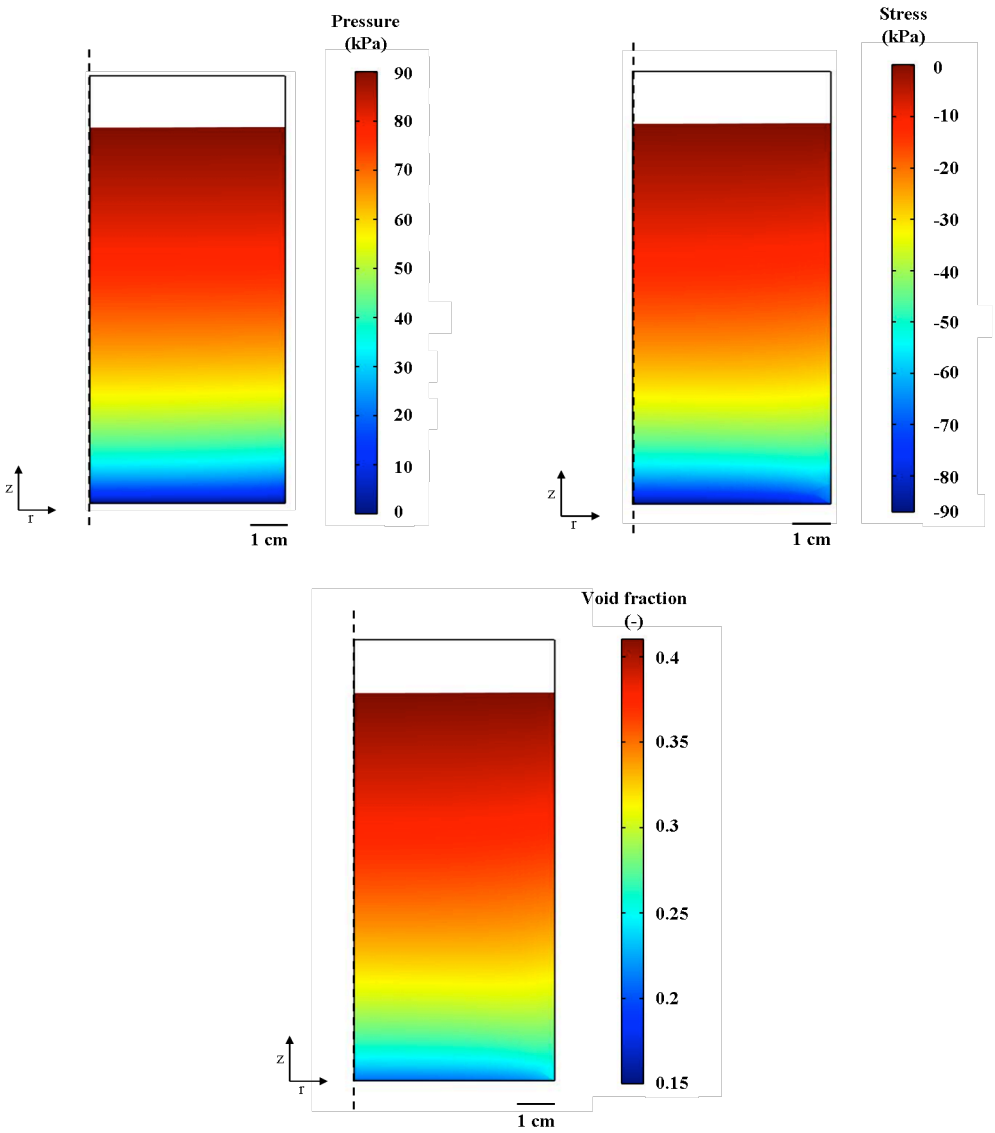

Figure 4.3 *Pressure, stress, and voidage fraction profile of a 0.86L chromatographic column (100 mm in diameter, and 110 mm in height) packed with P6XL, at the point the column achieves critical velocity.*

achieving critical velocity. The initial bed height is 110 mm, and it is 97 mm when the critical velocity achieved. The liquid pressure is applied at the top of column. Here the pressure is from liquid pumped through the column, and it is an external

force on the packing material. The stress is an internal parameter of the solid phase. From the stress profile graph in Figure 4.3, it is obvious that the stress developed at the bottom and near the column wall is lower than it is in the central region of the bed. That is again because of the wall support.

4.4 Conclusions

In this chapter, a mathematical model has been established to describe the pressure-flow profile, and bed compression. The model was established using Darcy's Law and solid mechanics from Biot's theory. The finite element method to solve the differential equations arising from the use of these theories was made. The inverse method was applied through combining Comsol Multiphysics and Matlab to find out the best fitted parameters in the empirical equation. This model provides estimates of the pressure-flow and bed height-flow profile which all match well the experimental data. It can also simulate the parameters (including the pressure, flow, bed displacement, stress, and strain) distribution in chromatographic columns under operating conditions. This achievement will help in the next study of the impact that including cylindrical column inserts installed in the column makes on the value of critical velocity.

In the next chapter, the structural mechanics models now created will be applied to describe the pressure-flow behaviors and the distribution of stresses within a

laboratory chromatography column supported by internal inserts. The model will then be used to optimize the diameter and height of the insert, so as to maximize the critical velocity, allowing higher throughput to be achieved. This will provide a thorough understanding of the effect of the inserts on the stress distribution in the column, setting up rules for the dimensions of the column insert to be used to maximise the operational linear velocity without the need for laboratory intensive experiments.

Chapter Five: Application of a two-dimensional structural mechanics model for predicting the pressure-flow profile and compression properties during operation of columns with internal inserts

5.1 Introduction

In Chapter Four, a mathematical model was established to describe the pressure-flow profile, and bed compression in a chromatography column. In this model, empirical equations were specified to describe the mechanical properties of the packed material (P6XL), involving Young's modulus and voidage fraction. In this chapter, these empirical model equations will be used to predict the hydrodynamics and bed consolidation in chromatographic columns containing various column inserts with negligible thickness. In Chapter Three, experimental data were presented on the effect of inserts on the column critical velocity. Conclusions were drawn from these data, including how longer inserts could lead to larger critical velocity increment, identification of the best insert diameter, which could increase the critical velocity at about 75% of the column diameter, which provide similar the inner and outer insert cross-sectional areas for flow, and the fact that a larger critical velocity increment with more inserts are used. In this chapter, all these conclusions will be supported by simulation results of pressure-flow and bed compression in column with inserts. This mode is also able to return values of parameters, such as liquid pressure, solid phase stress, bed voidage fraction, and

bed displacement distribution in column with inserts, which cannot be accessed by experiments alone.

Chromatographic process development takes place in lab-scale, using column with diameters less than 30 mm. The experimental work in this study followed this. Model establishment in this study was conducted at pilot scale with a 100 mm diameter column. The reason is that the column inserts make more impact at larger scales. In this chapter, simulations will be applied for columns having different insert dimensions and number of inserts. Changes in column pressure-flow profile for these various conditions are more obvious in a larger column.

5.2 Results and discussion

In Chapter Four, the coefficients in equations which describe Young's modulus and bed voidage fraction (equations 4.19 and 4.20) were found out by least-square regression from pressure-flow experimental data at a 100 mm diameter column packed to 110 mm bed height. The simulation results were in good agreement with the experimental data in Figure 4.1. In this section, these coefficients were then employed to simulate the pressure-flow profile and level of bed compression occurring in chromatographic columns supported by column inserts. Firstly, the empirical equations which expressed Young's modulus and bed voidage fraction were validated by comparing the simulation results and experimental data. Contour plots of key parameters such as the level of axial-stress, bed voidage fraction, and

displacement would be presented to highlight the effect of inserts on the pressure-flow distribution in a column. The model was then used to estimate the insert length and diameter which maximize the critical velocity values. The effect of supporting the column with extra inserts is presented at the end of the chapter.

5.2.1 Comparing simulation and experiment results

Figure 5.1 shows the experimental pressure-flow data and simulation profiles, for a chromatographic column containing one and two inserts. The empirical equations of Young Modulus and bed void fraction determined in Chapter Four were used in these cases. The simulated pressure-flow velocity behavior match well the results from experimental runs. Therefore it can be concluded that the model developed in Chapter Four can be used to simulate the pressure-flow profile in chromatography column packed with column inserts.

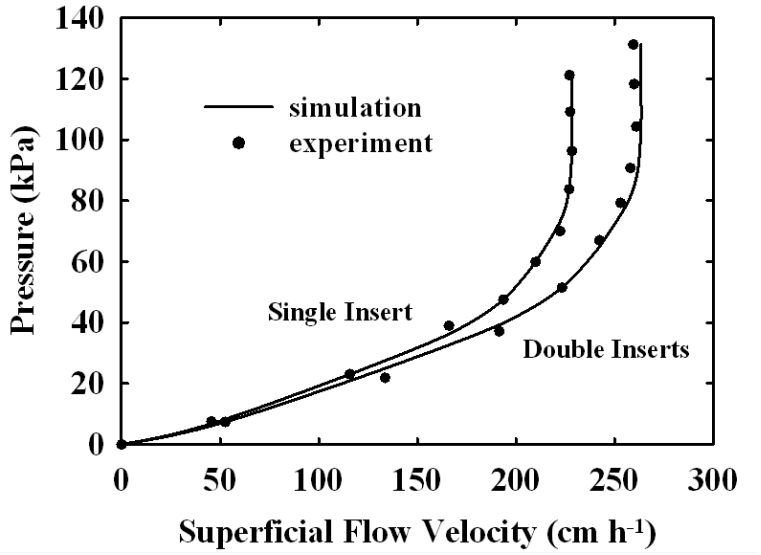

Figure 5.1 *Experimental (●) versus simulated (——) pressure-flow data for chromatographic column packed with column inserts. In practice, the column was 100 mm in diameter, and packed to 110 mm bed height. The column inserts were 30 mm diameter for single insert, and 30 mm & 75 mm for double inserts. All column inserts were 45 mm in length, and 1.1 mm in thickness. The packed material was P6XL.*

5.2.2 Key parameter profiles in columns with single insert

Figure 5.2 shows the key parameters profiles, including axial-stress, bed voidage fraction, and displacement, in the two-dimensional cylindrical coordinate system. The simulation was operated in a 100 mm diameter column packed to 110 mm bed height with P6XL. A single insert, (dimension are shown in Figure 5.2), was placed inside the column. The axial-stress profile shows that it is stressed significantly at the positions of the top of column insert, and at the bottom region without column insert support. In the bed voidage fraction distribution of Figure 5.2, it is clear that,

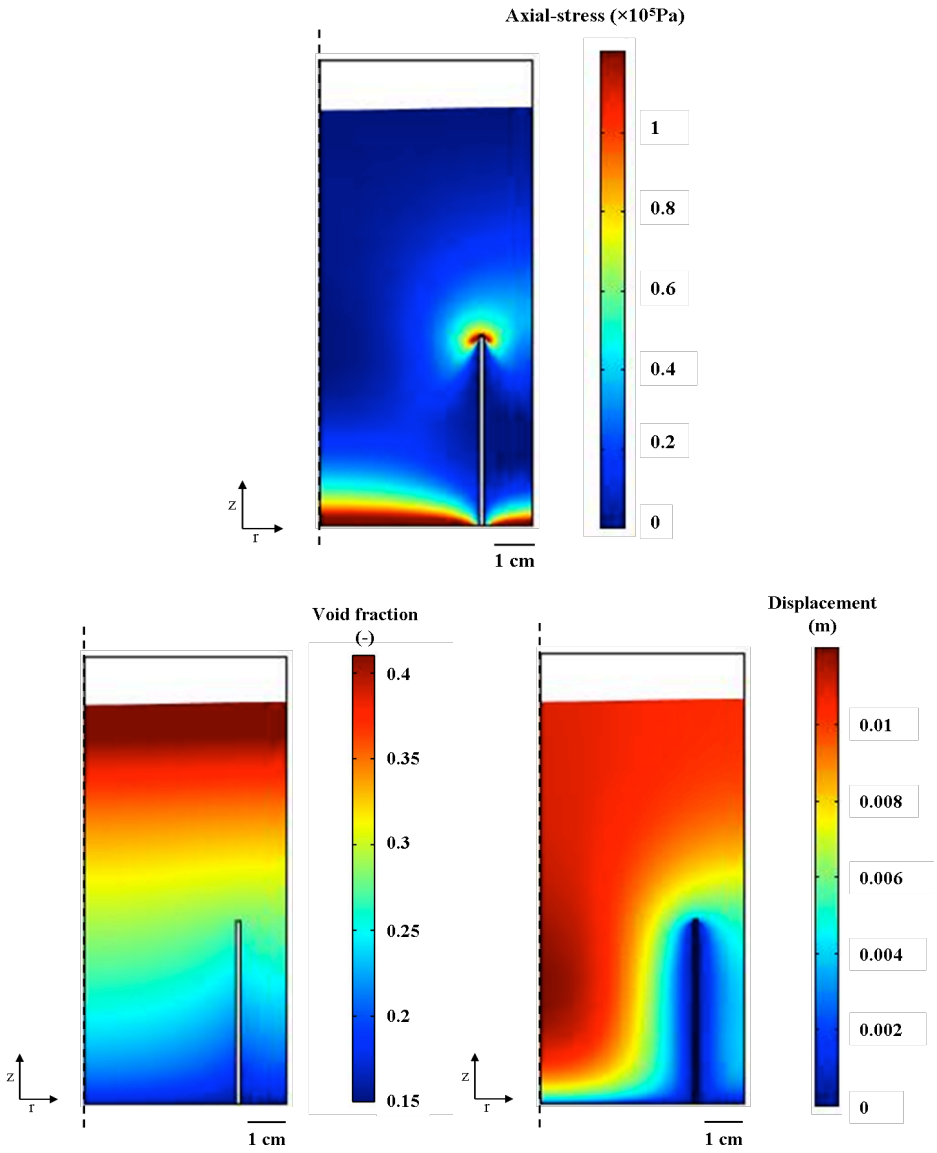

Figure 5.2 *Axial-stress, voidage fraction, and bed displacement profile of a 0.86 L chromatographic column (100 mm in diameter, and 110 mm in height) packed with single column inserts (75 mm in diameter and 45 mm in length), at the point the column achieves critical velocity. The packed material was P6XL.*

when a column insert is present there is a radial difference in voidage. The porosity is lower near the column insert than in any other position in the column. This is the result of the fictional force between the beads of the resin and the insert/column

walls, retarding bed compression this causes a relatively higher porosity close to the column insert walls and a lower bed displacement. In Figure 5.2, the bed displacement is more pronounced in the center of the column than it is near the insert. The bed displacement is also affected by the level of the frictional force between the column insert and the wall. This frictional force acts against the compression direction, and it can delay bed compression.

5.2.3 Simulation on the effect of insert length on critical velocity

Figure 5.3 shows the simulation results on the effect of insert length on critical velocity of the column when packed with a single insert. From the model established in Chapter Four, the simulations were run for insert lengths from 7.5 mm to 90 mm with a step size of 30 mm (12 intervals). The critical velocity increased linearly with insert length. The linear relationship is shown below:

$$u_{crit} = u_{crit0} + \alpha L_{insert} \tag{5.1}$$

where u_{crit} is the critical velocity, cm h^{-1}, u_{crit0} is the critical velocity in a column without insert(s), cm h^{-1}, L_{insert} is the insert length, mm, and α is the empirical constant. In this case for 100 mm diameter column packed to 110 mm bed height with P6XL having single insert system, α=0.19.

The results can be explained by the fact that the larger contact area with longer insert could generate a higher fictional force. This in turn provides more wall support, and raises the critical velocity. However, there is a practical limit to the

column bed height which can benefit from the increasing insert length, as discussed in Section 3.2.3. The maximum insert length was restricted to be no more than 90% of the flow packed bed height.

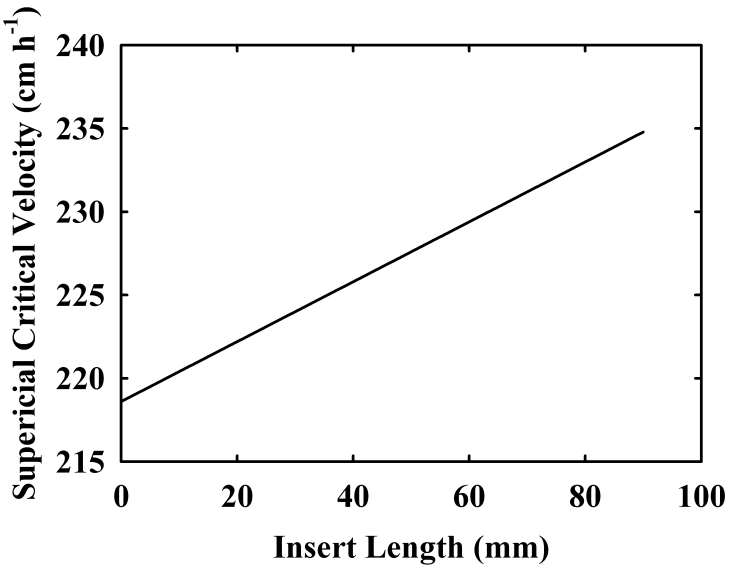

Figure 5.3 *Simulation result on the impact of column insert length on superficial critical velocity. The simulation was conducted at a 100 mm diameter column packed to 110 mm bed height. The inserts were 30 mm in diameter and 1.1 mm in thickness. The simulations were conducted for insert length ranging from 7.5 to 90 mm.*

5.2.4 Simulation on the effect of insert diameter on critical velocity

Figure 5.4 shows the simulation results on the effect of insert diameter on the critical velocity of a column packed with single insert. The simulations were run for different insert diameters ranging from 7.5 to 90 mm (step size: 7.5 mm). The insert

length was kept constant at 45 mm. The following empirical equation was used to express the critical velocity as a function of column diameter:

$$u_{crit} = u_{crit0} + \alpha\left(D_{insert}\right)^3 + \beta\left(D_{insert}\right)^2 + \delta\left(D_{insert}\right) \quad (5.2)$$

where u_{crit} is the critical velocity, cm h^{-1}, u_{crit0} is the critical velocity in column without insert(s), cm h^{-1}, D_{insert} is the insert diameter, mm. α, β, and δ are coefficients. In this case for 100mm diameter column packed to 110 mm bed height with P6XL having single insert system, their values are -5×10^{-5}, 4.2×10^{-3}, and 0.19 respectively.

Figure 5.4 describes the effect of insert diameter on the critical velocity. It can be seen that the critical velocity increases with insert diameter till the point where the insert diameter becomes 77.5 mm. A higher insert diameter decreases the critical velocity. A possible explanation for this may be how large the distance between the insert and the column wall is in comparison with the diameter of the column. When the distance between insert and column wall is small, the outer insert wall and the column wall provide support in a small fraction of the resin, which contained in the annulus forming between the insert and the column wall. By contrast, the resin in the inner part of column cannot be supported well due to large insert diameter (the insert is too close to column wall). This causes the overall critical velocity to decrease for inserts which are too close to the column wall (in this case for insert diameter >77.5 mm).

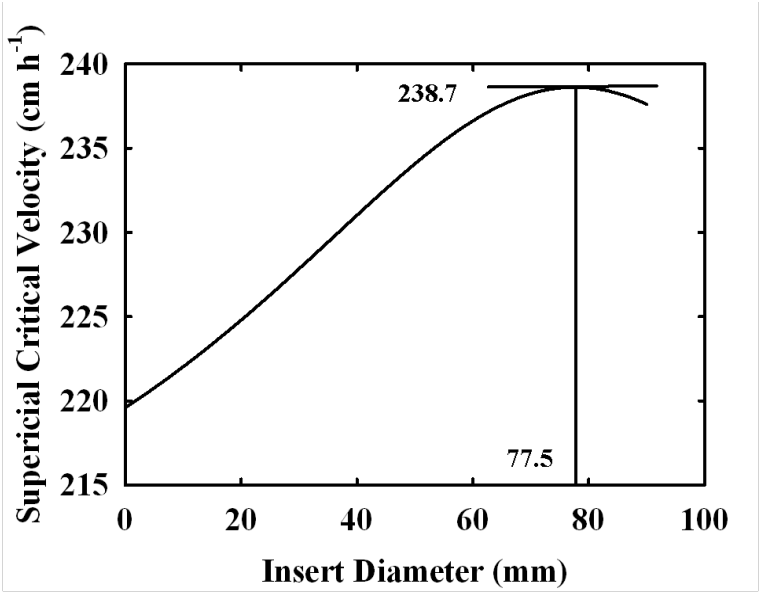

Figure 5.4 *Simulation result on the impact of column insert length on superficial critical velocity. The simulation was conducted at a 100 mm diameter column packed to 110 mm bed height. The inserts were 45 mm in length and 1.1 mm in diameter. The insert diameter of the simulation was from 7.5 to 90 mm.*

5.2.5 Simulation the effect of column insert number on critical velocity

Figure 5.5 shows the bed voidage faction and displacement profile in chromatographic column packed with double and triple inserts. Here, the length of column insert is 45 mm, (total bed height: 110 mm). The reason of choosing this length insert is that it could be clear to see the voidage fraction and displacement profile at the top region without insert and the bottom region with column inserts. The choice of double and triple column inserts diameters could lead the distance between inserts and column wall same in the two-dimensional cylindrical coordinated system.

Figure 5.5 shows that at the region near the column inserts, the bed voidage fraction is higher at the region near the column inserts than in all other point in the column located at the same bed height level. The bed displacement is also retarded by the presence of inserts. The higher voidage fraction led to a higher permeability, as predicted by Kozeny-Carman equation and therefore a larger critical velocity could be achieved. Bed voidage increased and displacement was decreased when more than one inserts were supporting the column. These changes though are not significant when the number of inserts is larger than three (for this column diameter).

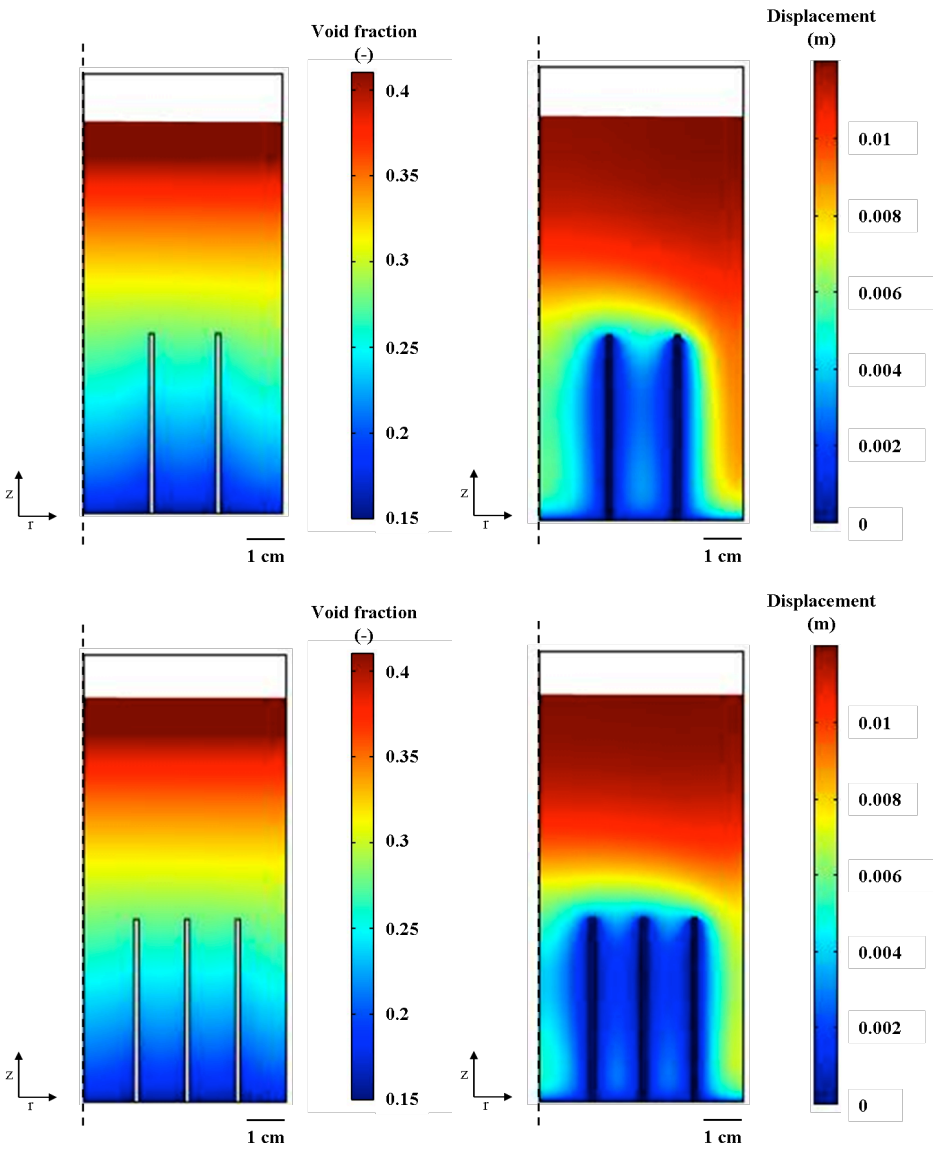

Figure 5.5 *Bed Voidage fraction, and displacement profile of a 0.86 L chromatographic column (100 mm in diameter, and 110 mm in height) packed with double column inserts (32 mm & 64 mm in diameter and 45 mm in length) and triple column inserts (25 mm & 50 mm & 75 mm diameter and 45 mm in length), at the point the column achieves critical velocity. The packed material was P6XL.*

Table 5.1 shows critical velocity values derived from simulations when a column was packed with more than one insert. It can be seen that the benefit from

increasing insert number reduces with higher insert numbers.

Table 5.1 Critical velocity increment with insert number

Insert number	1	2	3	4
Diameter (mm)	75	32&64	25&50&75	10&20&30&40
Critical velocity increment	8%	16%	20%	22%

The initial critical velocity was 219 cm h^{-1}.

5.3 Conclusions

In this chapter, a structural mechanics model has been used to simulate the pressure-flow profile and the level of compression in chromatographic columns, supported with column inserts. The empirical equations for Young's modulus and bed voidage fraction, developed in Chapter Four, were also applied for the case of columns supported with inserts. The effect of column inserts on key parameters describing column pressure-flow behavior, involving pressure, axial-stress, bed voidage fraction and displacement were also presented. The pressure-flow simulations were in good agreement with the experimental results.

The effect of insert dimensions (length and diameter) was also studied. Simulations showed that the longer the column insert is, the higher the critical velocity will be. It was shown also that the critical velocity is linearly dependent on the length of the insert. Additionally, it was shown that an increase of insert diameter causes an

increase on the critical velocity till the point where the distance between the insert and column wall becomes too small. In this case that most of the resin is in the inner part of the insert and the wall support is equal to the wall support without the insert.

The last part of the simulations was to show the effect of using more than one insert to support the column. When more inserts than one insert are placed in the column, the wall support increases and consequently the bed displacement decreases. However the benefit from increasing the number of the inserts to achieve even higher critical velocity diminishes when the number of inserts is greater than three. The number of the inserts though depends on the diameter of the column. A wider column would have required more than 3 inserts to maximize critical velocity. It is also a function of the compressibility of the resin.

Chapter Six: Conclusions and Future Work

6.1 Conclusions

The objective of the project, which is investigating the column inserts affecting chromatographic process hydrodynamics, has been achieved by a combination of experimental work to study the effects of cylindrical inserts on the hydrodynamic performance of chromatography column packed with compressible materials, together with a the simulation study of the pressure-flow profile and bed consolidation.

For the experimental study, a series of chromatography columns of different diameters (16, 50, and 100 mm) employed for critical velocity and column efficiency tests. The columns were packed with soft matrices of different level of compressibility, including Sepharose 4B, Sepharose 6b-CL, and P6XL.

The impact of column inserts on critical velocity can be summarised as:

(1) The inserts when placed at the bottom of a column make the most impact on the critical velocity increment. All experimental and simulation study followed this insert position. For determining the effect of insert position, the experiment was conducted only with an XK16 column and it shows inserts making more impact on critical velocity increment when it rests on the bottom of the columns. From the simulation result we predict there is more stress at the bottom part of the column.

Therefore, inserts at the bottom of the column could increase the critical velocity more in all column diameters.

(2) The more compressible the matrix, the greater the impact on the critical velocity of including column inserts.

(3) For a constant packed bed height, the larger the column is in diameter, the greater the increase in the critical velocity with the inclusion of column inserts (the insert diameter/column diameter is constant).

(4) The longer an insert the greater the increase in the critical velocity, but (practically) the insert length can not exceed 90% of packed bed height.

(5) With the change of insert diameter, the critical velocity keeps increasing with insert diameters to the point at which the insert diameter is about 77.5% of the column diameter. At this insert diameter, the inner and outer cross-sectional area becomes equal. The empirical equations for critical velocity versus insert length and insert diameter were developed.

(6) The impact of numbers of column insert on critical velocity was also studied. Multiple column inserts raise, the critical velocity but the benefit diminishes beyond n=3.

The column inserts have a positive effect on the critical velocity, but a negative effect on column efficiency. The theoretical plate number and bed asymmetry both decrease with use of column inserts. With larger inserts (more in length and in diameter) and the greater number, the plate number decreases. The large plate

number corresponds also to a broader peak area, and would lead to low level of resolution. For bind-and-elute chromatographic processes, the broadened peak would cause a larger volume of elution buffer, and a low concentration of product. However, the decrement of plate number for single insert was only about 5%, whilst the increment in critical velocity was about 10%. Moreover, the critical velocity impacts the whole chromatographic separation operating flowrate, whilst the peak broadening is only relevant during the elution step. The overall impact of column insert on chromatographic process productivity is positive, but it will need further study to establish the balance of critical velocity increment and plate number decrement.

A two-dimensional hydrodynamics and solid mechanics model was established to simulate the pressure-flow profile and bed deformation during flow. A finite element method was applied to solve the differential equations in Darcy's Law, which is used to describe the liquid phase fluid flow, and in Biot's theory, which is used to describe the compressible packed material consolidation of the solid phase in a chromatography column. The inverse method was applied to locate the best-fit parameters in the empirical equations (4.27 and 4.28) which describe the Young's modulus versus bed voidage fraction, and the bed voidage fraction versus pressure drop. The simulation results were matched against the experimental data for a chromatography column pressure-flow relationship and bed displacement versus flowrate without inserts.

The model was then applied to predict the pressure-flow, and bed consolidation in chromatography column with inserts. The simulation results and experimental data were matched. The flow velocity, liquid pressure, axial-stress, bed displacement, and voidage fraction distribution in the column with inserts were presented. The model enabled the best dimension of insert, which can lead the most critical velocity increment to be located. For a single insert, a 77.5 mm in diameter and 90 mm in length insert placed in 100 mm diameter column packed to about 110 mm bed height could make most impact on critical velocity increment about 16%. The model was also applied to predict the pressure-flow profile, and bed deformation when more inserts were used, and the results again showed the critical velocity increased when more with more inserts were used. However, this benefit was limited due to change the column efficiency as more inserts were used, and the volume of column inserts could not be ignored when lots of inserts (>3) were applied (Chapter Three). With this model, the properties (voidage fraction with pressure, Young's modulus with voidage fraction) of packing material could be found from experiments at small scale. Then with these properties, the hydrodynamic performance of large scale could be predicted with packing material properties. Moreover, the effect of column insert on critical velocity could also be predicted.

6.2 Future directions

6.2.1 Impact of column inserts on process productivity

In this thesis, the work was focused on the hydrodynamics of chromatographic columns. Both practical work and simulation approaches were used to establish the effect of on column inserts on the pressure-flow profile and on bed consolidation. In future work, the impact of column inserts on process productivity should be studied. Here the impact on mass transfer will also be concerned. The column inserts could increase the flow performance by providing extra wall support. However, in bind and elute chromatography mode, the larger flow velocity normally could cause a lower dynamic binding capacity (Sofer, 1997), whilst in flow-through mode, lower resolution could happen with a higher flowrate, and the theoretical plate number decrement with column inserts should also be considered here. Therefore, the overall effect of column inserts on process productivity for the whole chromatographic process, including column equilibration, sample loading, one or more wash steps, and product elution, should be studied. The column inserts could increase the operating flowrate in these stages, but decrease the column efficiency. The balance of these effects should be studied in a new model which describes the process productivity versus operating flowrate profile.

6.2.2 Insert material

In this study, the column inserts were constructed of plastic and stainless steel. The

mobile phase was RO water and 100m NaCl. The column packed material was agarose base material of different level of compressibility. The interaction between the column inserts and mobile phase/solid phase in the column was not considered. However, with chromatographic processes for bioproduct separation, the feedstock would be more complicated, and the column packed material would carry various ligands. Therefore, the material of the column inserts is important. Ideally the column inserts should only affect the hydrodynamics and bed consolidation, and have no interaction with the packed matrices, feedstock or buffer.

6.2.3 Industry scale study

The experimental work was on lab-scale to pilot-scale chromatographic columns (XK 16, XK 50, and BPG 100) and the simulation study was on pilot-scale column (BPG 100) in this study. All these columns were packed to about 100 mm bed height. The aspect ratio (column diameter/column bed height) was under 2, where the wall support clearly affects the critical velocity. The critical velocity change with more than 3 inserts is not very obvious.. For chromatography scale up to industry scale, it usually keeps the bed height, and increases the bed diameter. The aspect ratio could be over 2, and the wall support is negligible. Therefore, to take the benefit from wall support provided by column inserts, multi-insert (more than three) might be placed, and should be studied further for industry scale columns, (D>>100 mm).

References

1. Aggarwal, S. 2009. What's fueling the biotech engine-2008. *Nature Biotechnology,* 27**,** 987-993.

2. Aggarwal, S. 2011. What's fueling the biotech engine-2010 to 2011. *Nature Biotechnology,* 29**,** 1083-1089.

3. Aldington, S. & Bonnerjea, J. 2007. Scale-up of monoclonal antibody purification processes. *Journal of Chromatography B,* 848**,** 64-78.

4. Aldridge. 2006. Downstream processing needs a boost. *Genetic Engineering and Biotechnology News*.

5. Baru, M. B., Danilov, A. V. & Vagenina, I. V. 2003. Size exclusion chromatography on soft and semi-rigid packing materials in the dynamic axial compression mode. *Journal of Biochemical and Biophysical Methods,* 57**,** 115-142.

6. Bear, J. 1972. *Dynamics of Fluids in Porous Media,* New York, American Elsevier.

7. Beyzavi, K. 1999. *Adsorbents, Inorganic. In Encyclopedia of Bioprocess Technology: Fermentation, Biocatalysis, and Bioseparation,* New York, John Wiley and Sons.

8. Biot, M. A. 1941. General theory of three-dimensional consolidation. *Journal of Applied Physics,* 12**,** 155-164.

9. Biot, M. A. 1962. Mechanics of deformation and acoustic propagation in porous media. *Journal of Applied Physics,* 33**,** 1482-1498.

10. Bird, R. B., Stewart, W. E. & Lightfoot, E. N. 1960. *Transport Phenomena,*

New York, Wiley.

11. Boomsma, K. & Poulikakos, D. 2002. The effects of compression and pore size variations on the liquid flow characteristics in metal foams. *Journal of Fluids Engineering,* 124**,** 263-272.

12. Boschetti, E. 1994. Advanced sorbents for preparative protein separation purposes. *Journal of Chromatography A,* 658**,** 207-236.

13. Bottari, E. & Goretti, G. 1978. New method for estimation of the parameters in the Van Deemter equation. *Journal of Chromatography A,* 154**,** 228-233.

14. Burton, S. C. & Harding, D. R. K. 1998. Hydrophobic charge induction chromatography: Salt independent protein adsorption and facile elution with aqueous buffers. *Journal of Chromatography A,* 814**,** 71-81.

15. Carlsson, F., Axelsson, A. & Zacchi, G. 1994. Mathematical modelling and parametric studies of affinity chromatography. *Computers & Chemical Engineering,* 18**,** 657-661.

16. Carta, G. & Jungbauer, A. 2010. *Protein Chromatography: Process Development and Scale-up,* Weinheim, Wiley-VCH.

17. Chang, Y.-C., Gerontas, S. & Titchener-Hooker, N. J. 2012. Automated methods for accurate determination of the critical velocity of packed bed chromatography. *Biotechnology Progress,* 28**,** 740-745.

18. Chase, H. A. 1984. Prediciton of the preformance of preparative affinity chromatography. *Journal of Chromatography A,* 297**,** 179 -202.

19. Chen, F., Drumm, E. C. & Guiochon, G. 2005. Stress distribution and dimensional changes in chromatographic columns. *Journal of Chromatography A,* 1083**,** 68-79.

20. Chen, J., J. , Tetrault & Ley, A. 2008. Comparison of standard and new generation hydrophobic interaction chromatography resins in the monoclonal antibody purification process. *Journal of Chromatography A,* 1177**,** 272-281.

21. Chen, Q., Suki, B. & An, K.-N. 2003. Dynamic mechanical properties of agarose gel by a fractional derivative model. *2003 Summer Bioengineering Coference.* Florida.

22. Cherrak, D. E., Al-Bokaria, M., Drumm, E. & Guiochon, G. 2001. Behavior of packing materials in axially compressed chromatographic columns. *Journal of Chromatography A,* 943**,** 15-31.

23. Cherrak, D. E. & Guiochon, G. 2001. Phenomenological study of the bed-wall friction in axially compressed packed chromatographic columns. *Journal of Chromatography A,* 911**,** 147-166.

24. Clonis, Y. D. 2006. Affinity chromatography matures as bioinformatic and combinatorial tools develop. *Journal of Chromatography A,* 1101**,** 1-24.

25. Colby, C. B., O'neil, B. K. & Middelberg, A. P. 1996. A modified version of the volume avergaded continuum theory to predict pressure-drop across compressible packed beds of Sepharose big beads SP. *Biotechnology Process,* 12**,** 92-99.

26. Craig, L. C. 1944. Identification of small amounts of organic compounds by distribution studies: II. Separation by counter-current distribution. *Journal of Biological Chemistry,* 155**,** 519-534.

27. Curting, J. 2007. *History of chromatography: process chromatography: five decades of innovation*. BioPharm international.com. [Accessed 2009].

28. Danilov, A. V., Vagenina, I. V., Mustaeva, L. G., Moshnikov, S. A., Gorbunova, E. Y., Cherskii, V. V. & Baru, M. B. 1997. Liquid

chromatography on soft packing material, under axial compression: Size-exclusion chromatography of polypeptides. *Journal of Chromatography A,* 773**,** 103-114.

29. Davies, P. A. & Bellhouse, B. J. 1989. Permeability of beds of agarose-based particles. *Chemical Engineering Science,* 44**,** 452-455.

30. Dephillips, P. & Lenhoff, A. M. 2000. Pore size distributions of cation exchange adsorbents determined by inverse size-exclusion chromatography. *Journal of Chromatography A,* 883**,** 39-54.

31. Devault, D. 1942. The theory of chromatography. *Journal of the American Chemical Society* 65**,** 532-540.

32. Drgan, V., Novic, M. & Novic, M. 2009. Computational method for modeling of gradient separation in ion-exchange chromatography. *Journal of Chromatography A,* 1216**,** 6502-6510.

33. Foley, J. P. & Dorsey, J. G. 1983. Equations for calculation of chromatographic figures of merit for ideal and skewed peaks. *Analytical Chemistry,* 55**,** 730-737.

34. Freitag, R., Frey, D. & Horváth, C. 1994. Effect of bed compression on high-performance liquid chromatography columns with gigaporous polymeric packings. *Journal of Chromatography A,* 686**,** 165-177.

35. Ganetsos, G. & Barker, P. E. 1993. *Preparative and Production Scale Chromtography,* New York, Marcel Dekker Inc.

36. Gerontas, S., Asplund, M., Hjorth, R. & Bracewell, D. G. 2010. Integration of scale-down experimentation and general rate modelling to predict manufacturing scale chromatographic separations. *Journal of Chromatography A,* 1217**,** 6917-6926.

37. Guiochon, G. 2002. Preparative liquid chromatography. *Journal of*

Chromatography A, 965**,** 129-161.

38. Guiochon, G., Drumm, E. & Cherrak, D. 1999. Evidence of a wall friction effect in the consolidation of beds of packing materials in chromatographic columns. *Journal of Chromatography A,* 835**,** 41-58.

39. Guiochon, G., Farkas, T., Guan-Sajonz, H., Koh, J.-H., Sarker, M., Stanley, B. J. & Yun, T. 1997. Consolidation of particle beds and packing of chromatographic columns. *Journal of Chromatography A,* 762**,** 83-88.

40. Guiochon, G., Felinger, A., Shirazi, D. G. & Katti, A. M. 2006. *Fundamentals of Preparative and Nonlinear Chromatography, 2nd ed.* , Amsterdam, Netherlands, Academic Press.

41. Guiochon, G. & Sarker, M. 1995. Consolidation of the packing material in chromatographic columns under dynamic axial compression. I. Fundamental study. *Journal of Chromatography A,* 704**,** 247-268.

42. Guiochon, G. & Tarafder, A. 2011. Fundamental challenges and opportunities for preparative supercritical fluid chromatography. *Journal of Chromatography A,* 1218**,** 1037-1114.

43. Harrison, R. G., Todd, P. W., Rudge, S. R. & Petrides, D. 2003. *Bioseparation Science and Engineering. ,* New York., Oxford University Press.

44. Hashim, M. A. & Chu, K. H. 2009. Modeling the performance of protein-A affinity columns using asymptotic solutions. *Separation and Purification Technology,* 68**,** 279-282.

45. Hellström, J. G. I. & Lundström, T. S. Year. Flow through porous media at moderate reynolds number. *In:* International Scientific Colloquium, 2006 Riga.

46. Hjertén, S. 1961. Agarose as an anticonvection agent in zone electrophoresis.

Biochimica et Biophysica Acta, 53**,** 514-517.

47. Hjertén, S. 1964. The preparation of agarose spheres for the chromatography of molecules and particles. *Biochimica et Biophysica Acta,* 79**,** 393-398.

48. Janson, J. C. 1971. Columns for large-scale gel filtration on porous gels. Fractionation of rape seed proteins and insulin. *Journal of Agricultural and Food Chemistry,* 19**,** 581-588.

49. Johansson, B. L., Belew, M., Eriksson, S., Glad, G., Lind, O., Maloisel, J. L. & Norrman, N. 2003. Preparation and characterization of prototypes for multi-modal separation media aimed for capture of negatively charged biomolecules at high salt conditions. *Journal of Chromatography A,* 1016**,** 21-33.

50. Jungbauer, A. 1993. Preparative chromatography of biomolecules. *Journal of chromatography A,* 639**,** 3-16.

51. Keener, R. N., Fernandez, E. J., Maneval, J. E. & Hart, R. A. 2008. Advancement in the modeling of pressure-flow for the guidance of development and scale-up of commercial-scale biopharmaceutical chromatography. *Journal of Chromatography A,* 1190**,** 127-140.

52. Keener, R. N., Maneval, J. E. & Fernandez, E. J. 2004. Toward a Robust Model of Packing and Scale-Up for Chromatographic Beds. 2. Flow Packing. *Biotechnology Progress,* 20**,** 1159-1168.

53. Keener, R. N., Maneval, J. E., Ostergren, K. C. E. & Fernandez, E. J. 2002. Mechanical deformation of compressible chromatographic columns. *Biotechnology Process.,* 18**,** 587-596.

54. Knox, J. H., Laird, G. R. & Raven, P. A. 1976. Interaction of radial and axial dispersion in liquid chromatography in relation to the “infinite diameter effect”.

Journal of Chromatography, 122**,** 129-145.

55. Koh, J.-H., Broyles, B. S., Guan-Sajonz, H., Hu, M. Z. C. & Guiochon, G. 1998. Consolidation and column performance of several packing materials for liquid chromatography in a dynamic axial compression column. *Journal of Chromatography A,* 813**,** 223-238.

56. Lambe, W. T. & Whitman, R. V. 1969. *Soil Mechanics,* New York, Wiley.

57. Laub, C. 2003. Reproducible preparative liquid chromatography columns. *Journal of Chromatography A,* 992**,** 41-45.

58. Lawrence, S. 2007. Billion dollar babies-biotech drugs as blockbusters. *Nature Biotechnology,* 25**,** 380-382.

59. Müller, E. 2005. Properties and characterization of high capacity resins for biochromatography. *Chemical Engineering & Technology,* 28**,** 1295-1305.

60. Martin, A. & Shadday, J. 2006. A one-dimensional transient model of down-flow through a swelling packed porous bed. *Chemical Engineering Science,* 61**,** 2688-2700.

61. Martin, A. J. & Synge, R. L. 1941. Separation of the higher monoamino-acids by counter-current liquid-liquid extraction: the amino-acid composition of wool. *Biochemical Journal,* 35**,** 91-121.

62. Mccue, J. T., Cecchini, D., Chu, C., Liu, W.-H. & Spann, A. 2007. Application of a two-dimensional model for predicting the pressure-flow and compression properties during column packing scale-up. *Journal of Chromatography A,* 1145**,** 89-101.

63. Mitchell, J. K. & Soga, K. 2005. *Fundamentals of Soil Behavior,* New York, Wiley.

64. Mohammed, A. W., Stevenson, D. G. & Wankat, P. C. 1992. Pressure drop correlations and scales-up of size exclusion chromatography with compressible packing. *Industrial & Engineering Chemistry Research,* 31**,** 561-575.

65. Nagaraj, T. S. & Srinivasa Murthy, B. R. 1983. Rationalization of Skempton's compressibility equation. *Geotechnique,* 33**,** 413-425.

66. Nagaraj, T. S. & Srinivasa Murthy, B. R. 1986. A critical reappraisal of compression index equations. *Geotechnique,* 36**,** 135-138.

67. Naveh, D. & Siegel, R. C. 1991. Large-scale downstream processing of monoclonal antibodies. *Bioseparation,* 1**,** 351-366.

68. Ostergren, K. C. E., Trägårdh, A. C., Enstad, G. G. & Mosby, J. 1998. Deformation of a chromatographic bed during steady-state liquid flow. *AIChE Journal,* 44**,** 2-12.

69. Ostergren, K. C. E. & Trägårdh, C. 1997. Numerical study of two-dimensional compaction, flow, and dipersion in a chromatographic column. *Numerical Heat Transfer, Part A: Applications: An International Journal of Computation and Methodology,* 32**,** 247 - 265.

70. Ostergren, K. C. E. & Trägårdh, C. 1999. Modelling and analysis of axial flow through and compression of a non-rigid chromatographic bed. *Chemical Engineering Journal,* 72**,** 153-161.

71. Parker, K. H., Mehta, R. V. & Caro, C. G. 1987. Steady flow in porous, elastically deformable materials. *Journal of Applied Mechanics,* 54**,** 794-800.

72. Pelosi, G. 2007. The finite-element method, Part I: R. L. Courant [Historical Corner]. *Antennas and Propagation Magazine, IEEE,* 49**,** 180-182.

73. Peterson, E. & Sober, H. 1954. Chromatography of proteins. I Cellulose ion-exchange adsorbents. *Journal of the American Chemical Society,* 76**,**

751-755.

74. Petricevic, J., Forempoher, G., Ostojic, L., Mardesic-Brakus, S., Andjelinovic, S., Vukojevic, K. & Saraga-Babic, M. 2011. Expression of nestin, mesothelin and epithelial membrane antigen (EMA) in developing and adult human meninges and meningiomas. *Acta Histochemica,* 113**,** 703-711.

75. Porath, J. & Flodin, P. 1959. Gel filtration: A method for desalting and group separation. *Nature.*

76. Reddy, J. N. 1993. *An Introduction to the Finite Element Method,* Texas, McGraw-Hill, Inc.

77. Reddy, R. K. & Joshi, J. B. 2010. CFD modeling of pressure drop and drag coefficient in fixed beds: Wall effects. *Particuology,* 8**,** 37-43.

78. Reichert, J. M. 2008. Monoclonal Antibodies as Innovative Therapeutics. *Current Pharmaceutical Biotechnology,* 9**,** 423-430.

79. Roque & Lowe 2004. Antibodies and genetically engineered related molecules: Production and purification. *Biotechnology Progress,* 20**,** 639-654.

80. Roque, A. C., Gupta, G. & Lowe, C. R. 2005. Design, synthesis, and screening of biomimetic ligands for affinity chromatography. *Methods in Molecular Biology,* 310**,** 43-62.

81. Rubin, M. B. & Einav, I. 2011. A large deformation breakage model of granular materials including porosity and inelastic distortional deformation rate. *International Journal of Engineering Science,* 49**,** 1151-1169.

82. Said, W., Nemer, M. & Clodic, D. 2011. Modeling of dry pressure drop for fully developed gas flow in structured packing using CFD simulations. *Chemical Engineering Science,* 66**,** 2107-2117.

83. Salvalaglio, M., Zamolo, L., Busini, V., Moscatelli, D. & Cavallotti, C. 2009. Molecular modeling of Protein A affinity chromatography. *Journal of Chromatography A,* 1216**,** 8678-8686.

84. Sarker, M. & Guiochon, G. 1995. Study of the operating conditions of axial compression columns for preparative chromatography. *Journal of Chromatography A,* 709**,** 227-239.

85. Sarker, M. & Guiochon, G. 1996. Consolidation of the packing material in chromatographic columns under dynamic axial compression III. Effect of the nature of the packing solvent on the consolidation and performance of axial compression columns. *Journal of Chromatography A,* 741**,** 165-173.

86. Sarker, M., Katti, A. M. & Guiochon, G. 1996. Consolidation of the packing material in chromatographic columns under dynamic axial compression II. Consolidation and breakage of several packing materials. *Journal of Chromatography A,* 719**,** 275-289.

87. Schiff, D. & Agostino, P. B. 1996. *Practical Engineering Statistics,* New York, John Wiley & Sons.

88. Shadday, J. M. A. 2006. A one-dimensional transient model of down-flow through a swelling packed porous bed. *Chemical Engineering Science,* 61**,** 2688-2700.

89. Shalliker, R. A., Broyles, B. S. & Guiochon, G. 2000. Physical evidence of two wall effects in liquid chromatography. *Journal of Chromatography A,* 888**,** 1-12.

90. Shalliker, R. A., Broyles, B. S. & Guiochon, G. 2003. Axial and radial diffusion coefficients in a liquid chromatography column and bed heterogeneity. *Journal of Chromatography A,* 994**,** 1-12.

91. Skempton, A. W. & Jones, O. T. 1944. Notes on the compressibility of clays. *Quarterly Journal of the Geological Society,* 100**,** 119-135.

92. Smith, C. 2005. Striving for purity: Advances in protein purification. *Nature Methods in Molecular Biology,* 2**,** 71-76.

93. Snyder, L. R. & Kirkland, J. J. 1979. *Introduction to Modern Liquid Chromatography,* New York, Wiley.

94. Sofer, G. & Hagel, L. 1997. *Handbook of Process Chromatography: A Guide to Optimization, Scale-up, and Validation,* San Diego, Academic Press.

95. Sofer, G. K. & Nystrom, L.-E. 1989. *Process Chromatography; A Practical Guide,* San Diego, Academic Press.

96. Soriano, G. A., Titchener-Hooker, N. J. & Shamlou, P. A. 1997. The effects of processing scale on the pressure drop of compressible gel supports in liquid chromatographic columns. *Bioprocess and Biosystems Engineering,* 17**,** 115-119.

97. Stanley, B. J., Sarker, M. & Guiochon, G. 1996. Consolidation of the packing material in chromatographic columns under dynamic axial compression IV. Mechanical properties of some packing materials. *Journal of Chromatography A,* 741**,** 175-184.

98. Stickel, J. J. & Fotopoulos, A. 2001. Pressure-flow relationships for packed beds of compressible chromatography media at laboratory and production scale. *Biotechnology Progress,* 17**,** 744-751.

99. Subramanian, G. 1995. *Process Scale Liquid Chromatography,* New York, VCH publishers.

100. Thommes, M. E. 2007. Alternatives to chromatographic separations. *Biotechnology Progress,* 23**,** 42-45.

101. Tiselius. 1948. *Nobel Lecture* [Online]. Available: http://nobelprize.org [Accessed Feb 2009].

102. Tiselius, A. 1952. *Presentation Speech* [Online]. Available: http://nobelprize.org [Accessed Feb 2009].

103. Tran, R., Joseph, J. R., Sinclair, A., Bracewall, D., Zhou, Y. & Titchener-Hooker, N. J. 2007. A framework for the prediction of scale-up when using compressible chromatographic packings. *Biotechnology Process,* 23**,** 413-422.

104. Tripathy, S. & Mishra, A. 2011. On the use of Skempton's compression index equation. *Geotechnical and Geological Engineering,* 29**,** 129-135.

105. Tswett, M. 1906. Ber. Dtsch. *Botan. Ges,* 24**,** 384-393.

106. Van Deemter, J. J., F.J. Zuiderweg & A. Klinkenberg 1956. Longitudinal diffusion and resistance to mass transfer as causes of non ideality in chromatography. *Chemical Engineering Science,* 5**,** 271-289.

107. Wang, J. 1984. Young's modulus of porous materials Part 1 Theoretical derivation of modulus-porosity correlation. *Journal of Materials Science,* 19**,** 801-808.

108. Yuan, Q. S., Rosenfeld, A., Root, T. W., Klingenberg, D. J. & Lightfoot, E. N. 1999. Flow distribution in chromatographic columns. *Journal of Chromatography A,* 831**,** 149-165.

109. Yun, T. & Guiochon, G. 1994. Modeling of radial heterogeneity in chromatographic columns Columns with cylindrical symmetry and ideal model. *Journal of Chromatography A,* 672**,** 1-10.

110. Zhu, J., Katti, A. M. & Guiochon, G. 1991. Comparison of various isotherm models for predicting competitive adsorption data. *Journal of Chromatography*

A, 552**,** 71-89.

Appendix

Paper by the Author

Lan, T., Gerontas, S., Smith, G. R., Langdon, J., Ward, J. M. & Titchener-Hooker, N. J. 2012. Investigating the use of column inserts to achieve better chromatographic bed support. *Biotechnology Progress,* 28**,** 1285-1291.